Deciphering fermionic matter: from holography to field theory

Meszéna, B.

Deciphering Fermionic Matter: from Holography to Field Theory

Proefschrift

ter verkrijging van
de graad van Doctor aan de Universiteit Leiden,
op gezag van Rector Magnificus
prof. mr. C.J.J.M. Stolker,
volgens besluit van het College voor Promoties
te verdedigen op woensdag 21 december 2016
klokke 13.45 uur

door

Balazs Meszena

geboren te Boedapest, Hongarije in 1989

Promotor:	Prof. dr K. E. Schalm
Promotiecommissie:	Prof. dr S. S. Lee (McMaster University, Hamilton, Canada)
	Dr P. Strack (University of Cologne, Duitsland)
	Prof. dr E. R. Eliel
	Prof. dr ir T. H. Oosterkamp
	Prof. dr J. Zaanen

Casimir PhD series, Delft-Leiden 2016-35
ISBN 978-90-8593-228-9
An electronic version of this thesis can be found at
https://openaccess.leidenuniv.nl
Cover design: Proefschriftmaken.nl —— Uitgeverij BOXPress
Printed & Lay Out by: Proefschriftmaken.nl —— Uitgeverij BOXPress

The research presented in this thesis was founded by Leiden University through a Huygens fellowship.

Contents

Chapter 1

Introduction

One of the most challenging area in theoretical physics is that of strongly coupled many-body systems. Most of our knowledge and intuition come from perturbative descriptions especially in quantum mechanical systems. It is a priori rather remarkable that this seemingly limited tool can teach us so much about nature and can describe a large number of phenomena effectively. The modern understanding of this phenomenon is due to Wilson [1]. He introduced the idea of renormalization and universality which can be thought of as a metatheory of physical laws. Its strength relies on the fact that it is not necessary to refer closely to particular details of the system we wish to study. Wilsonian universality tells us that even given the unimaginably large number of possible interactions between the constituents, its consequences can be put into three categories with respect to its behavior at large distances. Most of the interactions turn out to be irrelevant and their effects are negligible at large distances. Only for a finite number of relevant couplings is the interaction important. In the marginal case, the interaction is equaly important in the UV and in the IR. Therefore, universality tells us that many systems behave perturbatively at low energy, despite the fact that the couplings may be large at high energy.

There are also, however, systems (with relevant coupling), where we do know the microscopic physics but we do not have an algorithm which transforms a microscopic model to experimental predictions (which can be tested and compared to the model). This happens both in high-, and low-energy physics. The classical example is the theory of the strong force, QCD. It is perturbative at high energy (above $300MeV$), therefore it is possible to test the details of quark interaction in high-energy scattering experiment. However, QCD at everyday scales (describing for example the spectrum of mesons and baryons) is out of the range of applicability of weak-coupling physics. We will see in this thesis that many examples of such theories also exist in condensed matter physics. In these cases, one knows the UV theory very well (electrons interacting with each other

and with ions in the lattice via Coulomb interaction) but in some classes of materials we cannot predict macroscopic measurable properties such as conductivity or photoemission spectra in the IR regime (in which we are mostly interested).

This calls for new approaches. In bosonic systems it is possible to use Monte Carlo methods to calculate equilibrium quantities by considering the discretised version of the relevant quantum field theory in hand in imaginary time. The greatest achievements of this type of techniques is the determination of the proton mass with 2% accuracy using a discretised version of quantum chromodynamics [4]. It took, however, more than 20 years of research to achieve this goal and the power of a supercomputer due to the huge computational demands of the simulation (both in terms of CPU and memory). Even with their success, these numerical approaches have limited range of applicability.

Achieving this precision is only possible in equilibrium and it is even harder to simulate real time dynamics. For this, one would need to analytically continue the numerical data from imaginary to real time (from Matsubara frequencies to real frequencies) which would require the knowledge of the spectrum of very large frequencies with high accuracy. A common trick is to try to fit a physically motivated analytical expression (e.g. Pade approximant) to the high frequency regime.

A far more fundamental problem arises in fermionic strongly coupled system at finite density. These systems are especially hard to solve due to the fermion sign problem [2]. It means that even in an equilibrium Monte-Carlo simulation, the weight of each configuration is not a real, positive number as in the bosonic case but complex which leads to oscillatory behavior. It is in fact claimed that simulating fermionic systems is NP hard [2, 3].

Because of these difficulties of applying numerical methods to quantum many-body physics, investigating and improving analytical approaches is of high importance. In Chapter 2-4 of this thesis, we will apply several promising techniques to strongly correlated fermionic systems. To give a background, in this chapter, we will introduce these systems together with analytical, non-perturbative methods. Specifically, we will describe large-N methods, conformal field theories and holography (AdS/CFT).

1.1 Phases of fermionic matter: Fermi and non-Fermi liquids

1.1.1 Fermi liquids

Let us summarize first what are the most important characteristics of the most common fermionic system for which we do have a successful description: the Fermi liquid. Landau's Fermi liquid theory relies on the fact that the interactions become weak (they are irrelevant in the Wilsonian language) well below the scale of the Fermi momentum. This results in an infinitely long lived spectrum of quasiparticles at the Fermi surface. Though the values of explicit parameters (such as lifetime, quasiparticle residue) vary among materials, the qualitative features are the same.

Both theoretically and experimentally a very relevant quantity (which can be measured by ARPES) is the spectral function. This gives the spectrum of excitations and is computed through the imaginary part of the single particle Green's function. In case of a Fermi liquid with momentum near the Fermi surface, the form of the Green's function is:

$$G_R(k,\omega) = \frac{Z_k}{\omega - v_F\left(k - k_F\right) + \Sigma(k,\omega)} + G_{incoh}(k,\omega), \tag{1.1}$$

with the self energy being quadratic in the frequency and temperature [17] $\Sigma_{FL}(k,\omega) = iC_k\left(\omega^2 + T^2\right)$. At the Fermi surface ($\omega = 0$), the lifetime of the quasiparticle is infinite (at zero temperature), while for $\omega > 0$, it stays finite. The spectral function is given by

$$A(k,\omega) = \frac{ImG_R}{2\pi}, \tag{1.2}$$

and it is plotted in Fig. 1.1 for a free Fermi gas and an interacting Fermi liquid (at zero temperature). This quantity can be measured by inverse photoemission experiments (ARPES) and is a valuable tool to confirm either Fermi liquid behavior or deviation from it.

The occupation number (shown in Fig. 1.2) can be also calculated from the spectral function

$$n_k = \int_{-\infty}^{0} d\omega A(k,\omega). \tag{1.3}$$

The quasiparticle residue Z_k sets the magnitude of the discontinuity at k_F in the occupation number.

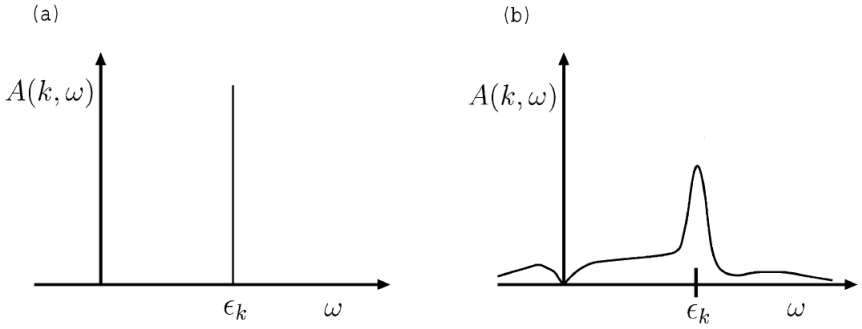

Figure 1.1. Spectral function as a function of frequency for a fixed momentum in the case of a a) free Fermi gas, b) interacting Fermi liquid (from [27]). The quasiparticle nature of these states is manifest in the form of a delta-function peak for the free Fermi gas. In case of the Fermi liquid, the peak broadens due to the interactions.

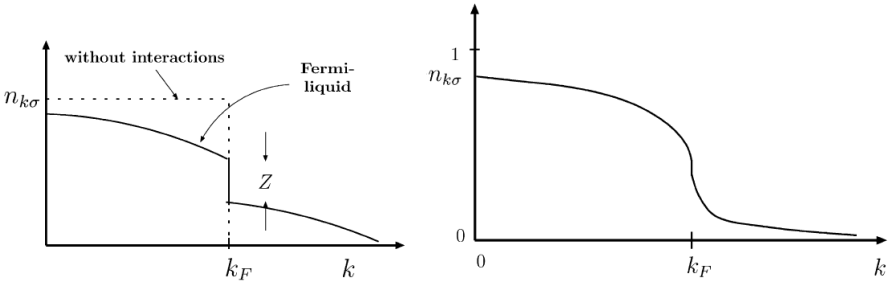

Figure 1.2. Occupation number of a a) Fermi liquid, b) marginal Fermi liquid, which we will introduce in Section 1.1.3 (from [27]).

1.1.2 Conductivity of Fermi liquids

Let us study an other very relevant feature of a Fermi liquid: its resistivity. Experiments show that the DC resistivity scales as T^2 (as in Fig. 1.4) at low temperature (for a clean sample) when electron-electron scattering is the dominant process. The form of the spectral function we saw in the previous section and the temperature profile of the conductivity are not independent. Let us see how these two important experimental quantities are related to each other.

The frequency dependent conductivity is related to the retarded current-current correlator (Π^R) according to the Kubo formula

$$\sigma_{xx}(\omega) = -\lim_{\vec{q}\to 0}\left(\frac{1}{i\omega}\Pi^R_{xx}(\omega,\vec{q})\right). \tag{1.4}$$

Here, the retarded quantity can be obtained from the Euclidean version using the usual analytical continuation

$$\Pi^R(\omega,\vec{q}) = \Pi(iq_n,\vec{q})|_{iq_n\to\omega+i\epsilon} \tag{1.5}$$

where in our notation $q = (iq_n,\vec{q})$ indicate both frequency and momentum dependence. As indicated we are interested in the diagonal part of the conductivity tensor.

The diagonal part of Π is defined by

$$\Pi_{xx}(q) = -T\langle J_x(q)J_x(-q)\rangle, \tag{1.6}$$

with $J_x(q)$ the momentum space current. Its form (depicted in Fig. 1.3) can be deduced from the $\psi^+(x)\nabla\psi(x)$ real space expression:

$$J_x(q) \sim T\sum_{ik_n}\int d^dk\,(2k_x+q_x)\,\psi^+(k)\psi(k+q), \tag{1.7}$$

where d is the number of space dimensions.

In general, in an interacting theory calculating (1.6) is difficult. Formally, there is an exact relation (Schwinger-Dyson equation) which connects it with the Green's function and three point vertex (Fig. 1.3):

$$\Pi_{xx}(iq_n,0) = T\Sigma_{ik_n}\int d^dk\,(2k_x)^2\,G\left(ik_n+iq_n,\vec{k}\right)G\left(ik_n,\vec{k}\right)\cdot \tag{1.8}$$

$$\cdot\,\Gamma\left(ik_n+iq_n,ik_n;\vec{k}.\vec{k}\right). \tag{1.9}$$

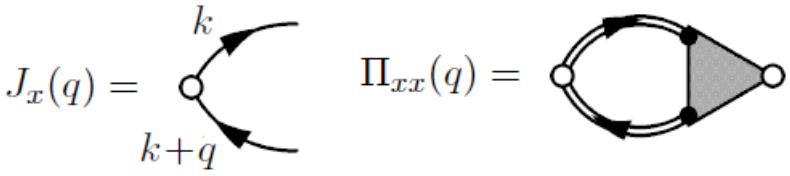

Figure 1.3. Left: Current vertex. Right: Schwinger-Dyson equation connecting the current-current correlator with the exact Green's function (double line) and irreducible three-point vertex (from [46]).

We can express the retarded version of Π by ignoring the vertex corrections (i.e. we set Γ to a constant) and using the substitution (1.5):

$$\Pi^R_{xx}(\omega, 0) = \int d^d k \, (2k_x)^2 \int_{-\infty}^{\infty} \frac{d\omega_1}{2\pi} \frac{d\omega_2}{2\pi} \frac{f(\omega_1) - f(\omega_2)}{\omega_1 - \omega - \omega_2 - i\epsilon} A\left(\omega_1, \vec{k}\right) A\left(\omega_2, \vec{k}\right), \tag{1.10}$$

where $f(\omega)$ is the Fermi-Dirac distribution. We have used the relation between the spectral function and the (Euclidean) Green's function

$$G\left(ik_n, \vec{k}\right) = \int_{-\infty}^{\infty} \frac{d\omega}{2\pi} \frac{A(\omega, \vec{k})}{ik_n - \omega}, \tag{1.11}$$

and the Matsubara sum

$$T \sum_{ik_n} \frac{1}{ik_n - \omega} = f(\omega). \tag{1.12}$$

We can obtain the DC conductivity from (1.10) by evaluating one of the frequency integral at infinitesimal ω

$$\sigma_{DC} \sim \int d^d k \, (2k_x)^2 \, d\omega_1 \frac{df(\omega_1)}{d\omega_1} \left(A\left(0, \vec{k}\right)\right)^2. \tag{1.13}$$

Ignoring the vertex correction is safe in case of the Fermi liquid (interaction is irrelevant). Note, however that this approximation is questionable for a system with relevant interactions.

One can simplify (1.13) by realizing that at low temperature, the derivative of the Fermi-Dirac distribution is a delta-function. Furthermore, the spectral function is highly peaked around the Fermi surface and in first approximation it only depends on $k_\perp$, the distance between $\vec{k}$ and

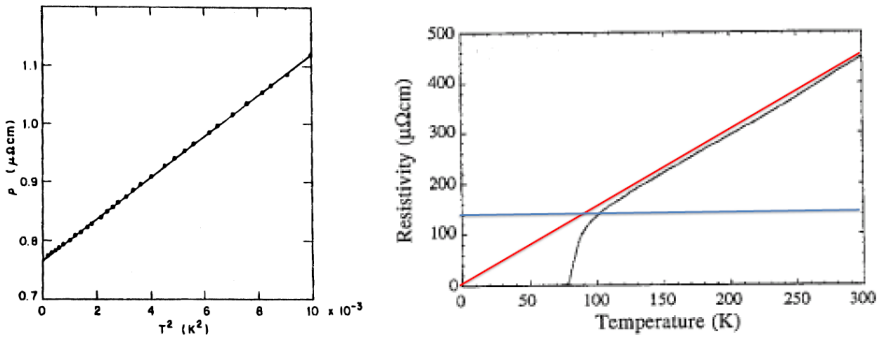

Figure 1.4. DC resistivity as a function of temperature in the case of a a) Fermi liquid and b) non-Fermi liquid (from [28] and [29] respectively). The horizontal line represents the estimated Mott-Ioffe-Regel bound.

the Fermi surface. We can therefore approximate the conductivity as

$$\sigma_{DC} \sim k_F^{d+1} \int dk_\perp A\left(0, k_\perp\right)^2 . \tag{1.14}$$

Using that $\Sigma_{FL}\left(0, \vec{k}\right) = C \cdot iT^2$ for a Fermi liquid, we arrive at the formula

$$\sigma_{DC} \sim k_F^{d+1} \int dk_\perp \frac{\Sigma''^2}{\left(\left(vk_\perp\right)^2 + \Sigma''^2\right)^2} = k_F^{d+1} \int dk_\perp \frac{c \cdot T^4}{\left(\left(vk_\perp\right)^2 + c^2 T^4\right)^2} . \tag{1.15}$$

By changing the integration variable $k_\perp \to T^2 k_\perp$, we see that the temperature scaling of the conductivity is $\sigma_{DC} \sim T^2$. Strictly speaking, there is an oversight in this computation. In a translationally invariant system the DC conductivity is always infinite. A precise calculation that includes weak translational symmetry breaking (by introducing a lattice for example) gives the same answer, however.

1.1.3 Strongly correlated fermions: Non-Fermi liquids

In 1986, a remarkable discovery happened which was unexpected for most of the physics community: the discovery of high-temperature superconductivity in cuprate systems, where the resistivity dropped to zero at $34K$ [44, 43]. Soon, new compounds were found for which the critical temperature was above the boiling temperature of liquid nitrogen ($77K$). Until

then, the theory of superconductivity was believed to be completely described with the BCS theory: phonon interaction mediated Cooper pairs condense at low temperature. However, it predicts that the critical temperature can not be higher than $30K$. On further examination these new types of material turned out to display a lot more unconventional features other than its high critical temperature. A very notable surprising feature is that at temperature above T_c the normal (not superconducting) phase exhibits behavior which cannot be describe with Fermi liquid theory.

Many electronic materials have been discovered since which display unconventional behavior. What is common in these different systems is first of all the layered structure (with CuO_2-planes in the case of the cuprates). This is believed to be the central cause of strongly coupled physics. This also means that important features of the system are captured by models in $d = 2$ spatial dimension. Secondly, these class of materials have a distinctive behavior as a function of a doping parameter x. These systems have very rich phase diagram. A simplified version of it is shown in Fig. 1.5. For large doping we have a normal Fermi liquid phase with sharp Fermi surface. In the other limit, for low doping the system is a Mott insulator with antiferromagnetic properties (or other type of phase). The most interesting regime is between these phases at intermediate doping. For low temperature, this is the exotic superconducting phase discovered in 1986.

The distinctive feature is that it is believed that under the superconducting dome there is a quantum critical point (QCP). The notion of a quantum critical point is very general and is important in bosonic systems as well. For a QCP to exist in a quantum system one needs a tunable parameter r in the Hamiltonian. This parameter can be for example an external magnetic field, pressure or the doping fraction as we described above in case of the cuprates. At zero temperature there can exist a critical value of this parameter r_c such that the groundstate of the system for $r < r_c$ can not be continously deformed into the groundstate for $r > r_c$. In other word, the system undergo a zero temperature phase transition as one tune r. If this transition is second order at the critical point ($r = r_c$), all correlation function possess a scaling symmetry, i.e.

$$\vec{x} \to s\vec{x}, \qquad t \to s^{\mathbf{z}} t, \tag{1.16}$$

similarly to thermal phase transitions. The exponent $\mathbf{z}$ is called the dynamical critical exponent, and it tells us the different scaling between time

and spatial variables. If $\mathbf{z} = 1$, we are dealing with a relativistic system with scaling symmetry. In that case the symmetry group is conjectured to be always enhanced with the special conformal transformations, arriving at a conformal field theory (CFT). We will study CFTs in more depth in Section 1.2.2.

The quantum critical point although seems to be special just one point in the phase diagram. However, if we consider now the system at finite temperature, originated from the QCP the properties in a cone-like region are still governed by the QCP. In this region therefore, the physics is also universal. The cuprates (and also other types of strongly correlated materials) exhibit such a cone. This region is the strange metallic phase and it can be obtained by heating up the system near optimal doping (see in Fig. 1.5). This is in contrast with conventional superconductors described by BCS-theory, where the normal metallic phase is of a Landau Fermi liquid. This is why it is believed that high T_c superconductivity is governed by a QCP.

The strange metallic phase has linear-T resistivity (as opposed to the T^2 resistivity of Fermi liquids) up to very high temperatures (as is depicted in Fig. 1.4b). From this experimental fact (anomalously large resistivity in the normal phase) alone one can conclude that non-quasiparticle type of physics is at work. To see this, let us use the Drude formula to obtain a resistivity bound for quasiparticle transport. In that case, the resistivity can be expressed as a function of the scattering time τ

$$\rho = \frac{m}{ne^2\tau}, \tag{1.17}$$

where n is the density of charge carriers. For a quasiparticle, τ can be approximated by $v_F\tau \sim l_{MFP}$, where v_F is the Fermi velocity and l_{MFP} is the mean free path. The resistivity is therefore inversely proportional to the mean free path:

$$\rho \sim \frac{k_F}{ne^2} \cdot \frac{1}{l_{MFP}} < \frac{k_F}{ne^2} \cdot \frac{1}{a}. \tag{1.18}$$

However, the mean free path cannot be smaller than the lattice spacing of the material and therefore, an upper bound exists (the Mott-Ioffe-Regel bound) for the resistivity. If in a material, quasiparticle transport is at work, its resistivity should saturate at high temperature.

A phenomenological description of the strange metallic phase can be given in terms of the so-called marginal Fermi-liquid. In this approach

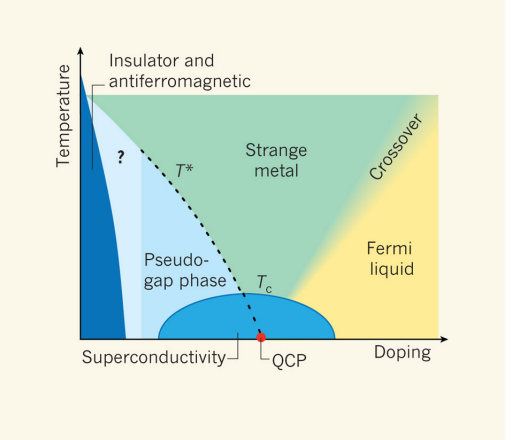

Figure 1.5. Schematic phase diagram of the cuprates (from [31]).

one fits the ARPES data (at low temperature) with the Green's function of the form [26]:

$$G_{MFL}(k,\omega) = \frac{Z}{v_F(k-k_F) - \omega - \Sigma(\omega)}, \tag{1.19}$$

with

$$\Sigma_{MFL}(\omega) = \lambda\left(\omega \log\left(\frac{x}{\omega_c}\right) - i\frac{\pi}{2}x\right), \tag{1.20}$$

where $x = \max(|\omega|, T)$. This results in an occupation number as in Fig. 1.2 b). Note that the discontinuity disappears, signaling again that we are not dealing with a gas of quasiparticles. Furthermore, as opposed to the Fermi liquid the self energy is completely independent of the momentum. We will see that this type of Green's function can be obtained by assuming that the fermions are interacting with a $\mathbf{z} = \infty$ critical system with large number of degrees of freedom. In this thesis we will meet other forms of Green's functions for non-Fermi liquids coming from different considerations.

We can connect this form of Green's function with the linear-T resistivity using (1.14) with $Im\,(\Sigma_{MFL}) \sim T$ and changing the integration variable to $k_\perp \to Tk_\perp$. We emphasise, however, that this derivation was based on the assumption that vertex-corrections can be neglected.

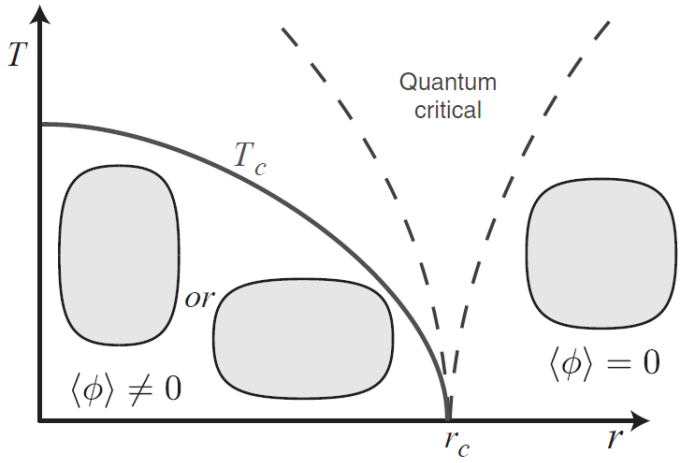

Figure 1.6. Phase diagram of the Ising-nematic transition (from [11]).

1.1.4 Ising-nematic transitions: quantum critical boson coupled to a Fermi surface

One can ask from a theoretical point of view, what kind of (effective) fermionic Lagrangian can result to non-Fermi liquid behavior. A natural attempt would be to introduce a four-fermion interaction between the fermions. However, in $d \geqslant 2$ such an interaction is generically irrelevant (with the well-known exception of BCS instability), therefore does not destroy the quasiparticle properties near the Fermi surface and we are still left with a Landau Fermi Liquid.

The simplest (continuum) model in which non-Fermi liquid behavior appears involves a fluctuating massless bosonic order parameter. The origin of the order parameter can be different, but for concreteness we will discuss the Ising-nematic transition observed for example in $YBa_2Cu_3O_y$ [30]. Here, in the unordered phase, the electronic correlations have C_4 rotation symmetry originated from the underlying lattice. In the ordered phase this rotation symmetry is spontaneously broken to C_2 as it is depicted in Fig. 1.6.

The order parameter can be described with the Landau-Ginzburg relativistic action [11]

$$S_b = \int d^d x d\tau \left[\frac{1}{2} \left((\partial_\tau \phi)^2 + (\nabla \phi)^2 + r\phi^2 \right) + u\phi^4 \right], \tag{1.21}$$

and the interaction with the fermions (we neglect the spin degrees of freedom of the fermions) is

$$S_{int} \sim \lambda \int d\tau \int d^d k d^d q d(k) \phi(q) \psi^+ \left(k + q/2\right) \psi \left(k - q/2\right). \qquad (1.22)$$

Of course, the free fermionic part of the action has the usual form of

$$S_f = \int d\tau \int \frac{d^d k}{(2\pi)^d} \psi^+(k) \left(\partial_\tau + \epsilon(k)\right) \psi(k). \qquad (1.23)$$

In $d = 2$ dimensions, in which we are most interested, the coupling λ is relevant. The parameter which controls the quantum phase transition is the mass term r in the bosonic part. In the massive case $r > 0$ we can integrate out the boson below the scale $\omega < r$, therefore the shape of the Fermi surface does not change. For $r < 0$ however ϕ acquire a non-zero (uniform) expectation value $\langle \phi \rangle \neq 0$ and its effect on the fermions is such that the shape of the Fermi surface changes. To achieve the C_2 symmetric shape (as in Fig. 1.6) we can choose $d(k) \sim \cos k_x - \cos k_y$. The most interesting question however, is what happens to the system when we tune r to criticality ($r = 0$).

Hertz-Millis approach

The model in the previous section was studied already in the 70's by Hertz [15]. His approach was to integrate out the fermions and derive an effective action for the order parameter. After the evaluation of the fermionic path integral one obtains for the partition function

$$Z = \int \mathcal{D}\phi \det\left(G^{-1}\left[\phi\right]\right) e^{-S_b[\phi]} = \int \mathcal{D}\phi \exp\left(-S_b[\phi] - S_{det}\left[\phi\right]\right), \quad (1.24)$$

where $G^{-1}\left[\phi\right] \sim G_0^{-1} + \lambda\phi$, with G_0 being the free fermion propagator, is the inverse of the fermion Green's function in the presence of a scalar field in real space - we assume $d(k) = 1$ for simplicity. The effective action from the determinant can be formally written as

$$S_{det} = -Tr \log G^{-1}\left[\phi\right]. \qquad (1.25)$$

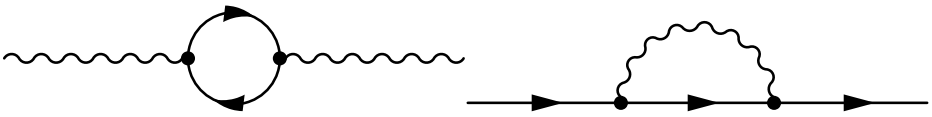

Figure 1.7. One-loop diagrams in the theory of fermions and quantum critical bosons. On the left: boson polarization diagram (Landau damping). On the right: fermion self energy correction.

This quantity has the usual non-local expansion in the coupling constant:

$$Tr\log G^{-1}[\phi] \sim \lambda^2 \int d^{d+1}Xd^{d+1}Y G_0\left(X-Y\right)^2 \phi\left(X\right)\phi\left(Y\right) \tag{1.26}$$

$$+\lambda^3 \int d^{d+1}Xd^{d+1}Yd^{d+1}Z G_0\left(X-Y\right)G_0\left(Y-Z\right)\cdot \tag{1.27}$$

$$\cdot G_0\left(Z-X\right)\phi\left(X\right)\phi\left(Y\right)\phi\left(Z\right)+..., \tag{1.28}$$

involving closed fermion loops with n propagators which result in effective interaction terms in the form of ϕ^n. Here, we used the simplified notation X, Y and Z for the spatial coordinates and imaginary time variables. The assumption of the Hertz-Milis approach is that the terms with $n > 2$ can be neglected in the low frequency limit [15]. Therefore only the one-loop Landau damping diagram (see the left figure in Fig. 1.7) contributes to the boson correction. This has the form $\Pi_{LD} = \gamma\left|\frac{\omega}{k}\right|$ in momentum space [11].

We arrive therefore to the modified boson action after including the one-loop polarization

$$S_{Hertz} = \frac{1}{2}\int \frac{d^dkd\omega}{(2\pi)^{d+1}}\left(k^2+\gamma\left|\frac{\omega}{k}\right|+r\right)|\phi(k,\omega)|^2$$
$$+u\int d^dxd\tau\phi^4(x,\tau).$$

The ω^2 bare kinetic term was neglected based on that for small frequencies the polarization (Landau damping) term dominates.

The quadratic part of this action is invariant under the scaling

$$\vec{x}\to s\vec{x}, \qquad t\to s^{\mathbf{z}}t, \qquad \phi\to\phi s^{1-\frac{d+\mathbf{z}}{2}} \tag{1.29}$$

if we choose $\mathbf{z}$ to be 3. Using this we can deduce that the dimension of the quartic coupling u is $\dim[u] = 1-d$. Therefore, under this scaling the boson self-interaction is irrelevant for $d > 1$.

However, the above argument of Hertz and Millis is questionable in the case of $d = 2$ dimensions. It ignores how the boson-fermion coupling λ scales, and in $d = 2$ it is relevant. In this case ignoring the terms with $n > 2$ from (1.28) is no longer self-consistently justified. Therefore, more careful analysis are needed for the problem. After the next section about large-N methods we will list some newer approaches from the literature. Then in Chapter 3 and 4 we will study the problem in detail in the so-called quenched approximation.

1.2 Non-perturbative methods

$d = 2$ fermions coupled to a QCP is an example of an important physical systems where perturbative methods cannot be applied. Therefore we need to seek alternative ways to deal with such problems. Non-perturbative methods are only exact in case of very special theories. For a reasonably generic case, one needs to use some form of approximation. Therefore, it is important to be familiar with more than one technique and to study the strongly coupled system at hand with several different approaches, since they can shed light to different aspects of the physics.

In this chapter we will give a brief introduction of some of these methods, namely large-N theories, conformal field theory and finally AdS/CFT correspondence (and holography in general). It is far from the complete list of important techniques, however. We must for example mention Wilsonian-, and functional renormalization group approaches, Monte-Carlo simulations and the use of dualities as the most successful ones. Integrability, supersymmetry and localization are also very useful and well studied methods with more limited applicability however than RG techniques.

1.2.1 Large-N theories

When dealing with strongly coupled systems one can not rely on the smallness of the coupling constant. Therefore, to gain insight of the system, it is possible to extend the theory with another parameter and use it as a control parameter. One standard way is to take multiple copies of the fields. This means adding additional degrees of freedom, therefore making the theory more classical than the original one. Large-N extensions have an important role in strongly coupled physics (both in condensed matter,

and high energy physics) on its own and they are crucial ingredients of the AdS/CFT correspondence as well.

Of course this extension can be implemented in different ways. We will review here the vector large-N and the matrix large-N models.

Vector large-N models

For the sake of concreteness, let us consider the following $O(N)$ bosonic model:

$$S = \int d^d x dt \left[-\frac{1}{2}\partial_\mu \phi_i \partial^\mu \phi^i - \frac{m^2}{2}\phi_i \phi^i - \frac{\lambda}{4!}\left(\phi_i \phi^i\right)^2 \right], \tag{1.30}$$

where $i = 1, ..., N$ indicates the different species of bosons. This is called a vector model because ϕ transforms in the fundamental represenation of $O(N)$. The coupling has the (naive) scaling dimension $3 - d$ therefore it is relevant in $d = 2$.

We can introduce a non-dynamical auxilary field σ by writing

$$Z = \int D\phi \exp\left(-S\right) = c \cdot \int D\phi D\sigma \exp\left(-S_{\psi\sigma}\right), \tag{1.31}$$

where c is a field-independent, irrelevant constant. The extended action has the form

$$S_{\psi\sigma} = \int d^d x dt \left[-\frac{1}{2}\partial_\mu \phi_i \partial^\mu \phi^i - \frac{m^2}{2}\phi_i \phi^i + \frac{6}{\lambda}\sigma^2 - \sigma \phi_i \phi^i \right] \tag{1.32}$$

Since in this form the ϕ integrals are gaussian, we can evaluate the path integral explicitly

$$Z = c \cdot \int D\sigma \exp\left(-S_\sigma\right), \tag{1.33}$$

with

$$S_\sigma = N \int d^d x dt \left(\frac{6}{\tilde{\lambda}}\sigma^2 + \frac{i}{2}\log\left(-\Box + m^2 + \sigma\right)\right), \tag{1.34}$$

where we have rescaled the coupling constant $\tilde{\lambda} = N\lambda$.

If N is large, than the path integral is dominated by the saddle point of S_σ and therefore, the theory can be analysed by semi-classical methods. Note, that we would arrive to similar results if we had started with N species of fermions transforming in the fundamental representation of $O(N)$. We have seen therefore that introducing N can help solving the original model.

Matrix large-N models

There is another way how one can introduce multiple similar degrees of freedom: by considering matrix valued fields. This is very natural in high-energy physics. The prime examples of the matrix valued large-N limit is the study of QCD and non-Abelian gauge theories in general. There the meaning of the parameter N there is the number of colors of the quarks (N_c). The theory has a local $SU(N_c)$ symmetry. The matter fields (quarks) transform in the fundamental representation, while the force-carriers (gluons) transforms in the adjoint matrix representation. The ($SU(N)$ invariant) action for the gauge-fields and quarks is

$$S = \int d^d x dt \left[-\frac{1}{4g_{YM}^2} Tr\left(F_{\mu\nu}F^{\mu\nu} + \bar{\psi}\gamma^\mu D_\mu \psi\right)\right], \tag{1.35}$$

where $D_\mu = \partial_\mu - iqA_\mu$ and the non-abelian field strength can be deduced from the matrix valued gauge connection

$$F_{\mu\nu} = \partial_\mu A_\nu - \partial_\nu A_\mu - i\left[A_\mu, A_\nu\right]. \tag{1.36}$$

The matrix form of the vector potential can be written as $A_\mu = A_\mu^a T_a$ with T_a being the generators of $SU(N)$.

However, the notion of matrix large-N limit is more general and can be applied to scalar field theories as well. Let's consider therefore the "ϕ^4 type theory":

$$S = \frac{1}{g^2}\int d^d x dt \left[Tr\left(-\partial_\mu \Phi^+ \partial^\mu \Phi - m^2 \Phi^+\Phi\right) - \frac{1}{4!} Tr\left(\Phi^+\Phi\Phi^+\Phi\right)\right]. \tag{1.37}$$

The dynamics of this theory is different from the vector large-N case. First of all, note that the single trace structure of the interaction $Tr\left(\Phi^+\Phi\Phi^+\Phi\right)$ prevent us to introduce an auxilary field in the form of (1.32). If we had a double trace type of interaction $\left(Tr\left(\Phi^+\Phi\right) Tr\left(\Phi^+\Phi\right)\right)$ which is a different way of generalizing, the method of the previous section would apply. However, as we will see there is a notion of classicalisation here as well. For simplicity we will consider the symmetry group to be $U(N)$. As for gauge theories, Φ transforms in the adjoint representation $\Phi \to U^{-1}\Phi U$.

The interesting limit here was first introduced by t'Hooft [12]. He studied the special limit where one keeps the combination $\lambda = g^2 N$ fixed while taking $N \to \infty$. To determine the N dependence of Feynman diagrams it is very useful to introduce the so-called double line notation where for the

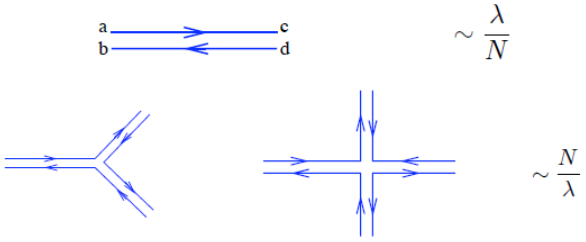

Figure 1.8. The propagator and verticies in a matrix theory with double line notation. The propagator scales as $1/N$, while each vertices as N^1 (from [45]).

propagators we draw two lines representing the two indices of the field Φ^i_j (see in Fig. 1.8). In this convention we can directly read off from (1.37) what is the N dependence of a diagram. A propagator contributes with $g^2 \sim \lambda/N$, while a vertex is proportional to N/λ. Furthermore, every index loop comes with an additional factor of N. We see therefore that the N dependence of a diagram is N^{V-P+L}, where V, P and L stand for the number of vertices, propagators and index loops respectively.

Note, that we can attach a topological meaning to this result. To demonstrate this, we consider vacuum diagrams. Let associate to each diagram a triangulation of a two dimensional manifold (as in Fig. 1.9) where the propagators are the edges, and the interior of each index loops are the faces. In this construction the exponent of the N dependence is $F - E + V = \chi = 2 - 2h$ (F, E and V are being the faces, edges and vertices of the triangulation respectively), which is the Euler characteristic of the triangulation with h the number of holes. $\chi = 2$ ($h = 0$) corresponds to a triangulation of a sphere, where $h \neq 0$ corresponds to a triangulation of a torus with h holes. Therefore, the more complex the topology of a diagram, the more subleading it is in terms of N.

The interesting quantities are correlation functions of $U(N)$ invariant ("gauge-invariant") operators. If the symmetry is gauged then the physical observables are only single- and multitrace combination of the elementary fields: i.e. $Tr\left((\Phi^+\Phi)^n\right)$, $Tr\left(\Phi^+\Phi\right) Tr\left(\Phi^+\Phi\right)$. If the symmetry is not gauged then the physical Hilbert space is larger but we will still call these operators gauge-invariant and the consequences of the large-N limit will be identical.

Let's first examine the two-point function of a single trace operator (we take $\mathcal{O}_4 = Tr\left(\Phi^+\Phi\Phi^+\Phi\right)$ for concreteness). We can write it as a

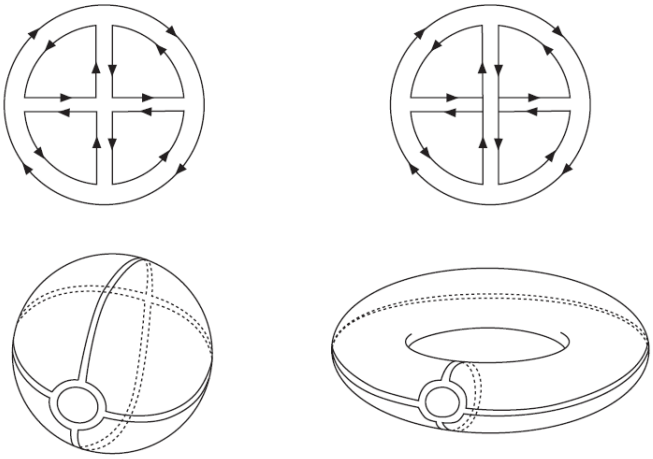

Figure 1.9. Two vacuum diagram in a matrix theory (with both cubic and quartic coupling). The left diagrams scales as N^2, while the right as N^0. This fact is also manifested in the fact that with the left diagram it is possible to tringulate a sphere while the right one only can be drawn to a torus (from [45]).

sum of the disconnected and connected component.

$$\langle \mathcal{O}_4 \mathcal{O}_4 \rangle = \langle \mathcal{O}_4 \rangle \langle \mathcal{O}_4 \rangle + \langle \mathcal{O}_4 \mathcal{O}_4 \rangle_c \tag{1.38}$$

Using the double line notation it is easy to see that while both the connected and the disconnected piece have the same number of vertices and propagators (at leading order), the connected one has less index loops (see in Fig. 1.10). Therefore if $\langle \mathcal{O}_4 \rangle$ is non-vanishing, the two-pont function is dominated by the disconnected component. However, this expectation value is often zero (in a CFT it is always vanishing) and the leading behavior of the correlation function is non-trivial. The connected component scales as $\langle \mathcal{O}_4 \mathcal{O}_4 \rangle_c \sim N^2$ and therefore it become infinite in the $N \to \infty$ limit. To avoid this, one usually renormalizes the single-trace operators of the theory such that its connected two-point function does not scale with N (for example $\frac{1}{N}\mathcal{O}_4 = \tilde{\mathcal{O}}_4$). After this normalization there is no additional freedom in the definition of multi-trace operators.

In similar way we can show that the higher-point functions always factorizes. To illustrate this, let us consider the four point function of (the already properly normalized operator) $\mathcal{O}_2 = \frac{1}{N} Tr\,(\Phi^+ \Phi)$:

$$\langle \mathcal{O}_2 \mathcal{O}_2 \mathcal{O}_2 \mathcal{O}_2 \rangle = \langle \mathcal{O}_2 \mathcal{O}_2 \mathcal{O}_2 \mathcal{O}_2 \rangle_c + \langle \mathcal{O}_2 \mathcal{O}_2 \rangle_c \langle \mathcal{O}_2 \mathcal{O}_2 \rangle_c + ... \tag{1.39}$$

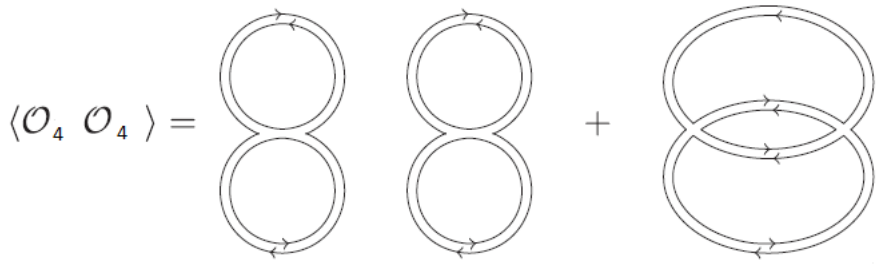

Figure 1.10. The two-point function of a single-trace operator can be split into a disconnected and a connected piece (from [8]). Both type of diagrams have the same number of propagators and vertices but the connected diagrams have less index loops, therefore they are subleading in N.

The disconnected piece (which can no longer vanish under any circumstances) scales as N^0 but the connected one goes to zero in the large-N limit.

$$\langle \mathcal{O}_2 \mathcal{O}_2 \mathcal{O}_2 \mathcal{O}_2 \rangle_c \sim N^{-2} \to 0. \tag{1.40}$$

As we will see in the forthcoming sections, the vanishing of the non-trivial component of higher point functions of single-trace operators in the large-N limit has important consequences in AdS/CFT as well.

Large-N approaches to quantum critical fermions

Large-N type approaches are important in condensed matter physics as well. As we have seen the quantum critical fermion model introduced in Section 1.1.4 in $d = 2$ dimensions is strongly coupled. To analyse the system (at least qualitatively) a usual approach is to generalize the theory and introduce multiple species of bosons (N_b) and fermions (N_f). One then can hope for a non-perturbative solution in a certain limit (typically large-N limit).

Since we have two parameters (N_b, N_f), there are in principle a lot of possible extension of the theory.

- One approach is to take the vector large-N_f limit while keeping $\lambda\sqrt{N_f}$ fixed [20, 21, 24]. In this case at one-loop the Landau damping (left of Fig. 1.7) or boson polarization diagram is $\mathcal{O}(N_f^0)$ but the fermion self energy correction (right of Fig. 1.7) is $\mathcal{O}(N_f^{-1})$. This limit is extensively studied by renormalization group methods up to four loops. However as pointed out in [24] it is questionable

whether it is a controllable expansion is since there are infinitely many diagrams with the same power of N_f.

- It is also possible to consider large N matrix theories with $SU(N)$ symmetry [26–29]. In this case the fermions transform in the fundamental representation (therefore there are $N_f = N$ number of them), while the bosons transform in the adjoint representation (so there are $N_b = N^2$ of them). The scaling of the coupling is chosen to be such that $\lambda\sqrt{N}$ is fixed similarly to the previous case (and the t'Hooft limit). Since $N_b \gg N_f$ the Landau damping is subleading compare to the fermion self energy. In the original problem ($N_f = N_b = 1$), the Landau damping believed to be an important effect at low frequencies. With this limit therefore one can qualitatively study the physics above this scale. At higher order for $N_f \to \infty$ the so-called rainbow diagrams give the dominant contributions to the self energy as we will explain in Chapter 3.

1.2.2 Conformal field theories

We now turn our attention to conformal field theories which are another type of important non-perturbative systems where we have (somewhat better) mathematical control. We have seen that studying critical points are crucial in understanding strongly correlated systems. In the Wilsonian language, at a general point in the RG flow one can compute the β function of the coupling (for example with momentum decimation)

$$\beta(g) = \mu \frac{\partial g}{\partial \mu} \tag{1.41}$$

When this function vanishes $\beta(g^\star) = 0$ for some values (g^*) of the coupling, the renormalization group flow ends in fixed point and the system has the scaling symmetries (1.16). If the dynamical critical exponent is unity, i.e. time and spatial dimensions scales at the same way (the system is "relativistic"), these symmetries enhanced with the so-called special conformal symmetry and the system is conformally invariant. In most of the condensed matter applications, the vanishing β function is at only a special value of the coupling ($g^\star$) so the critical point is isolated. We will see however, that in certain supersymmetric theories it is possible, that the β function vanishes for all values of the coupling.

This large symmetry group offers us another way to study strongly correlated systems non-perturbatively. $1+1$ dimensional theories turned

out to be special in such a way that the symmetry group is even larger than in $d > 1$ spatial dimensions. In some cases (in the so-called minimal models and Liouville theory), this imposes such large constraints on the correlation functions that the theory can be solved exactly via the conformal bootstrap. This program was an active area of reasearch in the 70's and 80's and recently it has received renewed attention with systems in higher dimensions. We will focus here on $d > 1$, and study features which are generic so we do not need to restrict ourselves to $1 + 1$ dimension.

Since the strategy with these systems is to squeze out as much physics as possible from the symmetry properties we should start with the algebra. Let us study therefore the properties of this symmetry group (in $d > 1$) which is realized in $\mathbf{z} = 1$ critical points. For concreteness we will focus here on the Euclidean case. In the following table we summarize the (finite) coordinate transformations and its generators:

Transformation	Generator
Translation $x'^{\mu} = x^{\mu} + a^{\mu}$	$P_{\mu} = -i\partial_{\mu}$
Rotation $x'^{\mu} = M^{\mu}_{\nu} x^{\nu}$	$L_{\mu\nu} = i\left(x_{\mu}\partial_{\nu} - x_{\nu}\partial_{\mu}\right)$
Dilatation $x'^{\mu} = s x^{\mu}$	$D = -i x^{\mu}\partial_{\mu}$
Special Conformal Transformation $x'^{\mu} = \frac{x^{\mu} - b^{\mu} x^2}{1 - 2b\cdot x + b^2 x^2}$	$K_{\mu} = -i\left(2x_{\mu}x^{\nu}\partial_{\nu} - x^2\partial_{\mu}\right)$

These generators satisfy the following algebra

$$[D, P_{\mu}] = iP_{\mu} \tag{1.42}$$

$$[D, K_{\mu}] = -iK_{\mu} \tag{1.43}$$

$$[K_{\mu}, P_{\nu}] = 2i\left(\eta_{\mu\nu}D - L_{\mu\nu}\right) \tag{1.44}$$

$$[K_{\rho}, L_{\mu\nu}] = i\left(\eta_{\rho\mu}K_{\nu} - \eta_{\rho\nu}K_{\mu}\right) \tag{1.45}$$

$$[P_{\rho}, L_{\mu\nu}] = i\left(\eta_{\rho\mu}P_{\nu} - \eta_{\rho\nu}P_{\mu}\right). \tag{1.46}$$

Here $\eta_{\mu\nu} = diag(1, ..., 1)$ is the Euclidean metric.

This group is called the conformal group and denoted by $SO(d+2, 1)$. It turns out that it is isomorphic to the group of Lorentz transformations in $d + 3$ dimensions. Note the somewhat unconventional notation for the number of dimensions. Although we are in Euclidean signature, we still denote the number of spacetime dimensions $d + 1$ (d spatial dimensions and an imaginary time dimension) to keep our notation consistent with

the previous sections. In other words the conformal group in certain dimensions is always isometric to the Lorentz algebra with two extra dimensions (one space-like and one time-like). In the same manner, if our CFT has Lorentzian signature, then its symmetry group is isometric to $SO(d+1,2)$.

As in a (continuum) general quantum field theory one classifies states with respect to the symmetry elements of the Poincare group (translations and rotations), it is possible to introduce extra quantum numbers with the additional symmetries. Under translation and rotations a scalar operator transforms as

$$[P_{\mu,}\mathcal{O}(x)] = i\partial_\mu \mathcal{O}(x), \tag{1.47}$$

$$[L_{\mu\nu}, \mathcal{O}(x)] = -i\left(x_\mu \partial_\nu - x_\nu \partial_\mu\right)\mathcal{O}(x). \tag{1.48}$$

In a CFT the most important quantum number is the scaling dimension of the operator. A trivial example of a CFT is a massless, free scalar field. In this case the fundamental field ϕ is a primary operator (for $d > 1$) and its 'naive' dimension (the one we can deduce from the Lagrangian) and 'true' scaling dimension (the one appears in the propagator) are the same. In an interacting theory, this is not the case however. Therefore we will always mean the latter by scaling dimension. On the other hand there are special operators for which the scaling dimension does not renormalize even in a strongly interacting theory. In some examples this phenomenon is highly specific to the concrete theory i.e. in supersymmetric theories where the protection is due to supersymmetry. However, it is generic that the energy momentum tensor $T_{\mu\nu}$ and a global current J_μ possess the 'naive' dimensions due to their conservation laws. In d dimensions it means $\Delta_T = d+1$, $\Delta_J = d$.

If the scaling dimension of $\mathcal{O}$ is Δ at the fixed point, its commutator with the dilatation operator is

$$[D, \mathcal{O}(0)] = i\Delta\mathcal{O}(0). \tag{1.49}$$

We have one more generator: the one of the special conformal transformations. By definition, we call $\mathcal{O}$ a primary operator if its satisfies the commutation relation

$$[K_\mu, \mathcal{O}(0)] = 0. \tag{1.50}$$

There are also operators which have definite scaling quantum numbers but are not primaries. For example, if $\mathcal{O}$ is primary, then its derivatives

(for example $\partial_\nu \mathcal{O}$) are not. To see this, first we write the commutation relations (1.49), (1.50) for a general point x:

$$[D, \mathcal{O}(x)] = i\left(\Delta + x^\mu \partial_\mu\right) \mathcal{O}(x), \tag{1.51}$$

$$[K_\mu, \mathcal{O}(x)] = i\left(2x_\mu \Delta + 2x_\mu \left(x^\rho \partial_\rho\right) - x^2 \partial_\mu\right) \mathcal{O}(x). \tag{1.52}$$

If we differentiate these two properties, we can see that $\partial_\nu \mathcal{O}$ satisfies (1.49) with $\Delta_{\partial\mathcal{O}} = \Delta_\mathcal{O} + 1$. However, the commutator with K_μ is not of the form of (1.50)

$$[K_\mu, \partial_\nu \mathcal{O}(0)] = 2i\eta_{\mu\nu} \Delta \mathcal{O}(0) \neq 0. \tag{1.53}$$

Derivatives of a primary are called descendants and together with the primary operators they span the space of possible local operators. An important theorem of the field of conformal field theories is that states in the theory are in one-to-one correspondance with local operators. Therefore primary and descendant states also span the Hilbert space of the system.

The conformal symmetry has large implications for the form of correlation function in a CFT. We can concentrate on correlation function of primary operators, since every other quantities follows from them. For a primary $\mathcal{O}_1$ and $\mathcal{O}_2$ with conformal dimension Δ_1 and Δ_2 the two point function has the scaling form

$$\langle \mathcal{O}_1(x) \mathcal{O}_2(y) \rangle = \frac{1}{|x-y|^{2\Delta_1}} \delta_{\Delta_1, \Delta_2}. \tag{1.54}$$

The form of the three-point function of primary operators are also fixed by the conformal symmetry. Let us consider the $\mathcal{O}_1$, $\mathcal{O}_2$ and $\mathcal{O}_3$ with dimensions Δ_1, Δ_2, Δ_3. It turns out that the combinations

$$\alpha_{ijk} = \frac{\Delta_i + \Delta_j - \Delta_k}{2}, \tag{1.55}$$

where $i, j, k = 1, 2, 3$, determines the powers in the form of the three-point function in the following way:

$$\langle \mathcal{O}_1(x_1) \mathcal{O}_2(x_2) \mathcal{O}_3(x_3) \rangle = \frac{\lambda_{123}}{(x_{12})^{2\alpha_{123}} (x_{13})^{2\alpha_{132}} (x_{23})^{2\alpha_{231}}} \tag{1.56}$$

with $x_{ij} = x_i - x_j$.

Finally, for a four point function, conformal invariance cannot fix the form of momentum dependence completely, but it still restricts it. Taking

only one type of operator with conformal dimension Δ one can arrive to the formula

$$\langle \mathcal{O}(x_1)\,\mathcal{O}(x_2)\mathcal{O}(x_3)\,\mathcal{O}(x_4)\rangle = \frac{1}{(x_{12})^{2\Delta}(x_{34})^{2\Delta}} F(u,v), \tag{1.57}$$

where F is an arbitrary function which depends in the conformal cross ratios

$$u = \frac{x_{12}^2 x_{34}^2}{x_{13}^2 x_{24}^2} \tag{1.58}$$

$$v = \frac{x_{14}^2 x_{23}^2}{x_{13}^2 x_{24}^2}. \tag{1.59}$$

Large-N CFTs and generalized free field theory

So far we have introduced two type of systems in which one can use non-perturbative methods: large-N theories and conformal field theories. In the former one has a large number of degrees of freedom per spacetime point which supress 'quantumness' compare to system with a few degrees of freedom. In the latter one can use the large symmetry group to gain information about the correlation functions.

A natural question arises: what happens if we combine these two properties and consider large-N CFTs. We will focus on matrix type theories since we have seen that they are richer in the large-N limit. These systems first appeared in the study of supersymmetric gauge theories where due to supersymmtery (another symmetry which we can use for studying strongly coupled physics) one can analyze RG flows and fixed point structures non-perturbatively. We will review $\mathcal{N} = 4$ super Yang-Mills theory, the most symmetric field theory that exists in physics in Section 1.3. This is a very special system originally studied by string theorists and mathematical physicsis but it has become relevant in a much wider range of applications since the discovery of AdS/CFT and holography.

Let us put together what we know about correlation functions in a large-N CFT. The most important objects here are single trace primary operators. From large-N considerations we have seen that the higher-point correlation functions at leading order are gaussian. The two-point function, however, is not constrained and has the form of (1.54) with non-trivial scaling dimensions Δ. Because of these properties (non-trivial two-point but gaussian higher-point correlator) at infinite N we call these theories generalized free field (or generalized mean field) theories.

We also know more about the Hilbert space structure of the CFT at large N. If $\mathcal{O}$ is a single trace primary with conformal dimension Δ, then $\mathcal{O}^2$ is a multitrace primary with dimension 2Δ. Taking another example, it can be shown by differentiating (1.52) that $\partial_\nu \mathcal{O}\mathcal{O} - \mathcal{O}\partial_\nu \mathcal{O}$ is also primary with dimension $2\Delta + 1$. In general we can construct a whole new tower of primaries by sandwiching differential operators between two copies of $\mathcal{O}$ with the schematic form of

$$[\mathcal{O}\mathcal{O}]_{n,l} \sim \mathcal{O} \left(\overleftrightarrow{\partial}\right)^{2n} \overleftrightarrow{\partial}_{\mu_1} ... \overleftrightarrow{\partial}_{\mu_n} \mathcal{O}. \tag{1.60}$$

Due to large-N its dimension is the naive $\Delta(n, l) = 2\Delta + 2n + l$. However at finite N this gets corrected leading to an anomalous dimension $\gamma(n, l)$. These operators will play a crucial role in the interpretation of the results in Chapter 2.

1.3 AdS/CFT

In this section we will introduce probably the most exciting discovery of theoretical physics which connects many research areas. AdS/CFT (or holographic duality in general) is rooted in string theory. However, to motivate its results we will use the knowledge we introduced in the previous sections. AdS/CFT states the equivalence between certain quantum field theories in D dimensional flat space-time and quantum gravity in curved background in one dimension higher. Therefore from a fundamental physics point of view it gives us the possibility to study quantum gravity from perspective we are more familiar.

The AdS/CFT correspondence, however, has a very important feature which makes it even more remarkable and interesting for a wider range of audience. It is a weak-strong duality in the sense that when the gravity side is weakly coupled, the field theory is strongly coupled. This means that by studying weakly coupled gravitational systems we can deduce properties of strongly correlated ones.

In practice there are limitations of this method. Most notably, we understand this duality well for matrix large-N theories only. Moreover, in the cases where we do know the two sides in details, the field theories are close to QCD but very different from other areas of physics such as the condensed matter systems. However, even if we do not know the exact Lagrangian of the field theory (which in the case of strong coupling are

much less informative than in perturbative physics) this method can be very insightful about universal features.

Let us summarize the content of the original correspondance found in 1997 by Juan Maldacena [5]. The field theory consist $\mathcal{N} = 4$ super Yang-Mills theory in four space-time dimensions. $\mathcal{N}$ denote the number of generators of supersymmetry the system has. In flat space this corresponds to the largest supersymmetry group. This is actually so restrictive that it determines not only the total field content but also the interaction structure of the theory. The fields are:

- A_μ non-Abelian gauge field of some gauge group (say $SU(N)$)
- Four species of fermions ψ^a, where $a = 1, .., 4$ is the flavor index
- Six scalar fields X_i $i = 1, ..., 6$

The Lagrangian of the theory has the form

$$\mathcal{L}_{SYM} = -\frac{1}{4g_{YM}^2} Tr \left[F_{\mu\nu}F^{\mu\nu} + D_\mu X^i D^\mu X^i + \overline{\psi}^i \gamma^\mu D_\mu \psi^i + \left[X^i, X^j\right]^2 + ... \right], \tag{1.61}$$

where ... indicates Yukawa type of interactions between the scalars and fermions. These are necessary for supersymmetry.

This theory seems very complicated in terms of field content and interactions. However, this complicated structure results a very important simple observation. This theory has a vanishing β function for all value of g_{YM}. This feature has such important consequences in the properties of physical observables such as scattering amplitudes that it is reasonable to say that actually $\mathcal{N} = 4$ SYM is one of the simplest quantum field theory [40].

Maldacena conjectured that the theory above is equivalent to type IIB string theory living in the spacetime of $AdS_5 \times S_5$. Here S_5 denotes the five-dimensional sphere and AdS_5 is an Anti-de-Sitter spacetime which properties will be discussed shortly. This theory can be characterised by a number of parameters. In string theory we have a length parameter which describes the tension of the string (l_s), and a coupling constant g_s which is the strength of the interaction between different strings. Additionally, the AdS_5 background has a length scale L. The connection of the parameters between the two sides are:

$$4\pi g_s = g_{YM}^2 = \frac{\lambda}{N}, \tag{1.62}$$

$$\frac{L}{l_s} = \lambda^{1/4}, \tag{1.63}$$

where $\lambda = g_{YM}^2 N$ is the t'Hooft coupling of the $\mathcal{N} = 4$ SYM theory.

This immediately shows two limits which can be taken in order to obtain a tracktable duality. First of all the large-N limit $\lambda \ll N$ suppresses quantum gravity effects (which corresponds to small g_s). Also, to work with only supergravity fields (low energy mode of the string) instead of the entire string spectrum then we can take L/l_s large. This corresponds to the large t'Hooft coupling limit in the field theory. Note, that since we do not have a well established theory of non-perturbative strings, considering large N is crucial. It is, however, in principle possible to move away from the supergravity limit.

This prototype of holographic duality is very well tested in details. We will see that scaling dimensions in the field theory side correspond to the spectrum in the string theory. In the strongly coupled $\mathcal{N} = 4$ SYM theory there are special single trace operators, whose scaling dimensions can be determined with the help of integrability. These have been compared to the weakly coupled string theory spectrum and a perfect agreement was found [39].

1.3.1 AdS spacetime

To present the more general content of the correspondence let us study the structure of AdS spacetime. Specifically we will present two useful sets of coordinates: the global coordinates and the Poincare patch. In the former, the symmetries of the system are more manifest and it is useful when one is studying general features of the duality. The latter, however, is used more often in practical calculations and applications.

First, however let us make some coordinate independent remarks on AdS. This spacetime is a solution of the vacuum Einstein's equation with negative cosmological constant

$$R_{\mu\nu} - \frac{1}{2} g_{\mu\nu} \left(R - 2\Lambda\right) = 0. \tag{1.64}$$

By taking the trace of the equation (in Lorentzian signature) one can see that the curvature (Ricci scalar) is constant throughout the entire spacetime

$$R = \frac{2D}{D-2}\Lambda. \tag{1.65}$$

AdS has constant negative curvature and therefore it can be obtained by embedding a hyperboloid in a $D+1$ dimensional flat space with signature $(-,-,+,+,...)$

$$X_0^2 + X_{d+2}^2 - \Sigma_{i=1}^{d+1} X_i^2 = L^2, \tag{1.66}$$

where $d = D-2$ is the number of spacelike directions in our original spacetime and the AdS radius L is related to the Ricci curvature by

$$L^2 = -\frac{D(D-1)}{R}. \tag{1.67}$$

The solution of the constraint (1.66) can be parametrized in the following way

$$\begin{aligned} X_0 &= L\frac{\cos\tau}{\cos\rho}, \\ X_{d+2} &= L\frac{\sin\tau}{\cos\rho}, \\ X_i &= Lu_i \tan\rho. \end{aligned} \tag{1.68}$$

Here $\tau \in (-\infty, \infty)$ is a timelike coordinate, $\rho \in [0, \pi/2)$ is a spacelike compact coordinate and u_i $i = 1, ..., d+1$ are the component of a unitvector. With these coordinates the AdS metric can be deduced from the induced metric formula $g_{ab} = \partial_a X^\mu \partial_b X^\nu \eta^{(2)}_{\mu\nu}$, where $\eta^{(2)}_{\mu\nu}$ is the flat space metric with signature (-,-,+,+,...). The result is

$$ds^2 = \frac{L^2}{\cos^2\rho}\left(-dt^2 + d\rho^2 + \sin^2\rho d\Omega_d^2\right). \tag{1.69}$$

This shows that AdS is conformally equivalent to a cylinder as in Fig. 1.11. The global time coordinate runs parralel to the axis of the cylinder while ρ is the radial coordinate. The conformal boundary is at $\rho = \pi/2$. Note that although the coordinate ρ terminates at a finite value, the boundary is still infinitely far away from an arbitrary point with $\rho < \pi/2$ due to the conformal $1/\cos^2\rho$ factor in the metric.

An alternative way of parametrizing (part of) AdS space is with the

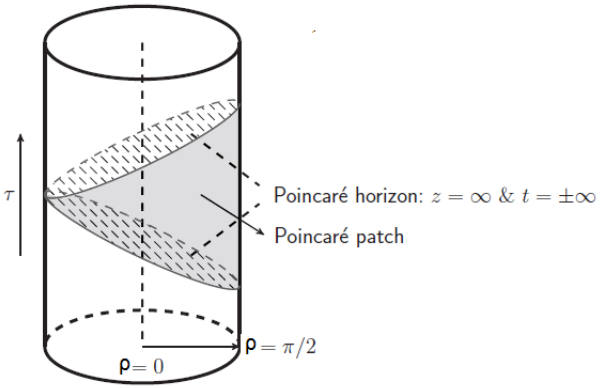

Figure 1.11. AdS spacetime and its parametrization with global coordinates and Poincare Patch coordinates in lorentzian signature. The shaded area indicates the region what the Poincare Patch covers (from [8]).

Poincare coordinates $(t, \vec{x}, z)$:

$$\begin{aligned} X_0 &= \frac{z}{2}\left(1 + \frac{L^2 + \vec{x}^2 - t^2}{z^2}\right) \\ X_{d+2} &= \frac{L}{z}t \\ X_{i<d+1} &= \frac{L}{z}x_i \\ X_{d+1} &= \frac{z}{2}\left(-1 + \frac{L^2 - \vec{x}^2 + t^2}{z^2}\right), \end{aligned} \tag{1.70}$$

where $z \in (0, \infty)$ is the radial coordinate and $x_i, t \in (-\infty, \infty)$ are very similar to Cartesian coordinates in flat space. With these coordinates the metric takes the form

$$ds^2 = \frac{L^2}{z^2}\left(-dt^2 + dz^2 + \Sigma_{i=1}^{d} dx_i^2\right). \tag{1.71}$$

An often used form of the metric (1.71) uses instead of z the radial coordinate we use $r = L^2/z$:

$$ds^2 = \frac{r^2}{L^2}\left(-dt^2 + d\vec{x}^2\right) + \frac{L^2}{r^2}dr^2. \tag{1.72}$$

In this parametrization, $r = \infty$ is the position of the boundary.

It is important to note that in Lorentzian signature the Poincare patch only covers a part of global AdS. This can be seen by expressing t from (1.68) and (1.70)

$$t = L\frac{\sin\tau}{\cos\tau - u_{d+1}\sin\rho}.$$

The limit $t \to \pm\infty$ corresponds to the case where the denominator vanishes which happens at finite value of τ.

The Euclidean version of the metric can be obtained by flipping the sign of the timelike coordinate. The relation between the embedding coordinates and the global coordinates are (1.68) with $\sin\tau \to \sinh\tau$ and $\cos\tau \to \cosh\tau$. Note also, that in this case the Poncare Patch covers the whole AdS spacetime.

AdS spacetime has a boundary related to the limit $\rho \to \pi/2$. This limit can be approached however in different ways. If we let $\rho \to \pi/2$ by keeping the other global coordinates (τ, Ω) fixed, we define a boundary surface with the topology of a sphere S_{D-1}. On the other hand, if we let the Poincare coordinate $z \to 0$ we arrive to a surface with flat metric and topology. Of course this later scaling can be also done in the global coordinates. To achive this, in the case of Euclidean signature we have to take the limit $\epsilon \to 0$

$$\rho = \frac{\pi}{2} - \epsilon e^{-\tau}. \tag{1.73}$$

In this case, the metric in the boundary surface is

$$ds^2 = \frac{1}{\cos^2\rho}\left(d\tau^2 + \sin^2\rho d\Omega^2\right) \to e^{2\tau}\left(d\tau^2 + d\Omega^2\right) = dr^2 + r^2 d\Omega^2, \tag{1.74}$$

where $r = e^{\tau}$. We obtain therefore the flat metric in polar coordinates. The most important property of AdS_D spacetime is that its isometry group (in Euclidean signature) is $SO(D,1)$. Therefore, the isometries of AdS are in one-to-one correspondence with the symmetries of a CFT in lower dimensions.

1.3.2 The dictionary

In the previous section we have already mentioned that the symmetries of a CFT in flat space and the isometries of curved AdS space-time are identical. This indicates that we have two different descriptions of the same physics. We now turn to the detailed dictionary between the two theories.

Since the Hilbert space of the two system is identical according to the conjecture, their partition function must be equal:

$$Z_{CFT}(N) = Z_{AdS}(N) = \int \mathcal{D}\phi \exp\left(iN^2 S_{AdS}\left(\phi\right)\right). \tag{1.75}$$

On the right-hand side ϕ is the set of all fields living in AdS. We explicitly indicated the N dependence in the exponent. In case of large-N we can approximate the path integral by its saddle point. In fact, it is the only limit where our correspondence is tractable.

The most important dictionary element is the rule to compute correlation functions for the field theory. This is called the Gubser-Klebanov-Polyakov-Witten (GKPW) rule after its inventors [6, 7]. Strictly speaking, this has a conjectural status (as everything else in holography) but it passed numerous non-trivial tests.

First, let us recall that a correlation function in field theory can be calculated by modifying the Lagrangian by adding source terms in the form:

$$\mathcal{L}(x) \to \mathcal{L}(x) - i\sum_i j_i(x)\mathcal{O}_i(x). \tag{1.76}$$

Having done this, one can compute any correlation function by first calculating the log of the partition function of the theory in the presence of the external sources $Z\left[J_i\right]$ and using the formula:

$$\left\langle \mathcal{O}_1\left(x_1\right)\mathcal{O}_2\left(x_2\right)...\mathcal{O}_n\left(x_n\right)\right\rangle = \prod_{i=1}^{n}\frac{\delta}{\delta j_i\left(x_i\right)}\log Z_{CFT}|_{j=0}. \tag{1.77}$$

The question is how to generalize (1.75), or in other words what the sources on the field theory side correspond to in the gravitational theory. The answer turns out to be somewhat counterintuitive: the sources in the field theory translate to a boundary condition for the fields ϕ in AdS. (1.75) generalizes to

$$Z_{CFT}[j] = \langle e^{\int d^{d+1}xj(x)\mathcal{O}(x)}\rangle_{CFT} = \int \mathcal{D}\phi e^{iN^2 S_{AdS}(\phi(x,r))|_{\phi(x,r=\infty)=j(x)}}, \tag{1.78}$$

where r is the radial coordinate with the property that the boundary is at $r=\infty$. As we discussed, in practice we choose N to be large so that we can approximate (1.78)

$$\int \mathcal{D}\phi e^{iN^2 S_{AdS}(\phi(x,r))|_{\phi(x,r=\infty)=j(x)}} \sim e^{iN^2 S_{on-shell}(\phi(x,r))|_{\phi(x,r=\infty)=j(x)}}. \tag{1.79}$$

To calculate a specific correlation function we need to go through the following steps. First we solve the classical equation of motions with general boundary conditions $\phi\left(\partial_{Bulk}\right)$. Then, this is substituted into S_{AdS} to obtain the on-shell action. Finally, according to (1.77), we differentiate (1.79) with respect to the boundary conditions.

There is one important detail in the above procedure which we did not touch upon. By considering the integral of the whole spacetime, the on-shell action $S_{on-shell}$ turns out to be infinite. To cure this divergence, we need to regularize our theory by cutting off the spacetime and place the boundary at a finite $r_{cutoff} = \epsilon^{-1}$ radius (instead having it at infinity). This property of the gravitational theory is actually not a surprise. The dual quantum field theory (as the majority of interacting QFTs) is expected to have UV divergencies. These divergences can be shown to translate to the infinite bulk action due to the infinite volume of AdS. This is one of the clearest examples of an aspect of AdS/CFT known as UV-IR duality because the cutoff r_{cutoff} is an IR regulator in the bullk. As in normal QFT the choice of regularization can be fixed by adding counterterms to the bulk action. To address these questions, a systematic treatment for a general class of spacetimes was developed under the name of holographic renormalization [42].

As the most elementary example let us take a massive scalar field in euclidean AdS with the action:

$$S = \frac{1}{2}\int d^{d+1}xdr\sqrt{g}\left(\partial_\mu\phi\partial^\mu\phi + m^2\phi^2\right), \tag{1.80}$$

By applying the GPKW rule to this case one obtains for the (boundary) 2-point function:

$$\left\langle \mathcal{O}\left(\vec{x}_1\right)\mathcal{O}\left(\vec{x}_2\right)\right\rangle = \frac{C_1}{\left|\vec{x}_1 - \vec{x}_2\right|^{2\Delta}}, \tag{1.81}$$

where C_1 is a constant and the power Δ denotes the combination

$$\Delta = \frac{d+1}{2} + \sqrt{\frac{(d+1)^2}{4} + m^2L^2}. \tag{1.82}$$

We can see that the result (1.81) has the scaling form (1.54) indicating that the dual field theory is a CFT.

To further verify this we can check the three-point function. For this, we need to introduce an interaction term in the bulk action:

$$S_{int} = \int d^{d+2}x\sqrt{g}\left(\frac{\lambda}{3!}\phi^3\right). \tag{1.83}$$

The result of the holographic calculation has the form:

$$\langle \mathcal{O}(\vec{x}_1)\,\mathcal{O}(\vec{x}_2)\,\mathcal{O}(\vec{x}_3)\rangle = \frac{C_2}{|\vec{x}_1-\vec{x}_2|^{\Delta}\,|\vec{x}_1-\vec{x}_3|^{\Delta}\,|\vec{x}_2-\vec{x}_3|^{\Delta}}, \tag{1.84}$$

with the coefficient C_2 being proportional to the coupling λ. This is also consistent with the CFT result (1.56). The relations (1.82) and (1.84) are crucial results. They tell us how to relate the conformal dimensions and OPE coefficients of an operator (which are boundary data) to the mass and coupling parameters in the bulk. It is also important to note that the above form of correlation functions implies that the operators in the CFT which have dual fields in the bulk are single trace primary operators.

We will shortly see that the GPKW rule extends to correlation functions of operators with more non-trivial index structure, such as $\langle T_{ij}(\vec{x}_1)\,J_k(\vec{x}_2)\,J_l(\vec{x}_2)\rangle$ (with T and J being the energy-momentum tensor and the conserved current respectively). These were computed in e.g. [41]. Again, the conformal symmetry allows one to determine the complex structure of this correlator and the holographic result is in perfect agreement.

As we mentioned, the GPKW rule is a bit counterintuitive. In many cases, it effectively reduces to a simpler prescription that gives the same results. Let us consider the correlation function of a scalar living in AdS spacetime with the action (1.80) (plus possible interactions such as (1.83)) $\langle \prec(\vec{x}_1,r_1)\,...\prec(\vec{x}_n,r_n)\rangle_{AdS}$. For example, the two point function (called also the bulk-to-bulk propagator) is the Green's function of the free equation of motion in AdS

$$\left(\nabla^{\mu}\nabla_{\mu}-m^2\right)\mathcal{G}(x_1,r_1;x_2,r_2) = \frac{1}{\sqrt{g}}\delta^{d+1}(x_1-x_2)\,\delta(r_1-r_2)\,. \tag{1.85}$$

We can obtain a correlation function in the boundary theory by considering the corresponding bulk n-point function and taking the radial coordinates r to the boundary while rescaling the expression it in the following way:

$$\langle \mathcal{O}(\vec{x}_1)\,...\mathcal{O}(\vec{x}_n)\rangle \sim \lim_{r_1,..,r_n\to\infty} r_1^{\Delta}...r_n^{\Delta}\langle \prec(\vec{x}_1,r_1)\,...\prec(\vec{x}_n,r_n)\rangle_{AdS}. \tag{1.86}$$

Although this method is more intuitive (and in some situation can be quicker way to calculate), the GPKW rule is easier to use if one consider non-conformal theories such as models with finite temperature and density.

1.3.3 Finite density and temperature

For most of the interesting systems in condensed matter physics the conformal symmetry is broken by several scales. The usefulness of AdS/CFT in applications originates from the fact that the original correspondence can be deformed in many ways. Specifically, we are often interested in systems at finite temperature and chemical potential. Let us summarize here how to incorporate these effects.

For the dual description of a chemical potential we need to first describe, how a $U(1)$ global conserved current J_μ translates into the bulk theory. Because it obeys the conservation law $\partial_\mu J^\mu = 0$, its conformal dimension is fixed to the canonical dimension which is $\Delta_J = d$ as we mentioned in Section (1.2.2). Furthermore, in the bulk, the corresponding field has to be a vector field. There is a slightly different analog of (1.82) which relates the conformal dimension and the mass in case of the spin-1 field which dictates that our dual vector field has to be massless. In other words it has to be invariant under gauge transformation so its action is fixed to usual Maxwell term:

$$S_A = -\frac{1}{4g_F^2}\int d^{d+1}xdrF^{\mu\nu}F_{\mu\nu}, \tag{1.87}$$

with $F_{\mu\nu} = \nabla_\mu A_\nu - \nabla_\nu A_\mu$. Interestingly, a global symmetry in the boundary translates into a local symmetry in the bulk.

A chemical potential μ means that we deform our original theory by $\delta S = \mu Q = \mu \int d^{d+1}xJ^0(x)$. By looking at (1.78) with the specific deformation of $j(x) = \mu$, $\mathcal{O}(x) = J^0(x)$ we can see that solving our bulk theory with the boundary condition $A_0(r \to \infty) = \mu$ corresponds to a boundary theory at finite density.

We can identify the dual of the energy-momentum tensor by similar logic. Its conformal dimension is also equal its canonical dimension $\Delta_T = d + 1$ as it is also a conserved current $\partial_\mu T^{\mu\nu} = 0$. This again results a masslessness condition for the spin-2 dual tensor field. However, the only consistent theory of interacting massless spin-2 fields is general relativity, therefore the dual field must be the metric tensor $g_{\mu\nu}$ itself. As a result, by studying the fluctuations of the metric (gravitational waves) in the bulk one can gain information about the energy and momentum dynamics.

So far in our introduction to AdS/CFT we have been discussing zero temperature physics. One of the most remarkable fact of AdS/CFT how naturally it can encode finite temperature systems. This is done by changing the bulk geometry so that it includes black holes. To see this, let us

write down the asymptotically AdS black hole solution (or black brane more precisely) with planar horizon (which is similar to the Schwarzschild solution in asymptotically flat space):

$$ds^2 = \frac{r^2}{L^2}\left(f(r)d\tau^2 + \Sigma_{i=1}^{d} dx_i^2\right) + \frac{L^2}{r^2 f(r)}dr^2, \tag{1.88}$$

with

$$f(r) = 1 - \frac{r_H^{d+1}}{r^{d+1}}, \tag{1.89}$$

where r_H is the position of the horizon of the black hole. The Hawking temperature of this black hole can be determined by the following argument. The solution (1.88) is plagued by an unphysical conical defect unless we make the (imaginary) time direction τ periodic ($\tau \sim \tau + \beta$) with the period

$$\beta = \frac{4\pi L^2}{r_H^2 f'(r_H)} = \frac{4\pi L^2}{(d+1)r_H}. \tag{1.90}$$

In the boundary field theory the time direction is identified with τ in the bulk and therefore it is also periodic. However, in thermal field theory a periodic imaginary time means that our system is considered in a heat bath with a temperature equal to the inverse of the time period:

$$T = \frac{(d+1)r_H}{4\pi L^2}. \tag{1.91}$$

This temperature in the dual CFT is thus given by the Hawking temperature of the bulk AdS black hole [11]. We can of course reverse this thought process and for a specific temperature T we can choose a horizon postition r_H to describe the dual gravitational system.

Usually, we are interested in systems which are at finite temperature and density at the same time. For this we need to combine the two descriptions and this calls for the black hole solutions of the Einstein-Maxwell action

$$S_{EM} = \int d^{d+2}x\sqrt{g}\left[\frac{1}{16\pi G}\left(R + \frac{d(d+1)}{L^2}\right) - \frac{1}{4g_F^2}F_{\mu\nu}F^{\mu\nu}\right], \tag{1.92}$$

with the boundary condition $A_0(r \to \infty) = \mu$. The solution for the metric is still in the form of (1.88) but with the emblackening factor

$$f_{RN}(r) = 1 + \frac{Q^2}{r^{2d}} - \frac{M}{r^{d+1}}, \tag{1.93}$$

where Q and M are the charge and mass of the black hole. The gauge field profile in this solution is

$$A_0 = \mu \left(1 - \frac{r_H^{d-1}}{r^{d-1}}\right). \tag{1.94}$$

This black hole, the charged Reissner-Nordstrom (RN) black hole, has two horizons in general but for us only the outer one (at position r_H) has importance. The relation between its position and the parameters of the black hole can be determined from the condition $f_{RN}(r_H) = 0$:

$$M = r_H^{d+1} + \frac{Q^2}{r_H^{d-1}}. \tag{1.95}$$

For studying a boundary theory at temperature T and chemical potential μ we need to choose the mass and the charge such that

$$T = \frac{(d+1)r_H}{4\pi L^2}\left(1 - \frac{(d-1)Q^2}{(d+1)r_H^{2d}}\right), \tag{1.96}$$

$$\mu = \frac{g_F Q}{2c_d\sqrt{\pi G}L^2 r_0^{d-1}}, \tag{1.97}$$

with

$$c_d = \sqrt{\frac{2(d-1)}{d}}. \tag{1.98}$$

This solution is especially interesting in the limit where the temperature goes to zero but the chemical potential is fixed. In this extremal limit the two separate horizons mentioned above merge and form a double horizon despite the fact that we are in zero temperature. It means that near the horizon the embleckening factor takes the form

$$f_{NH}(r) = d(d+1)\frac{(r - r_H)^2}{r_H^2} + ... \tag{1.99}$$

We can see the double zero of $f_{NH}(r)$ from this expression. If we define new near horizon variables

$$L_2 = \frac{L}{\sqrt{d(d+1)}}, \tag{1.100}$$

$$\zeta = \frac{L_2}{r - r_H} \tag{1.101}$$

then the near horizon metric can be written as

$$ds^2 = \frac{L_2^2}{\zeta^2}\left(d\tau^2 + d\zeta^2\right) + \frac{r_H^2}{L^2}\Sigma_{i=1}^{d} dx_i^2. \tag{1.102}$$

Comparing to the AdS metric in the coordinates (1.71) we recognize that here the space time is a product of two dimensional Anti-de-Sitter space and flat space resulting in the geometry of $AdS_2 \times \mathbb{R}^d$.

This is a remarkable result and has profound implication to the boundary field theory. According to holography, the radial direction can be thought of a flow of the renormalization group such that the UV of the field theory is characterized by the near boundary geometry and the IR is characterized by the near horizon geometry. Let us study the scaling properties of the UV and IR limit. The UV geometry is invariant under the relativistic, $\mathbf{z} = 1$ scaling

$$\tau \to s\tau, \qquad z \to sz, \qquad \mathbf{x} \to s\mathbf{x}, \tag{1.103}$$

while the IR $AdS_2 \times \mathbb{R}^2$ is invariant under

$$\tau \to s\tau, \qquad \zeta \to s\zeta, \qquad \mathbf{x} \to \mathbf{x}. \tag{1.104}$$

Comparing this with the general form of (1.16) we can see that the IR of the theory has the dynamical critical exponent of $\mathbf{z} = \infty$.

The extremal RN geometry therefore corresponds to a flow from a CFT with $\mathbf{z} = 1$ to a state with $\mathbf{z} = \infty$ upon turning on a chemical potential. This property is called "local quantum criticality" since only the time direction has scaling behavior.

The question arises whether it is possible to construct holographic examples with more general $\mathbf{z}$. The answer turns out to be yes, but for this we need to consider slightly more general models. The hint comes from the string theoretical construction of AdS/CFT. Generally, in a top-down construction there are numerous fields living in AdS but most of them have large masses so we can ignore them. However, there is a type of field which generically appears in the low-energy spectrum called the dilaton field. It is a scalar similar to the example above but it has unusual properties from a traditional field theory point of view. Namely it has non-linear and non-minimal coupling to the gauge field. The extended

theory is the "Einstein-Maxwell-dilaton" gravity [37, 36, 38, 35] with the Lagrangian

$$\mathcal{L} = R - \frac{1}{2}\left(\partial_\mu \phi\right)^2 - \frac{Z(\phi)}{4}F^2 - V(\phi). \tag{1.105}$$

We can think of this as modification of the pure "Einstein-Maxwell" theory that makes the gauge coupling dynamical $g_{F,eff} = Z^{-1}(\phi)$. This generalization is parametrized by two functions: $V(\phi)$ and $Z(\phi)$. Based on string theory arguments these are usually approximated by the exponential forms: $V(\phi) \sim e^{\alpha_2 \phi}$ and $Z(\phi) \sim e^{\alpha_1 \phi}$.

After solving the Einstein's equation for this type of theory, the IR metric (near $r = 0$) can be written in the following form

$$ds^2_{EMD} = r^{-2\theta/d}\left(r^{2\mathbf{z}}d\tau^2 + r^2 dx_i^2 + \frac{dr^2}{r^2}\right) + ..., \tag{1.106}$$

with

$$\theta = \frac{d^2\alpha_2}{\alpha_1 + (d-1)\alpha_2}, \qquad \mathbf{z} = 1 + \frac{\theta}{d} + \frac{2\left(d(d-\theta)+\theta\right)^2}{d^2(d-\theta)\alpha_1}. \tag{1.107}$$

We have a family of solution with two parameters. We do not touch upon the parameter θ here which is called the hyperscaling violation exponent and we set it to zero for our discussion (we choose $\alpha_2 = 0$). In this special case the metric (1.106) is the so-called Lifshitz solution, which is invariant under the scale transformation

$$\tau \to s^{\mathbf{z}}\tau, \qquad r \to s^{-1}r, \qquad \mathbf{x} \to s\mathbf{x}. \tag{1.108}$$

This means that the boundary field theory has the dynamical critical exponent $\mathbf{z}$.

1.3.4 Holographic fermions

So far we have been investigated holographic models in which the bulk action contains only bosonic fields. Now, we briefly study here the exciting case where the bulk conatains fermions as well. In the field theory side these correspond to fermionic single trace operators, e.g. $\mathcal{O}_\Psi \sim Tr\left(\phi\psi\right)$, where ϕ and ψ are bosonic and fermionic fundamental fields. The latter is quite natural from the perspective of the original correspondence since there the field theory is supersymmetric.

To study the properties of the fermion we need to incorporate the Dirac term into the gravitational action

$$S = \int d^{d+2}x\sqrt{-g}\left[\frac{1}{16\pi G}(R-2\Lambda) - \frac{1}{4g_F^2}F_{\mu\nu}F^{\mu\nu}\right. \tag{1.109}$$

$$\left. -i\bar{\Psi}\left(e_a^\mu\Gamma^a\left(\partial_\mu + \frac{1}{4}\omega_{\mu bc}\Gamma^{bc} - iqA_\mu\right) - m\right)\Psi\right], \tag{1.110}$$

where Γ^a are the gamma matrices, e_a^μ is the so-called vielbein defined with the help of the flat metric η as $e_a^\mu e_b^\nu \eta_{ab} = g^{\mu\nu}$ and ω is the spin connection with the properties

$$\partial_\mu e_\nu^a - \Gamma_{\mu\nu}^\sigma e_\sigma^a + \omega_{\mu\nu}^a e_\nu^b = 0. \tag{1.111}$$

Here we have restricted ourself to a bulk action containing only the metric, the gauge field and the fermion field. A natural generalization of this involves the dilaton field introduced in the previous section.

Probe limit

Solving (1.110) in generality is a very hard task and one needs additional approximations. Fermions are intrinsically quantum mechanical objects and therefore in the large-N (semiclassical) limit their backreaction to the geometry and gauge field is small. A natural simplification is to consider the fermion dynamics in the fixed background determined by the other fields. We have seen in Section 1.3.3 that this background is the charged Reissner-Nordstrom (RN) black hole.

The most interesting quantity to compute is the Green's function of the fermionic operators in the boundary field theory. In general, this can only be done numerically as in the first papers on this topic [10, 9, 34]. Later, the problem was reconsidered in a semi-analytical approach which uses the AdS_2 nature of the IR geometry [33, 32].

The key step in this method is to determine the IR AdS_2 Green's function $\mathcal{G}$ which is just the fermion retarded two-point function obtained using the $AdS_2 \times \mathbb{R}^2$ background (1.102) (we restrict ourselves to $d = 2$ dimensions). It has the form

$$\mathcal{G}_k(\omega) = c_k e^{i\phi_k}\omega^{2\nu_k}, \tag{1.112}$$

where c_k and ϕ_k are real, analytical function of the momenta k. The $\mathbf{z} = \infty$ local quantum critical scaling is manifest in the power law fre-

quency dependence. The exponent ν_k depends on the momentum, chemical potential and the parameters of the fermion (mass and charge):

$$\nu_k = \sqrt{\frac{2k^2}{\mu^2} + \frac{m^2}{6} - \frac{q^2}{3}}. \tag{1.113}$$

The full RN black hole geometry interpolates between the near horizon $AdS_2 \times \mathbb{R}^2$ and the near boundary AdS_4 region. It turns out by matching asymptotic expansions that the full Green's function G_R at low frequencies $\omega \ll \mu$ can be obtained from $\mathcal{G}$:

$$G_R(\omega, k) = \frac{b_+^{(0)} + \omega b_+^{(1)} + \mathcal{G}_k(\omega)\left(b_-^{(0)} + \omega b_-^{(1)}\right)}{a_+^{(0)} + \omega a_+^{(1)} + \mathcal{G}_k(\omega)\left(a_-^{(0)} + \omega a_-^{(1)}\right)}. \tag{1.114}$$

We ignored in the formula (real) terms of order ω^2. The coefficients $a_\pm^{(i)}$, $b_\pm^{(i)}$ which can be determined numerically, are real functions of the momentum and the parameters of the model (chemical potential, mass and charge of the fermion). The realness of these coefficients implies that the spectral function is proportional to the AdS_2 spectral function in the limit $\omega \to 0$

$$A(\omega, k) = ImG_R(\omega, k) \sim Im\mathcal{G}_k(\omega) + ..., \tag{1.115}$$

provided $a_+^{(0)} \neq 0$. This latter condition is satisfied when the mass to charge ratio m/q is large.

However, when m/q is small the coefficient $a_+^{(0)}$ can vanish linearly around a momenta k_F: $a_+^{(0)}(k) = v_F(k - k_F) + ...$. In this case (1.114) can be written near k_F in the familiar form of (1.1):

$$G_R(\omega, k) \approx \frac{Z}{\omega - v_F(k - k_F) - \Sigma(\omega, k)} + ..., \tag{1.116}$$

with the self-energy being of the form of

$$\Sigma(\omega, k) = -\frac{c_{k_F}}{a^{(1)}(k_F)} e^{i\phi_k} \omega^{2\nu_{k_F}} \sim \mathcal{G}_k(\omega). \tag{1.117}$$

The emergent parameters v_F and Z are functions of $a_\pm^{(i)}$ and $b_\pm^{(i)}$ evaluated at k_F.

We recognize parts of an interacting Fermion system as in the begining but also very different. The value of the power $2\nu_{k_F}$ is a very important

in the behavior of our result. If $\nu_{k_F} > 1/2$, then at low frequencies the linear bare term dominates over the self-energy. It means that the system has well-defined quasiparticles whose lifetime however is different from quasiparticles in on ordinary Landau type Fermi-liquid (which has $\Sigma \sim \omega^2$). In the case of $\nu_{k_F} < 1/2$ we arrive to a novel non-Fermi liquid state without quasiparticles. In the special (finetuned) case of $\nu_{k_F} \to 1/2$ the self-energy has the marginal Fermi-liquid form $\Sigma \sim \omega \log \omega$ we have seen in formula (1.19). We see therefore that within this simple holographic model one can get a whole zoo of fermionic behavior with or without Fermi surfaces and quasiparticles, including models that we have only postulated phenomenologically up to this point.

Semi-holography

The result (1.117) that the self-energy is proportional to the AdS_2 propagator has a very insightful interpretation. It tells us that we are dealing with a nearly free fermion interacting with a matrix large-N local quantum critical system. to see this let us consider the following effective theory [48]. Let χ be the nearly free fermion and ψ a fermionic operator of a strongly coupled theory whose Green's function has the of $\langle \psi\psi \rangle = \mathcal{G}$. We then couple χ and ψ with the following (sometimes called semi-holographic) action:

$$S = S(\Psi) + \int dt d^d x \left(\chi^\dagger \left(i\partial_t - \epsilon \left(i\nabla \right) + \mu \right) \chi + g\chi^\dagger \Psi + g\Psi^\dagger \chi \right). \quad (1.118)$$

Here $S(\Psi)$ is the action for the strongly coupled system. We have seen that in the matrix large-N limit the higher-point correlators vanishes. In this case the Dyson summation is exact for the χ fermion Green's function

$$\langle \chi^\dagger \chi \rangle = \sum_n g^n G_0 \left(\mathcal{G} G_0 \right)^n = \frac{1}{G_0^{-1} + g\mathcal{G}}, \quad (1.119)$$

where G_0 denotes the free Green's function for the fermion χ. We obtained therefore a result from our effective action which has the same form as the fully holographic result.

One can qualitatively understand this structure by analysing in details the properties of the fermion wavefunction in the RN background. The region where the AdS_4 and $AdS_2 \times \mathbb{R}^2$ geometry meet can be thought as a domain wall where the fermion wavefunction localizes an interacts

weakly with its enviroment. However this fermion can tunnel to the near horizon local critical region. The latter therefore acts as a heat bath for the particle.

In this view of splitting the full system to a nearly free fermion and a local quantum critical subsystem our holographic setup has similarities to the Hertz-Milis type model in Section 1.1.4 used for the Ising-nematic transition. There the fermions however was coupled to a $\mathbf{z} = 1$ critical system, namely to a massless scalar. In view of the disucssion there, the virtues and pitfalls of using AdS/CFT to study such theories should be clear. Nevertheless it is able to offer us novel insights into these complicated systems.

Instabilities

The above mentioned solutions for holographic fermions in the probe limit are very insightful but it turns out that in the parameter region where Fermi surfaces are found instabilities occur. The exponent of the AdS_2 Green's function (1.113) already signals this instality for the small m/q ratio. In that case ν_k become imaginary and $\mathcal{G}$ shows log-oscillatory behaviour. It means that to quantitatively study these holographic systems with Fermi surfaces one needs to take into account the fermion backreaction to the geometry (and to the other fields). Determining the new geometry is a hard task and extra assumptions are needed to make the theory tractable. One approach is to approximate the fermions as a fluid and study the self-gravitating star-like objects and the geometry they have created [14]. This approximation turns out to be good if the total charge of the system Q is much larger than the induvidual charge q of a fermion. The crucial difference compare to the RN black hole geometry is the absence of a horizon.

Another crude approach is to by hand cut off the AdS geometry at some radial distance z_W and consider the fermions in this background. In this case we arrive by construction to a state which is an interacting CFT in the UV and a free Fermi gas in the IR. We will review this approach in the next chapter in details.

We end this section with table (1.1) summarizing our review of the basics of AdS/CFT by indicating the main dictionary elements.

Boundary field theory	Bulk gravitational theory
Partition function	Partition function
Scalar operator $\mathcal{O}$	Scalar field ϕ
Energy-momentum tensor $T_{\mu\nu}$	Metric $g_{\mu\nu}$
Current of a global symmetry J_μ	Gauge field A_μ
Fermionic operator $\mathcal{O}_\psi$	Dirac field ψ
Spin, charge of the operator	Spin, charge of the field
Conformal dimension of the operator	Mass of the field
Global space-time symmetry	Isometry of the geometry
Global internal symmetry	Local (gauge) symmetry
Finite temperature T	Black hole with Hawking temparature T
Chemical potential μ	Boundary condition for the gauge field $A_0(r \to \infty) = \mu$
RG flow	Evolution in the radial direction

Table 1.1. (Non-complete) dictionary for holography.

1.4 This thesis

In the rest of this thesis we apply these techniques to problems in strongly correlated physics. Chapter 2, 3 and 4 are based on the research papers [14–16] respectively.

In Chapter 2 we study pairing induced superconductivity in large N strongly coupled systems at finite density using holographic methods described in the previous section. The goal of this direction is to understand the pairing instability occurring in non-Fermi liquids. We made the first step by studying the pairing of a holographic Fermi liquid (Fermi liquid which is an interacting CFT in the UV). To obtain this state, we introduce an IR hardwall in the background AdS geometry. This results in a discrete spectrum of fermions. Next, we add a dynamical order parameter field and couple it to the fermions with (a relativistic extension of) a BCS type interaction. We solve then (in fixed background) the scalar-gauge-fermion system self-consistently and study the behavior of the order parameter as a function of the relative scaling dimension of the scalar and fermion fields. When translating the bulk physics to the boundary we find novel results namely that the order parameter have resonances for specific scaling dimensions. We speculate about the origin of these and point out that operator mixing in the boundary field theory has an important role when the bulk theory has interaction terms.

In Chapter 3 we study a Fermi surface coupled to a quantum critical boson in $d = 2$ dimensions defined in Section (1.1.4). As we have seen, this model has a relevant interaction between the boson order parameter and the fermion, therefore perturbation theory is not applicable. Because of the fermion sign problem, we cannot use numerical Monte-Carlo methods either. Unlike previous studies which mostly use renormalization group technique we investigate the problem with a different approach. We show that when one excludes fermion loops (which is called the quenched approximation in high-energy physics) it is possible to compute the fermion spectral function exactly using the linear nature of the fermion dispersion relation near the Fermi surface. As we expect the resulting state is not a Fermi liquid. Instead, the original Fermi surface splits and forms three singularities at low energies where the Green's function has power law behavior with different exponents.

In Chapter 4 we continue our investigation of this Hertz-Millis quantum critical metal by weakening our approximations and allow fermion loops to be present. We show that if the Fermi surface curvature is small,

in first approximation it is consistent to correct the boson two-point function only at one-loop order. With this modified propagator we carry out a similar computation than in Chapter 3 to obtain the fermionic Green's function. In the UV/intermediate energy range the quenched approximation is still valid but at lower energies different behavior was found. Deep in the IR the result is very similar to the RPA form using a strongly Landau damped boson. Therefore this calculation shows how to connect the quenched result with the Landau damping dominated low energy regime.

Bibliography

[1] K. G. Wilson, "The renormalization group: critical phenomena and the Kondo," Rev. Mod. Phys. **47**, 4, 773.

[2] E. Y. Loh, Jr., J. E. Gubernatis, R. T. Scalettar, S. R. White, D. J. Scalapino, and R. L. Sugar, "Sign problem in the numerical simulation of many-electron systems," Phys. Rev. B 41, 9301 (1990).

[3] M. Troyer and U.-J. Wiese, "Computational Complexity and Fundamental Limitations to Fermionic Quantum Monte Carlo Simulations," Phys. Rev. Lett. 94, 170201 (2005), [cond-mat/0408370].

[4] S. Durr *et al.*, "Ab-Initio Determination of Light Hadron Masses," Science **322**, 1224 (2008) [arXiv:0906.3599 [hep-lat]].

[5] J. M. Maldacena, "The Large N limit of superconformal field theories and supergravity", Adv. Theor. Math. Phys. **2**, 231 (1998) [hep-th/9711200].

[6] S. S. Gubser, I. R. Klebanov and A. M. Polyakov, "Gauge theory correlators from noncritical string theory", Phys. Lett. B **428** (1998) 105 [hep-th/9802109].

[7] E. Witten, "Anti-de Sitter space and holography", Adv. Theor. Math. Phys. **2** (1998) 253 [hep-th/9802150].

[8] Y. Liu, K. Schalm, Y.-W. Sun, J. Zaanen, "Holographic duality for condensed matter physics", Cambridge University Press, 2015

[9] H. Liu, J. McGreevy and D. Vegh, "Non-Fermi liquids from holography", Phys. Rev. D **83** (2011) 065029 [arXiv:0903.2477 [hep-th]].

[10] M. Cubrovic, J. Zaanen and K. Schalm, "String Theory, Quantum Phase Transitions and the Emergent Fermi-Liquid", Science **325** (2009) 439 [arXiv:0904.1993 [hep-th]].

[11] S. W. Hawking, "Particle Creation by Black Holes", Commun. Math. Phys. **43** (1975) 199 [Erratum-ibid. **46** (1976) 206].

[12] G. 't Hooft, "A Planar Diagram Theory for Strong Interactions," Nucl. Phys. B **72** (1974) 461.

[13] S. Sachdev, "Quantum phase transitions," 2nd Edition, Cambridge University Press 2011

[14] A. Bagrov, B. Meszena and K. Schalm, "Pairing induced superconductivity in holography," JHEP **1409**,106(2014) [arXiv:1403.3699 [hep-th]].

[15] B. Meszena, P. Säterskog, A. Bagrov and K. Schalm, "Non-perturbative emergence of non-Fermi liquid behaviour in $d = 2$ quantum critical metals," Phys. Rev. B **94**, 115134, [arXiv:1602.05360 [cond-mat.str-el]].

[16] B. Meszena, P. Säterskog, and K. Schalm, "Non-perturbative correlation functions of a $d = 2$ quantum critical metal", to be appear

[17] J. A. Hertz, "Quantum critical phenomena," Phys. Rev. B **14** (1976) 1165

[18] M. A. Metlitski and S. Sachdev, "Quantum phase transitions of metals in two spatial dimensions: I. Ising-nematic order," Phys. Rev. B **82** (2010) 075127 [arXiv:1001.1153 [cond-mat.str-el]]

[19] M. A. Metlitski and S. Sachdev, "Quantum phase transitions of metals in two spatial dimensions: II. Spin density wave order," Phys. Rev. B **82** (2010) 075128 [arXiv:1005.1288 [cond-mat.str-el]]

[20] S. S. Lee, "Low-energy effective theory of Fermi surface coupled with U(1) gauge field in 2+1 dimensions," Phys. Rev. B **80** (2009) 165102; [arXiv:0905.4532 [cond-mat.str-el]]

[21] A. L. Fitzpatrick, S. Kachru, J. Kaplan and S. Raghu, "Non-Fermi liquid fixed point in a Wilsonian theory of quantum critical metals," Phys. Rev. B **88** (2013) 125116 [arXiv:1307.0004 [cond-mat.str-el]]

[22] A. L. Fitzpatrick, S. Kachru, J. Kaplan and S. Raghu, "Non-Fermi-liquid behavior of large-N_B quantum critical metals," Phys. Rev. B **89** (2014) 16, 165114 [arXiv:1312.3321 [cond-mat.str-el]]

[23] R. Mahajan, D. M. Ramirez, S. Kachru and S. Raghu, "Quantum critical metals in $d = 3 + 1$ dimensions," Phys. Rev. B **88** (2013) 11, 115116 [arXiv:1303.1587 [cond-mat.str-el]]

[24] G. Torroba and H. Wang, "Quantum critical metals in $4 - \epsilon$ dimensions," Phys. Rev. B **90** (2014) 16, 165144 [arXiv:1406.3029 [cond-mat.str-el]]

[25] A. V. Chubukov, and D. L. Maslov, "First-Matsubara-frequency rule in a Fermi liquid. I.: Fermion self-energy," Phys. Rev. B **86** (2012) 15, 155136 [arXiv:1208.3483 [cond-mat.str-el]]

[26] C. M. Varma, P. B. Littlewood, S. Schmitt-Rink, E. Abrahams and A. E. Ruckenstein, "Phenomenology of the normal state of Cu-O high-temperature superconductors," Phys. Rev. Lett. **63**, 1996 (1989).

[27] C. M. Varma, Z. Nussinov. W. van Saarloos, "Singular or non-Fermi liquids," Physics. Reports **86** (2002) 5-6, [arXiv:1208.3483 [cond-mat.str-el]]

[28] K. Andres, J. E. Graebner and H. R. Ott, "$4f$-Virtual-Bound-State Formation in $CeAl_3$ at Low Temperatures", Phys. Rev. Lett. **35** (1975) 1779

[29] A. W. Tyler and A. P. MacKenzie, "Hall effect of single layer, tetragonal $Tl_2Ba_2CuO_{6+\delta}$ near optimal doping", Physica C 282-287 (1997) 1185-1186

[30] R. Daou *et al.*, "Broken rotational symmetry in the pseudogap phase of high-T_c superconductor," Nature **463**, 519-522 (2009), [arXiv:0909.4430 [hep-lat]].

[31] C. Varma, "High-temperature superconductivity: Mind the pseudogap," Nature **468**, 184-185 (2010)

[32] T. Faulkner, H. Liu, J. McGreevy and D. Vegh, "Emergent quantum criticality, Fermi surfaces, and AdS(2)," Phys. Rev. D **83**, 125002 (2011) [arXiv:0907.2694 [hep-th]].

[33] N. Iqbal, H. Liu and M. Mezei, "Semi-local quantum liquids," JHEP **1204**, 086 (2012) [arXiv:1105.4621 [hep-th]].

[34] S. S. Lee, "A Non-Fermi Liquid from a Charged Black Hole: A Critical Fermi Ball," Phys. Rev. D **79**, 086006 (2009) [arXiv:0809.3402 [hep-th]].

[35] S. S. Gubser and F. D. Rocha, "Peculiar properties of a charged dilatonic black hole in AdS_5," Phys. Rev. D **81**, 046001 (2010) [arXiv:0911.2898 [hep-th]].

[36] K. Goldstein, S. Kachru, S. Prakash and S. P. Trivedi, "Holography of Charged Dilaton Black Holes," JHEP **1008**, 078 (2010) [arXiv:0911.3586 [hep-th]].

[37] C. Charmousis, B. Gouteraux, B. S. Kim, E. Kiritsis and R. Meyer, "Effective Holographic Theories for low-temperature condensed matter systems," JHEP **1011**, 151 (2010) doi:10.1007/JHEP11(2010)151 [arXiv:1005.4690 [hep-th]].

[38] B. Gouteraux and E. Kiritsis, "Generalized Holographic Quantum Criticality at Finite Density," JHEP **1112**, 036 (2011) [arXiv:1107.2116 [hep-th]].

[39] Z. Bajnok and R. A. Janik, "Four-loop perturbative Konishi from strings and finite size effects for multiparticle states," Nucl. Phys. B **807**, 625 (2009) [arXiv:0807.0399 [hep-th]].

[40] N. Arkani-Hamed, F. Cachazo and J. Kaplan, "What is the Simplest Quantum Field Theory?," JHEP **1009**, 016 (2010) [arXiv:0808.1446 [hep-th]].

[41] D. Chowdhury, S. Raju, S. Sachdev, A. Singh and P. Strack, "Multipoint correlators of conformal field theories: implications for quantum critical transport," Phys. Rev. B **87**, no. 8, 085138 (2013) [arXiv:1210.5247 [cond-mat.str-el]].

[42] K. Skenderis, "Lecture notes on holographic renormalization," Class. Quant. Grav. **19**, 5849 (2002) [hep-th/0209067].

[43] J. Zaanen, "A Modern, but way too short history of the theory of superconductivity at a high temperature," [arXiv:1012.5461 [cond-mat.supr-con]].

[44] G. Bednorz and K. A. Müller, "Possible high-T_c superconductivity in the $Ba-La-Cu-O$ system," Physik B - Condensed Matter (1986) 64: 189.

[45] A. V. Ramallo, "Introduction to the AdS/CFT correspondence," Springer Proc. Phys. **161**, 411 (2015) [arXiv:1310.4319 [hep-th]].

[46] H. Bruus and K. Flensberg, "Many-Body Quantum Theory in Condensed Matter Physics," Oxford University Press 2004

[47] S. A. Hartnoll and A. Tavanfar, "Electron stars for holographic metallic criticality," Phys. Rev. D **83**, 046003 (2011) [arXiv:1008.2828 [hep-th]].

[48] T. Faulkner and J. Polchinski, "Semi-Holographic Fermi Liquids," JHEP **1106**, 012 (2011) [arXiv:1001.5049 [hep-th]].

[49] J. Kaplan, "'Lectures on AdS/CFT from the Bottom Up", http://sites.krieger.jhu.edu/jared-kaplan/files/2016/05/AdSCFTCourseNotesCurrentPublic.pdf

Chapter 2

Pairing induced superconductivity in holography

2.1 Introduction

The puzzles posed by strongly correlated electron systems have been considerably illuminated in recent years by the application of gauge-gravity duality. This "holography", which translates the challenging strongly coupled dynamics to an equivalent weakly coupled gravitational theory in one dimension higher, has given qualitative new insights into quantum critical transport [1, 2], superconductivity beyond the weak coupling Bardeen-Cooper-Schrieffer (BCS) paradigm [3–5], and non-Fermi liquids [6, 7].

A simple way to pose the challenge of strongly coupled systems is that the familiar weakly coupled particles no longer exist as controlled excitations in this regime of the theory. Our microscopic understanding of the observed macroscopics in condensed matter usually rests on the notion of an electron(ic quasi)-particle — a charged spin 1/2 fermion — as the fundamental degree of freedom. The theory of Fermi-liquids and the BCS description of superconductivity are good examples of such weakly coupled systems. Even in strongly correlated phases, parts of this electron quasi-particle picture survive. The transition from such a strongly correlated phase to a superconducting phase is still thought to arise from fundamental electron pairing at the microscopic level. After all, these are the only relevant charge carriers in the system. The open puzzle in strongly correlated electron systems such as high Tc superconductors is the nature of the "glue": the interaction that allows pairs to form.

In this chapter we take this suggestion that simple pairing mechanisms should survive in strongly coupled systems to heart. While staying ignorant on the glue, it is a very natural step to incorporate the BCS

theory in the holographic framework. A straightforward reason to do so is to use this very well understood standard theory of superconductivity as a benchmark and inroad into a deeper understanding of holographic fermions. Although AdS/CFT models of superconductivity that have been constructed up to now are quite successful in capturing the main universal properties of real superconductors, they describe physics on the Landau-Ginzburg level of a scalar order parameter. In doing so it manifestly cannot reveal details of the underlying microscopic mechanisms that drive the superconducting instability, but it also ignores the Cooper pair origin of the order parameter. Our specific question here is whether holographic BCS can fill in the latter gap while being agnostic on the former, and serve as a good foothold for further research on this topic.

The most straightforward implementation of Cooper pairing in holography is to incorporate an attractive four-fermi interaction in the gravitational dual theory. In essence one now has a weakly coupled BCS interaction in the dual description of the strongly coupled theory. Pairing instabilities in this set-up were studied in [8], and the formation of a gap in the fermion spectral functions in a fixed Landau-Ginzburg holographic superconductor background, charactertistic of the broken groundstate, was shown in [9]; see also [11].

Both these studies consider the fermions as probes. Since then our understanding of holographic fermions has increased and we now understand that some of the peculiar holographic effects, in particular the non-Fermi-liquid behavior, arise from a coupling to an interacting critical IR [12]. We shall use that improved understanding to go beyond the probe limit and study the full condensation of any paired state, its subsequent groundstate and the self-consistent gap in the fluctuations around it. One way to fully treat the fermion physics is to approximate the fermions in the gravitational dual in a macroscopic fluid limit [13, 14]. In this electron star approximation it is possible to understand the full macroscopic features of the system as it includes gravitational backreaction. A companion article takes this approach [15]. The drawback of the fluid limit is that it essentially describes a system with infinitely many Fermi surfaces — one for each mode in the extra radial AdS direction. This is very unusual from a condensed matter point of view.

Here we pursue an approach that allows us to concentrate on the dynamics of a single Fermi surface. This requires us to consider the fermions quantum-mechanically. In the straightforward holographic set-up this

"quantum electron star" is fraught with subtle issues due to zero-point energy renormalization and its effect on the gravitational background [16, 17]. From the perspective of the field theory side this difficulty is the interaction with the large number of surviving IR degrees in addition to the Fermi-surface quasiparticle. As our first goal is to simply recover the physics of regular BCS in the dual description, the straightforward solution is to lift these extra IR degrees of freedom, and start with a regular confined Fermi-liquid. This can be done by the addition of a hard-wall [12, 16]. This also discretizes the infinite number of Fermi surfaces dual to each radial mode that the AdS theory describes. We then tune the chemical potential such that only a single Fermi surface is occupied. This has the added virtue that the gravitational backreaction will be small, and we are allowed to neglect it. In this straightforward set-up the bulk AdS computation reduces to a standard Hartree BCS calculation but with relativistic fermions in an "effective box" that is spatially curved. This has several technical consequences: working in $d = 3 + 1$ bulk dimensions, there is an effective spin-splitting in that the up and down spin fermions have different Fermi-momenta [18, 19]. Furthermore the non-trivial wavefunctions of the fermions enter into the gap equation. Accounting for this, we shall show that in this hard wall model conventional BCS maps cleanly between the dual gravitational theory and the strongly interacting field theory on the boundary.

To connect this closer to previous study [9] including the standard Landau-Ginzburg holographic superconductor, we next allow the gap-operator to become dynamical: i.e. we introduce a kinetic term for the scalar field in the gravitational bulk. The interpretation of this in the dual field theory is that we have explicitly added an additional charged scalar operator in the theory, that can independently condense. The characteristic quantum number of this new scalar operator in the strongly coupled critical theory is its scaling dimension. Following the well-known AdS/CFT dictionary, this translates into the mass of dual scalar field in the gravitational bulk. For very high mass/dimension the field/operator decouples and we have the conventional BCS scenario constructed earlier. For low masses, the field/operator starts to mix with the Cooper pair operator, and we observe a BCS/BEC crossover. Here we find a novel result. When the operator dimension is strictly degenerate with the that of the Cooper pair, the expectation values of each diverge. Nevertheless their sum — equal to the order parameter — and the gap stay finite. In effect

the extra scalar and the Cooper pair act as a π-Josephson pair in that the relative phase of the condensates is opposite.[1]

However, when the operator dimension is degenerate with that of a higher derivative cousin of the Cooper-pair — higher conformal partial wave — there is another resonance where the naive expectation values of each diverge. Arguably the gap should stay finite for any value of the scaling dimension. A direct application of AdS/CFT rules does not extract the gap cleanly and indicates that a clearer definition of the order parameter vev is needed in the AdS/CFT dictionary. We will address this in future work. Here we conclude by shownig that one can easily construct an expression that has the right order parameter property in that it stays finite. This postulated gap shows a clean BCS/BEC crossover.

2.2 Review of fermion spectra in the AdS dual: spin splitting

To start we shall recall a lesser known point of spectra of holographic fermions: the spectra depend on the spin [18, 19]. The spectra follow from the simplest AdS model of fermions, Einstein Dirac-Maxwell theory — we shall add the BCS interaction in later. The action is

$$S = \frac{1}{2\kappa^2}\int d^4x\sqrt{-g}\left(R + \frac{6}{L^2} - \frac{1}{4}F_{\mu\nu}F^{\mu\nu} + \overline{\Psi}\Gamma^\mu D_\mu\Psi - m_\Psi\overline{\Psi}\Psi\right), \quad (2.1)$$

Here the covariant derivative equals $D_\mu = \partial_\mu + \frac{1}{4}\omega_\mu^{ab}\Gamma_{ab} - iqA_\mu$, and $\overline{\Psi} = i\Psi^\dagger\Gamma^0$. For the background we choose a pure AdS_4 spacetime with AdS radius L equal to one, and cut-off by a hard wall at a finite value of the holographic direction $z = z_w$.

$$ds^2 = \frac{1}{z^2}\left(-dt^2 + dz^2 + dx^2 + dy^2\right), \quad z \in [0, z_w], \quad (2.2)$$

We shall consider a large charge $q \gg \kappa$ where it is consistent to ignore gravitational backreation. The cut off at z_w plays a double role. Together with the AdS potential well, it renders the interval along the holographic coordinate $0 < z < z_w$ effectively finite. This leads to quantization of fermionic energy bands $\omega_n(k)$ (where n is the discrete band number).

[1] Recall that the absolute phase of a condensate is unobservable.

Therefore, on the one hand, we have well-defined sharp long living quasiparticles, and on the other hand the removal of the geometry beyond z_w corresponds to a gapping out of normally present low energy deconfined degrees of freedom. This fundamental gap is also present in the fermion spectra itself. See Fig. 2.1(a). In this set-up we can arrive at the dual description of a single Fermi liquid by tuning the chemical potential such that exactly one band is partially occupied [12]. The charge density produced by the occupied fermions backreacts on the gauge field and its profile and the subsequent adjustment in the fermion spectra can be determined in a self-consistent Hartree manner [12]. Changing z_w changes the size of the gap and the level spacing (larger values of z_w correspond to smaller gap), but does not affect the qualitative picture. Only for strictly infinite z_w do we enter a new critical regime which requires a completely different analysis [16, 17]. We will keep z_w finite throughout and therefore set $z_w = 1$ for most of the remainder without loss of generality. Since all our computations will only depend on the combination qA_0, we also set $q = 1$ in every numerical calculation from hereon.

As we shall review now, due to the spin carried by the relativistic fermions there are actually two Fermi liquids. Moreover, the (background or self-generated) electric field provides a spin-orbit coupling that renders them slightly non-degenerate in the curved background geometry. In addition the lowest energy state is at a non-zero momentum value; this is known as the plasmino mode [18, 19]. This non-degeneracy of the different spin Fermi surfaces will be important in that it leads to a more complex pairing of the fermions.

The spectrum of the fermions is given by normalizable solutions to the Dirac equation. Eliminating the spin connection by rescaling

$$\Psi = (-gg^{zz})^{-1/4}\,\psi = z^{3/2}\psi, \tag{2.3}$$

Fourier transforming along the boundary directions, and making the assumption that the only non-vanishing component of the vector potential is A_0, the Dirac equation reduces to the eigenvalue problem

$$\left(i\Gamma^0\Gamma^z\partial_z + k_i\Gamma^i\Gamma^0 - qA_0 - i\frac{m_\Psi}{z}\Gamma^0\right)\psi = \omega\psi, \tag{2.4}$$

Hereinafter we use tangent-space gamma-matrices, and $i = 1, 2$ refers to the boundary spatial indices.

Due to the impenetrability of the hard wall we choose the canonical momenta to vanish at $z = z_w$:

$$\frac{1}{2}(1+\Gamma^z)\psi(z_w) = 0 \ , \quad A_0'(z_w) = 0. \tag{2.5}$$

At the boundary $z = 0$ we demand that the fermion and scalar fields are normalizable (i.e. vanish sufficiently fast), and the boundary value of the gauge field sets the chemical potential in dual field theory: $A_0(0) = \mu$.

The fermion spectra are determined together with the gauge field profile self-consistently by (numerical) iteration [12]: solve the Dirac equation for a given gauge field profile (for the initial profile $A_0(z) = \mu$). Then solve Maxwell equations $\nabla_\mu F^{\mu\nu} = -iq\langle\overline{\Psi}\Gamma^\nu\Psi\rangle$ with the source determined from the normalizable wave-functions. This gives a new gauge field profile for A_0, etc. the result converges to a self-consistent solution after a few iterations (Fig. 2.2).

The interesting feature of the spectrum is that each band has a fine structure. To understand the origin of this splitting we examine profiles of the two spinor modes corresponding to the first band. Fermion spectra are frequently analyzed using rotational invariance to rotate the momentum k_i parallel to the x-axis and choosing an appropriate basis of the gamma matrices one can simplify the problem [6]. It will, however, be useful for us to keep the rotational symmetry manifest. Our objective is to separate the radial evolution of the fermion from its spinorial structure as much as possible. We can solve the Dirac equation (2.4) with the ansatz

$$\psi_\pm(z) = A_\pm\left(z, |\vec{k}|\right) u_\pm\left(\hat{k}_i\right) + B_\pm\left(z, |\vec{k}|\right)\Gamma^0 u_\pm\left(\hat{k}_i\right), \tag{2.6}$$

where $A_\pm\left(z, |\vec{k}|\right)$ and $B_\pm\left(z, |\vec{k}|\right)$ are functions of the radial coordinate and $u_\pm\left(\hat{k}_i\right)$ are spinors (with unit norm) independent of z. The latter are defined by the following properties

$$\Gamma^z u_\pm\left(\hat{k}_i\right) = u_\pm\left(\hat{k}_i\right) \ , \quad \hat{k}_i\Gamma^i\Gamma^0 u_\pm\left(\hat{k}_i\right) = \pm u_\pm\left(\hat{k}_i\right), \tag{2.7}$$

where $\hat{k}_i$ is a unit (boundary) vector pointing to the direction of the momentum k_i. In the basis (2.15) (which we will use later in this chapter) and with a momentum parallel to the x-axis u_+ (u_-) is the spinor with only fourth (first) nontrivial component.

The Dirac equation implies that

$$\begin{pmatrix} \pm|\vec{k}| - qA_0(z) & i\frac{m_\Psi}{z} + i\partial_z \\ -i\frac{m_\Psi}{z} + i\partial_z & \mp|\vec{k}| - qA_0(z) \end{pmatrix} \begin{pmatrix} A_\pm\left(z, |\vec{k}|\right) \\ B_\pm\left(z, |\vec{k}|\right) \end{pmatrix} = \omega \begin{pmatrix} A_\pm\left(z, |\vec{k}|\right) \\ B_\pm\left(z, |\vec{k}|\right) \end{pmatrix}. \tag{2.8}$$

Provided the electrostatic potential is regular near the AdS boundary at $z = 0$, the asymptotic behavior of the solution is

$$\begin{pmatrix} A_\pm\left(z, |\vec{k}|\right) \\ B_\pm\left(z, |\vec{k}|\right) \end{pmatrix} = a \begin{pmatrix} 0 \\ 1 \end{pmatrix} z^{-m_\Psi} + b \begin{pmatrix} 1 \\ 0 \end{pmatrix} z^{m_\Psi} \ . \tag{2.9}$$

Normalizable solutions are those with $a = 0$. Note that the scaling dimension of the original fermion is $\Delta_\Psi = m_\Psi + \frac{3}{2}$ and we obtained the powers of z above as a result of the rescaling (2.3). In the IR, the boundary condition (2.5) implies that $A_\pm\left(z_w, |\vec{k}|\right) = 0$.

In the absence of an electric field (i.e. $A_0(z)$ is constant), the positive and negative modes have the same energy. In this case we can actually solve our problem exactly in terms of Bessel functions [12]

$$\begin{pmatrix} A_{\pm,n}\left(z, |\vec{k}|\right) \\ B_{\pm,n}\left(z, |\vec{k}|\right) \end{pmatrix} = N_\pm \sqrt{z} \begin{pmatrix} J_{m_\Psi - \frac{1}{2}}\left(\frac{j_n}{z_w} z\right) \\ i\frac{\pm|\vec{k}| - \sqrt{(j_n/z_w)^2 + \vec{k}^2}}{j_n/z_w} J_{m_\Psi + \frac{1}{2}}\left(\frac{j_n}{z_w} z\right) \end{pmatrix}, \tag{2.10}$$

with the dispersion relation $\omega_n = \sqrt{(j_n/z_w)^2 + \vec{k}^2} - q\mu$. Here j_n is the n-th zero of the Bessel function $J_{m_\Psi - 1/2}$, and $N_\pm$ is the normalization constant.

However, in the presence of an electric field in the bulk ($A_0'(z) \neq 0$) the positive and negative modes no longer have the same energy anymore. The reason is that the densities of the two modes (2.10) have different radial profiles. The "effective chemical potential" $A_0(z)$ felt by each mode is therefore different, if the gauge field has a non-trivial z dependence, and this results in a different energy shift for the two modes (Fig. 2.1(b)).

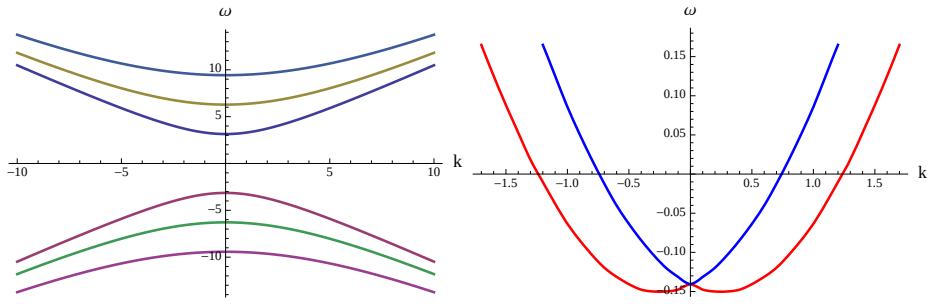

(a) (b)

Figure 2.1. (a): Fermionic spectrum in the AdS-hardwall background at zero chemical potential $z_w = 1$ and $m_\Psi = 1$(b): Spectrum of fermions with unit mass (and $z_w = 1$) in the presence of externally applied electric field $qA_0(z) = 4.5 - 2z$ (without backreaction). We can observe that degeneracy of the two spin states is resolved, and state of a minimal energy is at non-zero momentum. The red and blue curves correspond to positive $u_+(k)$ and negative $u_-(k)$ modes respectively. (When the electric field is self-generated by the fermions the effect is smaller, see Fig. 2.2(a))

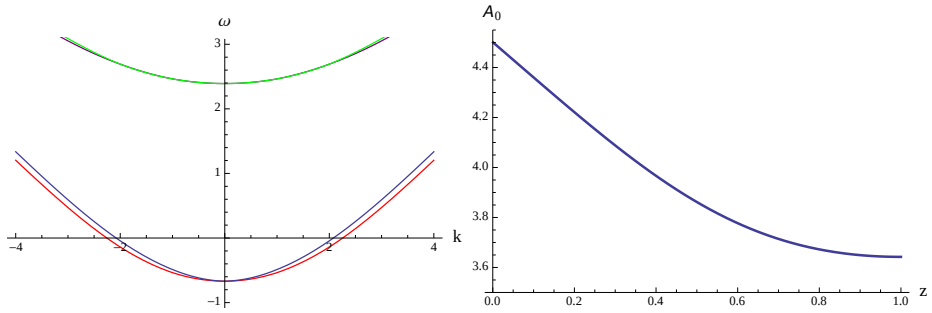

(a) (b)

Figure 2.2. (a): Fermionic spectrum in the self-consistent solution of the fermion+gauge field system at $q\mu = 4.5$, $z_w = 1$ and $m_\Psi = 1$. The red and blue curves represent the modes with positive and negative eigenvalues of $\hat{k}_i \Gamma^i \Gamma^0$ respectively. (b): The profile of the gauge field sourced by the fermions.

2.3 Self interacting fermions in AdS and a bulk BCS theory

2.3.1 Majorana interaction

To study pairing driven superconductivity we now add a quartic contact fermionic interaction in the bulk of AdS:

$$\mathcal{L}_{contact} = \frac{\eta_5^2}{m_\phi^2} z^6 \left(\overline{\psi^C}\Gamma^5\psi\right)^\dagger \left(\overline{\psi}\Gamma^5\psi^C\right), \quad \overline{\psi} = i\psi^\dagger\Gamma^0, \quad \psi^C = C\Gamma^0\psi^* \tag{2.11}$$

ψ^C here is a charge conjugated spinor, and the z^6 factor is due to the rescaling (2.3). One can also consider the naive relativistic generalization of the Cooper pair $\overline{\psi^C}\psi$. However to boil down to standard BCS in non-relativistic limit, where the coupling occurs in s-wave channel between states time-reversed to each other, the unique Lorentz invariant term is actually the Majorana coupling $\overline{\psi^C}\Gamma^5\psi$ (see e.g. [20] for details). We therefore focus only on this term.

As was shown in [18] the direction of the spin of each of the slightly offset modes is perpendicular to the momenta and the two modes have opposite spin. The zero-momentum pairing therefore occurs between opposite spin, without any mixing of the two fermion modes, see Fig. (2.3).

To analyze the interacting theory, we perform the standard Hubbard-Stratonovich transformation with the introduction of an auxiliary the scalar field $\phi(z)$ with charge $q_\phi = 2q$ dual to the superconducting condensate. The scalar part of the action thus takes the form

$$S = \int d^4x \left(i\eta_5^* \phi^* z^3 \overline{\psi^C}\Gamma^5\psi + \text{h.c.} - m_\phi^2\phi\phi^*\right) \tag{2.12}$$

This is the theory studied in [9, 8] with the kinetic term for the scalar turned off. We shall reintroduce this kinetic term in section 2.4.3.

2.3.2 Nambu-Gorkov formalism

The resulting system differs from standard BCS in that, as before, we are including the backreaction of the finite density fermions on the gauge field. Assuming translational invariance in the boundary directions, and restrict the scalar and the gauge field to depend only on z-coordinate, the

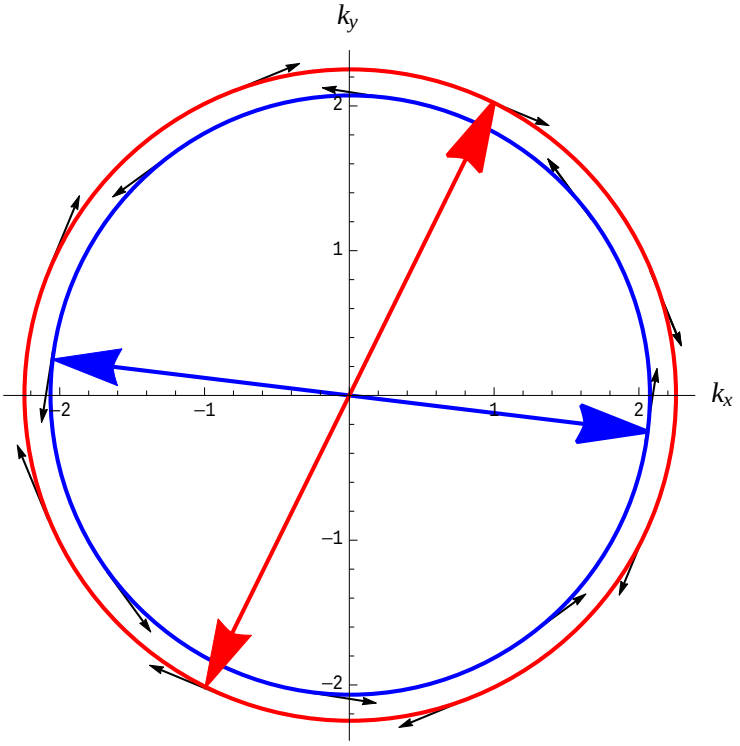

Figure 2.3. The two Fermi surfaces and the *BCS* pairing for the same parameters as in Fig. 2.2. The arrows indicates the direction of the spin of the modes. The pairing happens between opposite spins.

holographic BCS system is formed by

$$\begin{aligned} -m_\phi^2\phi(z) &= -i\eta_5^* z^3\langle\overline{\psi^c}\Gamma^5\psi\rangle, \\ z^2A_0'' - 2q_\phi^2A_0\phi^2 &= qz^2\langle\psi^+\psi\rangle. \end{aligned} \tag{2.13}$$

The fermionic expectation values are assumed to only depend on z as well; they are averaged over all other directions. To compute them, it is convenient to rewrite the action in a quadratic form in terms of the

Nambu-Gorkov spinors. We choose the following basis of gamma-matrices

$$\Gamma^0 = \begin{pmatrix} i\sigma_2 & 0 \\ 0 & i\sigma_2 \end{pmatrix}, \Gamma^1 = \begin{pmatrix} \sigma_1 & 0 \\ 0 & \sigma_1 \end{pmatrix}, \Gamma^2 = \begin{pmatrix} 0 & \sigma_3 \\ \sigma_3 & 0 \end{pmatrix}, \tag{2.14}$$
$$\Gamma^3 = \begin{pmatrix} \sigma_3 & 0 \\ 0 & -\sigma_3 \end{pmatrix}, \Gamma^5 = \begin{pmatrix} 0 & -i\sigma_3 \\ i\sigma_3 & 0 \end{pmatrix}.$$

and rewrite the fermionic part of the action as

$$S_D + S_M = \int d^4x \sqrt{g_{zz}} \left[\overline{\psi} \Gamma^\mu (\partial_\mu - iqA_\mu)\psi - m_\Psi \overline{\psi}\psi - \right. \tag{2.15}$$
$$\left. - i\eta_5^* \phi^* \overline{\psi^c} \Gamma^5 \psi + \text{h.c.} \right] = \int d^4x \overline{\chi} K \chi,$$

where the Nambu-Gorkov spinor χ equals

$$\chi = \begin{pmatrix} \psi_1 \\ \psi_2 \\ \psi_3^* \\ \psi_4^* \end{pmatrix}. \tag{2.16}$$

Taking the pure AdS metric (2.2) explicitly, and using rotational invariance of the problem to set $k_y = 0$, the kinetic matrix K equals

$$K = \begin{pmatrix} D_{11} & 2\eta_5 \frac{\phi}{z} \sigma_3 \\ -2\eta_5^* \frac{\phi^*}{z} \sigma_3 & D_{22} \end{pmatrix}, \tag{2.17}$$

with

$$D_{11} = i\sigma_2(\partial_0 - igA_0) + \sigma_1 \partial_x + \sigma_3 \partial_z - \frac{m_\Psi}{z}, \tag{2.18}$$

$$D_{22} = i\sigma_2(\partial_0 + igA_0) + \sigma_1 \partial_x - \sigma_3 \partial_z - \frac{m_\Psi}{z}. \tag{2.19}$$

The fermionic expectation values can be written in terms of the Nambu-Gorkov Green's function, which satisfies the equation

$$i\Gamma^0 K G_{\chi_i \chi_j^+}(t, \vec{x}; t', \vec{x}') \equiv (i\partial_0 - H)\, G_{\chi_i \chi_j^+}(t, \vec{x}; t', \vec{x}')$$
$$= i\delta(t - t')\delta(\vec{x}_\perp - \vec{x}'_\perp)\, \delta(z - z'). \tag{2.20}$$

Note the additional factor of $i\Gamma^0$ in our definition.

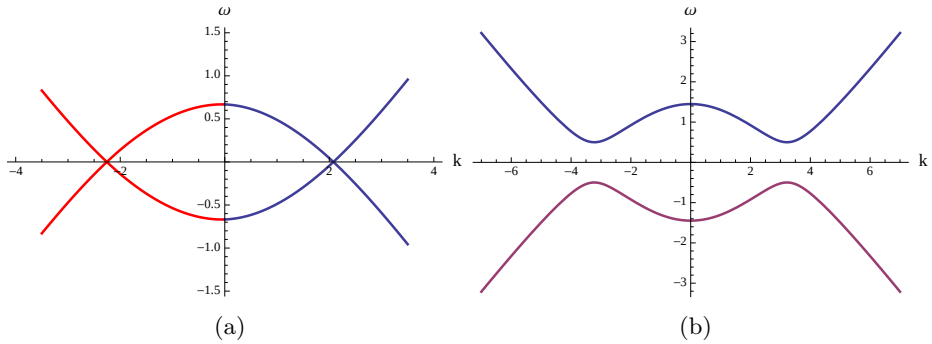

(a) (b)

Figure 2.4. (a): The lower two bands from Fig. 2.2 in the Nambu-Gorkov convention (with parameters $q\mu = 4.5$, $z_w = 1$, $m_\Psi = 1$). (b): Energy spectrum for constant gauge field $qA_0 = q\mu = 4.5$ and linear fixed scalar profile $\phi(z) = z$ at $\eta_5 = 0.25$ ($z_w = 1$, $m_\Psi = 1$). The spectrum is gapped at the Fermi surface.

We determine the Green's function by spectral decomposition. For this we solve the Dirac eigenvalue problem in presence of both the (back-reacted) scalar and gauge field

$$H(i\vec{k}, z)\chi_{\vec{k},n}(z) = \omega_{\vec{k},n}\chi_{\vec{k},n}(z). \tag{2.21}$$

Note, that the Nambu-Gorkov formalism flips the signs of some pieces of the spectrum. Fig. 2.4(a) shows how the two low-lying energy bands in Fig. 2.2(a) look like in the Nambu-Gorkov formalism.

It is convenient to write (2.21) in terms of $(\alpha_1, \alpha_2, \alpha_3, \alpha_4) = (\chi_1, i\chi_2, \chi_3, i\chi_4)$. In this way the redefined "Hamiltonian" H is real (but we will still denote it with H).

We will construct the spectrum numerically, but it is instructive to first consider a toy example. We wish to show that the fermion spectrum becomes gapped in the presence of a condensate for ϕ. Consider the special case when the gauge field is constant $A_0 = \mu$, and the scalar field profile is linear $\phi(z) = z$. Then it is possible to solve the Dirac equation exactly, and the dispersion relation (corresponding to the first band) takes the form (Fig. 2.4(b)):

$$\omega^2 = \left(q\mu - \sqrt{(j_1/z_w)^2 + k^2}\right)^2 + (2\eta_5)^2, \tag{2.22}$$

where j_1 is the first zero of the Bessel-function $J_{m_\Psi - 1/2}$. We visibly see the eigenvalue repulsion responsible for the opening of a gap.

2.3.3 Perturbative calculation of the scalar source

In the Nambu-Gorkov formalism it is straightforward to compute the form of fermionic bilinears sourcing the electric and scalar fields (see Appendix A for details).

$$\langle \psi^+ \psi \rangle = \frac{1}{2\pi} \sum_n \int dk|k| \left(\alpha_{k,n,1}^2 + \alpha_{k,n,2}^2 \right) \Theta\left(-\omega_{k,n}\right) \tag{2.23}$$

$$\langle \bar{\psi^C} \Gamma^5 \psi \rangle = \frac{i}{2\pi} \sum_n \int_{-\Lambda(\omega_D)}^{\Lambda(\omega_D)} dk|k| \left[\Theta\left(\omega_{k,n}\right) \left(\alpha_{k,n,1} \alpha_{k,n,4} - \alpha_{k,n,2} \alpha_{k,n,3} \right) \right] \tag{2.24}$$

where the sum is over the various bands (i.e. radial modes). The sum in the Cooper pair condensate needs to be cut-off at a momentum scale Λ in order to be well-defined. This momentum cut-off corresponds to an energy cut-off ω_D.[2] From now on we will be using real coupling constant $\eta_5^* = \eta_5$.

A direct discretization of the momentum integral in (2.24) is not the most reliable way to numerically computing the fermionic source for the scalar field because contributions from different momenta are sharply peaked around the Fermi surfaces. For higher numerical accuracy and analytical control we solve (2.21) perturbatively in the scalar field. For this we split the Hamiltonian into an unperturbed piece and an interaction piece $H = H_0 + V$, $H_0 = H|_{\eta_5 = 0}$. The typical spectrum for the unperturbed operator looks like the one in Fig. 2.4(a). With our choice of Gamma-matrices, the eigenspinor with the unperturbed energy $\omega_k^{(0)}$ and momentum parallel to the x-axis takes the form (we omit the band index)

$$\alpha_{k,+}^{(0)} = \begin{pmatrix} \xi_k \\ 0 \end{pmatrix} \tag{2.25}$$

where ξ_k is a two component spinor. There is also a mode

$$\alpha_{k,-}^{(0)} = \begin{pmatrix} 0 \\ i\sigma_2 \xi_k \end{pmatrix} \tag{2.26}$$

[2] We use the conventional BCS notation for this cut-off, although there is no explicit connection to any Debye frequency here as the origin of the four-fermion interaction is left in the dark.

with $-\omega_k^{(0)}$, for which only the lower two components are non-zero. Using nearly degenerate perturbation theory we find the matrix-element controlling the effect of the scalar field:

$$V_k = 2\eta_5 \int_0^{z_w} dz |\xi_k(z)|^2 \frac{\phi}{z}. \tag{2.27}$$

The new energy levels are

$$\omega_\pm = \pm\sqrt{\left(\omega_k^{(0)}\right)^2 + V_k^2}, \tag{2.28}$$

so the size of the gap is V_{k_F}. We show in the Appendix B that the scalar source has the following form in terms of the unperturbed wave-functions (considering only one fermion mode):

$$\langle \bar{\psi^C} \Gamma^5 \psi \rangle = -\frac{i}{4\pi} \int_{-\Lambda(\omega_D)}^{\Lambda(\omega_D)} dk|k| \frac{V_k}{\sqrt{\left(\omega_k^{(0)}\right)^2 + V_k^2}} |\xi_k(z)|^2. \tag{2.29}$$

2.3.4 Analytical study of the non-dynamical scalar: double gap equation

Eq.(3.8) is very similar to the standard BCS gap equation. The key difference is the way the spatial profiles ξ_k of the fermion wavefunctions modify both the gap V_k and the spatially varying profile of the pairing vev $\langle \bar{\psi^C} \Gamma^5 \psi \rangle$. Since the AdS geometry together with the hard wall confine the wavefunction, what we have essentially done is solve a relativistic BCS in a non-trivial potential.

There is one additional subtlety, in that the Fermi surfaces corresponding to the up-down spin are slightly split. Assuming, as is conventional, that the cut-off frequency is small enough, we are allowed to approximate V_k and ξ_k by their values at the Fermi surfaces. Doing so we can solve the gap equation

$$\phi(z) = \frac{z^3}{4\eta_5} \left[\gamma_1 V_1 \log\left(\frac{\omega_D + \sqrt{\omega_D^2 + V_1^2}}{V_1} \right) \rho_1(z) + \right. \tag{2.30}$$

$$\left. + \gamma_2 V_2 \log\left(\frac{\omega_D + \sqrt{\omega_D^2 + V_2^2}}{V_2} \right) \rho_2(z) \right], \tag{2.31}$$

where $\rho_1(z) = |\xi_{k_{F,1}}|^2$, $\rho_2(z) = |\xi_{k_{F,2}}|^2$ are the fermion wave functions at the two distinct Fermi surfaces, and $\gamma_{1,2} = \frac{\eta_5^2}{m_\phi^2 \pi} \frac{|k_{F1,2}|}{|\omega'(k_{F1,2})|}$. A brief inspection reveals that the gap equation only depends on the dimensionless combinations $\frac{\eta_5}{m_\phi}$ and $\frac{\eta_5}{\omega_D}$.

In Appendix 2.B.2 we show that the solution of the gap equation can be found in a form of linear combination of the two fermionic wave functions (up to an additional z^3 factor)

$$\phi = (C_1\rho_1(z) + C_2\rho_2(z))\, z^3. \tag{2.32}$$

For $C_1 \gg C_2$ ($C_2 \gg C_1$) the condensate profile is more similar to the wave-function at the first (second) Fermi surface. We obtain the coefficients

$$C_1 = (ax+b)\frac{\omega_D}{\eta_5} \exp\left(-\frac{bx+c}{\gamma_2}\right), \tag{2.33}$$

$$C_2 = (bx+c)\frac{\omega_D}{\eta_5} \exp\left(-\frac{bx+c}{\gamma_2}\right), \tag{2.34}$$

where x is the ratio of the two gaps $x = V_1/V_2$, satisfying the following equation

$$x^2 + \left(\frac{I_{22}}{I_{12}}\frac{\gamma_2}{\gamma_1} - \frac{I_{11}}{I_{12}}\right) x - \frac{\gamma_2}{\gamma_1} = \frac{\gamma_2}{b} x \log x. \tag{2.35}$$

Here I_{11}, I_{22}, I_{12}, a, b, c are functionals of the fermion profiles ρ_1, ρ_2, defined in (4.21), and (2.81) in Appendix B2.

In Fig. 2.5(b) we show the perturbative solutions to the gap equation for $\mu = 4.5$, $q = 1$, $m_\Psi = 1$ and for two different couplings. (In principle there are two solutions but one of these contains a node and is presumably energitically unfavored). We can see a cross-over when we tune the coupling η_5/m_ϕ (see also Fig. 2.6). For small (large) coupling the profile of the condensate is dominated by ρ_2 (ρ_1). Note that the gap at the first Fermi-surface (with fermion wave-function ρ_1) is always smaller than the gap at the second Fermi-surface.

The analysis above is all from the perspective of the bulk AdS physics. All the data of the dual strongly coupled field theory is directly inferred from it. The spectral condition for a normalizable mode is the same [12], hence a gap in the bulk spectra equals a gap in the boundary fermion spectrum. The CFT order parameter is by construction the leading non-zero component of the fermion bilinear vev $\langle \mathcal{O}_{U(1)} \rangle = \lim_{z\to 0} z^{-2\Delta_\Psi} \langle \overline{\Psi^C} \Gamma^5 \Psi \rangle$, where Δ_Ψ is the scaling dimension of the single trace fermionic operator

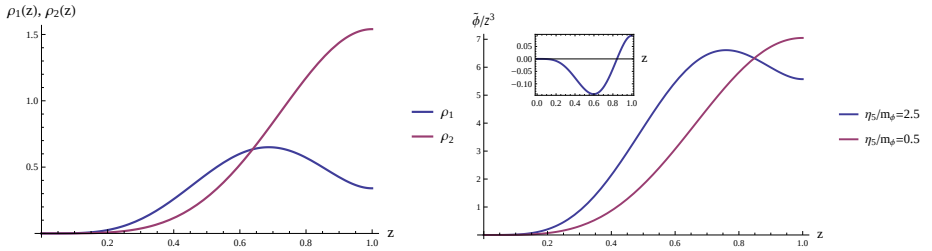

(a) (b)

Figure 2.5. (a): wave function profiles of the fermions at the two Fermi surfaces (ρ_1, ρ_2) $(q\mu = 4.5, z_w = 1, m_\psi)$. (b) The profiles of the stable solutions of the gap equation $\tilde{\phi} = \phi \exp\left(\frac{bx+c}{\gamma_2}\right)$ (rescaled by z^3) for $\eta_5/\omega_D = 0.5$, $\eta_5/m_\phi = 0.5$ and $\eta_5/m_\phi = 2.5$. Depending on the coupling the profiles are similar to the fermion wave-functions ρ_1, ρ_2. In the inset we plot the unstable solution for $\eta_5/m_\phi = 2.5$ (for the other value of the coupling this mode is exponentially small).

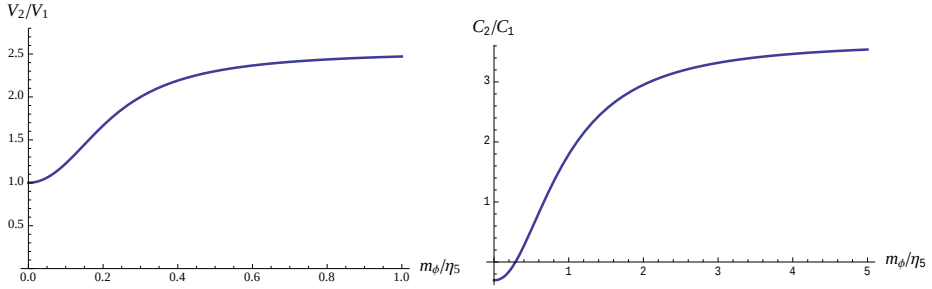

(a) (b)

Figure 2.6. (a): The ratio of the gaps (V_2/V_1) as a function of the inverse coupling m_ϕ/η_5 (for fixed $\eta_5/\omega_D = 0.5$). The other parameters are as in Fig. (2.5). For zero boson mass (or infinite coupling) the gaps have the same size but for non-zero mass (smaller coupling) V_2 is bigger and the ratio converges to the value 2.56. (b): The ratio of the coefficients C_2/C_1 as a function of the inverse coupling.

$\mathcal{O}_\Psi$ dual to the AdS Dirac field (each normalizable fermion wavefunction behaves as z^{Δ_Ψ}) [21, 22]. We thus neatly see how a bulk BCS coupling holographically encodes standard BCS in the dual CFT.

2.4 Fermionic ordering in holography

To establish a closer connection to previous works [9, 10] on fermionic aspects in holographically ordered ground states, we now introduce by hand a kinetic term for the scalar field ϕ. From the bulk perspective this would correspond to a situation where the coherence length (the inverse binding energy) of the Cooper pair is smaller than the relevant cut-off. From the dual boundary field theory perspective this corresponds to the introduction of an explicit scalar operator of scaling dimension

$$\Delta_\phi = \frac{3}{2} + \frac{1}{2}\sqrt{9 + 4m_\phi^2}. \tag{2.36}$$

We reserve the symbol Δ for the scaling dimensions of operators. It is not to be confused with the value of the gap. Again assuming translational invariance in the boundary directions, the bosonic equations now take the form

$$z^2\phi'' - 2z\phi' + z^2 q_\phi^2 A_0^2\phi - m_\phi^2\phi = -i\eta_5 z^3\langle\overline{\psi^c}\Gamma^5\psi\rangle, \tag{2.37}$$

$$z^2 A_0'' - 2q_\phi^2 A_0\phi^2 = qz^2\langle\psi^+\psi\rangle, \tag{2.38}$$

where $q_\phi = 2q$. In addition one has the Dirac equation

$$K(\phi, A_0)\chi = 0 \tag{2.39}$$

through which one defines the bulk expectation values on the right hand side. Here $K(\phi, A_0)$ is the kinetic matrix in (4.73),

The distinction between the model with a dynamical and non-dynamical scalar field is two-fold:

(1) Although physically the order parameter in the broken state cannot distinguish between a fermionic Cooper pair origin and a condensed scalar, in this holographic model they mathematically arise at different orders in the $1/N$ expansion. Recall that the coupling constant expansion in AdS/CFT maps to the $1/N$ matrix expansion of the dual field theory, whereas each AdS field is dual to a single trace composite operator. A Cooper pair is thus dual to double trace operator in the dual field theory which are always $1/N$ suppressed. This distinction is the same distinction between classical spontaneous symmetry breaking in a scalar field theory, and "quantum pairing" in BCS.

(2) Physically, strictly put the scalar is an additional degree of freedom (it will show up in the free energy). If the coherence length of the Cooper pair is smaller than the relevant cut-off, one should indeed introduce this operator separately. In this "strong coupling" (equal to small coherence length) limit, the dynamical scalar field can condense by itself. In the formulation here this is controlled by its mass. For high mass the field should decouple. This is dual to the statement that in the dual field theory the corresponding operator will have a very high scaling dimension and become extremely irrelevant. All the IR dynamics is then controlled by the fermions and we recover the standard BCS of the previous section. For low mass, however, the boson dynamics will start to compete with the fermion pairing and rapidly take over the symmetry breaking dynamics in the IR.

Tuning the scalar mass therefore controls a crossover between pure BCS theory and a classic BEC spontaneous symmetry breaking. Qualitatively one can thus consider the mass/scaling dimension of the scalar operator as a proxy for the coherence length of the Cooper pair. When it is large, the dynamics is pure BCS; as it becomes comparable to and smaller than the relevant cut-off, one should introduce the paired operator independently.

Writing out the spin components explicitly the full system of equations that we are attempting to solve is

$$
\begin{aligned}
& z^2\phi'' - 2z\phi' + 4q^2z^2A_0^2\phi - m_\phi^2\phi = \\
& = \frac{\eta_5 z^3}{2\pi}\sum_n \int_{-\Lambda(\omega_D)}^{\Lambda(\omega_D)} dk|k|\Theta\left(\omega_{k,n}\right)\left(\alpha_{k,n,1}\alpha_{k,n,4} - \alpha_{k,n,2}\alpha_{k,n,3}\right), \\
& z^2A_0'' - 8q^2A_0 = \frac{qz^2}{2\pi}\sum_n \int dk|k|\left(\alpha_{k,n,1}^2 + \alpha_{k,n,2}^2\right)\Theta\left(-\omega_{k,n}\right), \\
& \begin{pmatrix} \partial_z - \frac{m_\Psi}{z} & -(\omega-k) - qA_0 & 2\eta_5\frac{\phi}{z} & 0 \\ (\omega+k) + qA_0 & \partial_z + \frac{m_\Psi}{z} & 0 & 2\eta_5\frac{\phi}{z} \\ 2\eta_5\frac{\phi}{z} & 0 & \partial_z + \frac{m_\Psi}{z} & (\omega-k) - qA_0 \\ 0 & 2\eta_5\frac{\phi}{z} & -(\omega+k) + qA_0 & \partial_z - \frac{m_\Psi}{z} \end{pmatrix} \begin{pmatrix} \alpha_1 \\ \alpha_2 \\ \alpha_3 \\ \alpha_4 \end{pmatrix} = 0
\end{aligned}
\tag{2.40}
$$

Here all fields depend only on the radial direction z. For completeness we recall boundary conditions for each of the fields. At the impenetrable hard wall all canonical momenta should vanish. For the bosons this means

$$
\phi'(z_w) = 0\ , \quad A_0'(z_w) = 0\ ; \tag{2.41}
$$

for the fermions this can be achieved by the choice

$$\alpha_1(z_w) = \alpha_4(z_w) = 0 \tag{2.42}$$

At the AdS boundary, all field should be normalizable: they should vanish as a positive power of z. (For two of the fermion components this is automatic, see eq. (4.2)).

We will approach the fully interacting scalar-fermion system in three steps: we first set all fermions to vanish and construct the purely scalar holographic superconductor. Next we include fermions, but hold the BCS coupling $\eta_5 = 0$; this exhibits bose-fermi competition in the system. Finally we will analyze fully interacting system at $\eta_5 \neq 0$. Details of the numerical calculations are discussed in Appendix C.

2.4.1 Purely scalar holographic superconductor

First, as the scalar field in our system is a fully dynamical degree of freedom, it should condense for small enough mass even in absence of fermions [4, 23, 24]. This hardwall superconductor will be useful for later comparison.

Since we consider a pure hardwall AdS_4 spacetime without a black hole horizon, we study a $T = 0$ groundstate as a function of the mass/conformal dimension of the scalar field/dual scalar operator. Any phase transition is therefore of quantum origin. Note that the hard gap due to the hardwall directly implies that the physics is the same for any temperature $T < 1/z_w$. Only when $T > 1/z_w$ will the the black hole horizon become relevant to the geometry, see e.g. [25].

The numerics of the pure scalar system is particularly simple as there is no need to solve the integro-differential equations iteratively. Varying the scalar conformal dimension we indeed find a condensate value below a critical value (Fig. 2.7). We see a sharp second order phase transition as expected for spontaneous symmetry breaking. Scalar operators with smaller conformal dimensions (dual to lighter bulk scalar fields) are more likely to condense and yield an order parameter with higher density.

2.4.2 Bose-Fermi competition

The next step is to see what happens in a system where both scalar and fermionic fields are present, but interact with each other only via the gauge field A_0, and not directly (the Majorana coupling $\eta_5 = 0$ vanishes). For

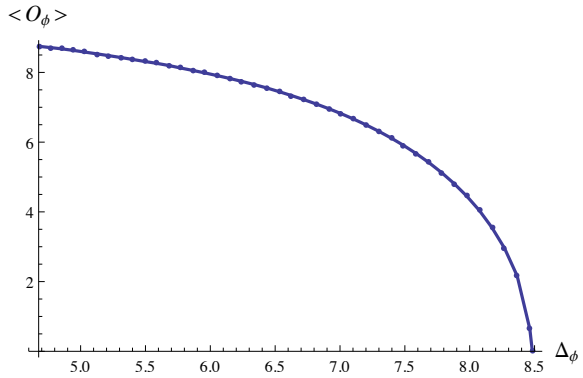

Figure 2.7. Condensate of a scalar order parameter in the boundary theory as a function of scalar conformal dimension at $\mu q = 4.5$, $z_w = 1$, $q_\phi = 2$.

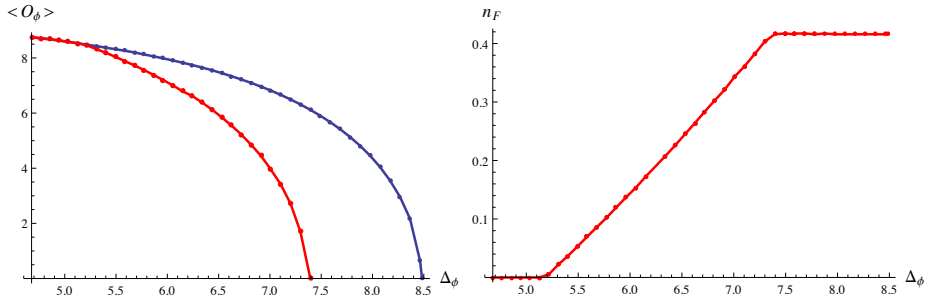

(a) (b)

Figure 2.8. (a): Comparision of the superconducting phase transition in a purely scalar system (blue curve) to the one in a system with fermions at $\eta_5 = 0$ (red curve). At small conformal dimension there is no difference between the phase curves at all, while for larger dimension we see effects of Bose-Fermi competition. (b): Total fermionic bulk charge as a function of scalar conformal dimension, $n_F = \int_0^{z_w} q z^2 \langle \psi^\dagger \psi \rangle dz$. Here $\mu q = 4.5$, $z_w = 1$, $q_\phi = 2$, $\omega_D = 0.7$.

the same parameters as in Fig. 2.7 for a scaling dimension of the fermionic operator $\Delta_\Psi = m_\Psi + 3/2 = 5/2$ we obtain a scalar condensate shown on Fig.2.8.

Comparing, the two condensate values become identical with the pure

hardwall superconductor without fermions for low enough Δ_ϕ. For these values the bulk scalar field is so light that it consumes all the energy in the system. Ceteris paribus we would need a higher chemical potential to make fermions occupy the first band and backreact on A_0.

At larger values of Δ_ϕ there is still a scalar condensate, but it is suppressed compared to the pure hardwall superconductor (Fig.2.8(a)). This can be easily understood in terms of canonical ensemble. For fixed total electromagnetic charge of the system, adding new constituents (fermions) would redistribute the available charge (Fig.2.8(b)) and the condensate of the original degrees of freedom would be suppressed. This effect has also been observed in a holographic set-up where the fermions are approximated in the fluid [26, 27]

2.4.3 A dynamical BCS scalar and a BCS/BEC crossover

Now we analyze the most interesting case and include the full dynamics for the scalar field ϕ. Let us give another reason why this is quite natural from the field theory perspective. The evolution in the radial direction in AdS captures the (leading matrix large N contribution to the) RG flow of the corresponding operator in the field theory. The BCS gap, proportional to the vev of the scalar field is certainly sensitive to the RG scale. Hence one expects it to change dynamically as a function of the radial direction. Strictly speaking the double trace pairing operator which sets the value of the gap is a subleading operator in large N and any running that deviates from its semiclassical scaling is therefore a quantum effect in the AdS gravity theory. This is the situation we studied in section 2.3.4. At the $1/N$ level, for small enough coherence length, the pair operator will become dynamical and qualitatively it ought to be given by the dynamical scalar we study here.

We will see a very interesting effect occurs in doing so. Because the scalar is sourced by the Cooper pair condensate, this changes near-boundary fall off of ϕ, and the standard holographic prescription for boundary field theory condensates has to be modified. Without the presence of a Cooper pair condensate, the zero momentum scalar mode equation in AdS_4 is a homogeneous (linear) differential equation

$$z^2\phi''(z) - 2z\phi'(z) + q_\phi^2 z^2 A_0^2(z)\phi(z) - m_\phi^2\phi(z) = 0. \tag{2.43}$$

Near the AdS boundary its solutions have the following form

$$\phi(z) = Az^{3-\Delta_\phi} \cdot \Big(1 + a_1 z + a_2 z^2 + ...\Big) + Bz^{\Delta_\phi} \cdot \Big(1 + b_1 z + b_2 z^2 + ...\Big),$$
$$\Delta_\phi = \frac{3}{2} + \frac{1}{2}\sqrt{9 + 4m_\phi^2}, \tag{2.44}$$

and in the standard quantization scheme the coefficient A of the non-normalizable solution corresponds to the source $J_{\mathcal{O}_\phi}$ for the operator $\mathcal{O}_\phi$ dual to ϕ, and the coefficient B of the normalizable solution to the vev $\langle \mathcal{O}_\phi \rangle$. Spontaneous symmetry breaking due to a condensation of the operator occurs for a solution in the absence of a source, i.e. with $A = 0$ as a boundary condition.

For the interacting scalar-fermion system this simple one-to-one correspondence between bulk asymptotics and boundary condensates needs modification. We must now consider the inhomogeneous differential equation

$$z^2\phi''(z) - 2z\phi'(z) + q_\phi^2 z^2 A_0^2(z)\phi(z) - m_\phi^2\phi(z) = -i\eta_5 z^3 \langle \overline{\psi^c}\Gamma^5\psi\rangle. \tag{2.45}$$

The solutions to this equation now include the particular solution responding to the inhomogeneous source in addition to the homogeneous solutions (4.76). For near boundary behavior of the source

$$\lim_{z\to 0} z^3 \langle \overline{\psi^c}\Gamma^5\psi\rangle \sim z^{2\Delta_\Psi} \tag{2.46}$$

the particular solution will behave in the same way (assuming $2\Delta_\Psi \neq \Delta_\phi$):

$$\begin{aligned} \phi(z) &= \phi_{hom}(z) + \phi_{part}(z) \\ \phi_{part}(z) &= \mathcal{P}_1 z^{2\Delta_\Psi} + \mathcal{P}_2 z^{2\Delta_\Psi+1} + \mathcal{P}_3 z^{2\Delta_\Psi+2} + ... \end{aligned} \tag{2.47}$$

This particular solution will control the dominant normalizable near boundary behavior for $\Delta_\phi > 2\Delta_\Psi$. This raises the question what we should use as the vev for the corresponding operator. The canonical AdS/CFT prescription

$$\langle \mathcal{O}_\phi \rangle = \lim_{z\to 0} z^{-d+1}\partial_z \Big(z^{d-\Delta_\phi}\phi(z)\Big) \tag{2.48}$$

no longer gives a viable answer. Let us exhibit this in detail. As an aside, note that the near-boundary behavior of the fermions does not change provided the solution for $\phi(z)$ is normalizable.

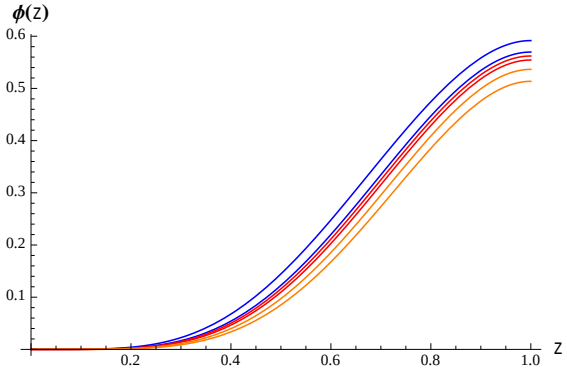

Figure 2.9. Profiles of the bulk scalar wavefunction $\phi(z)$ for $\Delta_\phi = 4.6765$, $\Delta_\phi = 4.8541$ (two blue curves), $\Delta_\phi = 4.9438$, $\Delta_\phi = 5.0341$ (two red curves, - proximity of the critical point), $\Delta_\phi = 5.379$, and $\Delta_\phi = 5.4925$ (two orange curves). Crossing the critical point $\Delta_\phi = 2\Delta_\Psi = 5$ does not lead to any singularities in the bulk wavefunction. The other parameters here are $\eta_5 = 1$, $\mu q = 4.5$, $z_w = 1$, $q_\phi = 2$, $\omega_D = 0.7$.

Denoting the coefficient B of the normalizable homogeneous solution with $B = \mathcal{H}_1$ we extract these coefficients from numerical solutions to the scalar and fermionic equations. (see Fig.2.10, 2.11). Immediately noticable are the singularities at $\Delta_\phi = 2\Delta_\Psi$ and $\Delta_\phi = 2\Delta_\Psi + 2$. Strictly speaking when $\Delta_\phi = 2\Delta_\Psi + n$ the expansion (2.47) breaks down and the solution has an extra logarithmic term

$$\phi(z) = \mathcal{H}_1 z^{2\Delta_\Psi + n} + ... + \mathcal{P}_1 z^{2\Delta_\Psi} + ... + \mathcal{P}_{n+1} z^{2\Delta_\Psi + n} \ln(z) + ... \quad (2.49)$$

The singular divergence of coefficients is a precursor of this logarithm. There is no singularity at $2\Delta_\Psi + 1$ because $\mathcal{P}_2$ happens to vanish in our case.[3]

The indisputable presence of these singularities or resonances can be readily seen by considering a simplified version of the scalar equation. Computing the series solution to the equation

$$z^2\phi'' - 2z\phi' - m_\phi^2\phi = \mathcal{S}_1 z^{2\Delta_\Psi} + \mathcal{S}_3 z^{2\Delta_\Psi + 2} \quad (2.50)$$

[3]This vanishing of $\mathcal{P}_2$ (due to the vanishing of $\mathcal{S}_2$) and the structure of the series expansion is determined by the solutions of the Dirac equation. For zero electric field each *even* coefficient would vanish in fact. Since the gauge field profile modifies the higher order coefficients in the series expansion of the Dirac equation, it can be shown that $\mathcal{S}_4 \neq 0$.

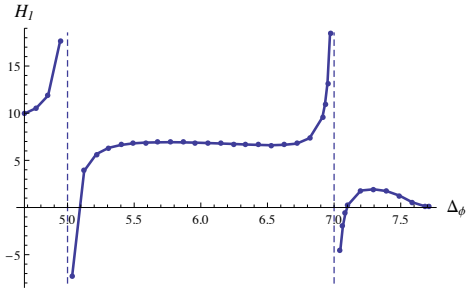

Figure 2.10. Dependence of the leading homogeneous coefficient in the scalar solution expansion on the conformal dimension of the field. Here $\mu q = 4.5$, $\eta_5 = 1$, $z_w = 1$, $q_\phi = 2$, $m_\Psi = 1$ (so $2\Delta_\Psi = 5$), $\omega_D = 0.7$.

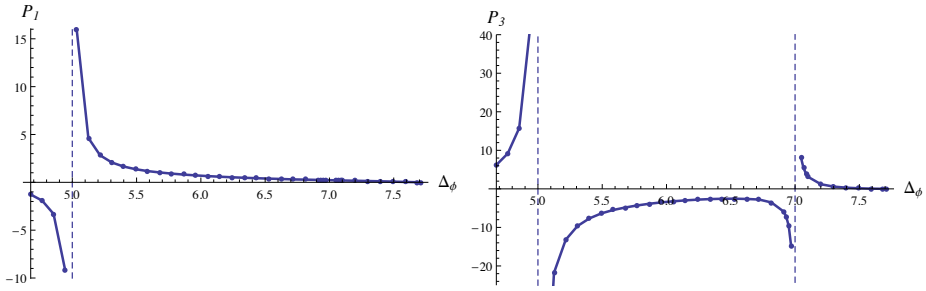

Figure 2.11. Dependence of the two leading particular coefficients in the scalar solution expansion on the conformal dimension of the field. Here $\mu q = 4.5$, $\eta_5 = 1$, $z_w = 1$, $q_\phi = 2$, $m_\Psi = 1$ (so $2\Delta_\Psi = 5$), $\omega_D = 0.7$.

one directly finds the "resonances"

$$\mathcal{P}_1 = \frac{\mathcal{S}_1}{2\Delta_\Psi(2\Delta_\Psi - 3) - \Delta_\phi(\Delta_\phi - 3)},$$
$$\mathcal{P}_3 = \frac{\mathcal{S}_3}{(2\Delta_\Psi + 2)(2\Delta_\Psi - 1) - \Delta_\phi(\Delta_\phi - 3)}. \tag{2.51}$$

Note that they are Feschbach-like resonances in that the singularity is a single rather than a double pole.

The question is how to extract the information of the strongly coupled dual field theory from this asymptotic behavior of the AdS scalar wavefunction. Despite these singularities in the coefficients, by construction the bulk scalar wavefunction is regular at all points (Fig.2.9). It is therefore physically natural to have regular observables in the boundary field theory as well. There are two obvious points to make here.

(1) Physically the origin of the order parameter is indistinguishable. One cannot tell whether the broken groundstate is caused by condensation of the Cooper pair or the scalar field.

(2) Mathematically, the regularity of the bulk solution directly implies that the homogeneous component $\mathcal{H}_1$ must have a similar resonance but with an opposite sign.

An obvious and physically motivated choice is to postulate that the actual order parameter is the simply the sum of the naive condensates, with the Cooper pair condensate $\mathcal{S}_1$ renormalized to $\mathcal{P}_1$: i.e.

$$\langle \mathcal{O}_\phi \rangle = \mathcal{H}_1 + \mathcal{P}_1. \tag{2.52}$$

Taking this linear combination does in fact lead to a cancelation of "resonances" and a smooth function at $\Delta_\phi = 2\Delta_\Psi$ (see Fig. 2.12). However, the reflection of the next resonance $\Delta_\phi = 2\Delta_\Psi + 2$ in the homogenous solution $\mathcal{H}_1$ remains. Likewise, a similar partial resolution occurs for the linear combination $\mathcal{H}_1 + \mathcal{P}_3$.

These "resonances" in $\mathcal{P}_i$ and their cancellation by (part of) the homogeneous solution $\mathcal{H}_1$ will in fact occur at every order of the expansion from the AdS boundary $z = 0$. It hints that the proper definition of the superconducting condensate should be given by a Δ_ϕ-dependent linear combination of the homogeneous $\mathcal{H}_1$ and particular coefficients $\mathcal{P}_1, \mathcal{P}_3, \mathcal{P}_5, ...$

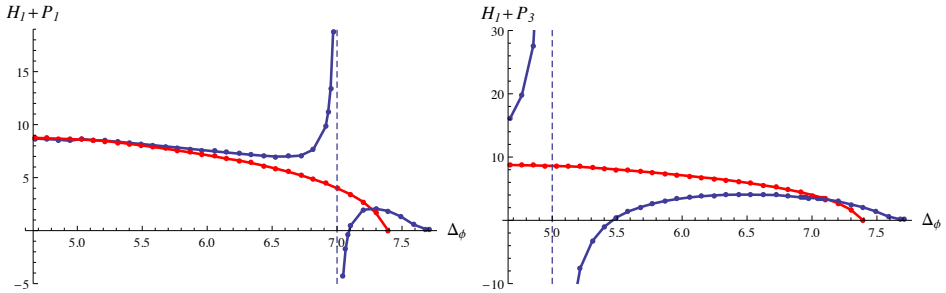

Figure 2.12. Linear combinations of the series expansion coefficients. Red curve represents the boundary scalar operator condensate $\langle \mathcal{O}_\phi \rangle$ as a function of its conformal dimension in presence of fermions at $\eta_5 = 0$ (the same as the red curve on Fig.2.8). The blue curve represent the linear combination $\mathcal{H}_1 + \mathcal{P}_1$ on the left plot, and $\mathcal{H}_1 + \mathcal{P}_3$ on the right one. Resonances in $\mathcal{H}_1$ and $\mathcal{P}_1$ precisely cancel each other at $\Delta_\phi = 2\Delta_\Psi$, and so do resonances in $\mathcal{H}_1$ and $\mathcal{P}_3$ at $\Delta_\phi = 2\Delta_\Psi + 2$. All parameters are as in Fig.2.10.

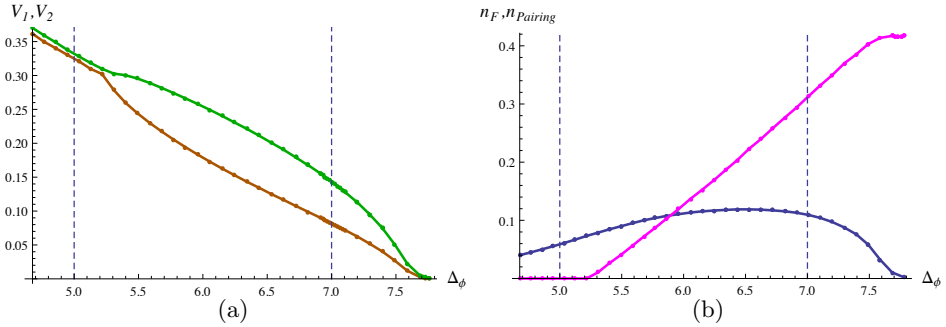

Figure 2.13. (a): Dependence of the two gaps V_1 (orange) and V_2 (green) on Δ_ϕ in the fully interacting case. (b): Dependence of the total fermionic bulk charge $n_F = \int_0^{z_w} qz^2 \langle \psi^\dagger \psi \rangle dz$ (magenta) and the total "number" of pairs $n_{Pairing} = -i\eta_5 \int_0^{z_w} z^3 \langle \overline{\psi^C} \Gamma^5 \psi \rangle dz$ (blue) on Δ_ϕ. One can see that while at small scalar conformal dimensions the fermionic bulk charge totally vanishes the number of Cooper pairs in the bulk theory stays finite. All parameters are as in Fig.2.10.

that is regular for all Δ_ϕ. One can readily construct such a combination, e.g.

$$\langle \mathcal{O}_\phi \rangle = \mathcal{H}_1 + \frac{1}{2}((2\Delta_\Psi + 2) - \Delta_\phi)\mathcal{P}_1 + \frac{1}{2}(\Delta_\phi - 2\Delta_\Psi)\mathcal{P}_3, \tag{2.53}$$

see Fig. 2.14(a). as a demonstration of the existence of a non-singular combination; though there is no proof at all that this constitutes the actual physical observable.[4]

Normally the strict application of the AdS/CFT dictionary does not assign any role to such higher order coefficients in the bulk wavefunction. It is clear, however, that the singularities arise solely from the extraction of the coefficients, whereas the full AdS wavefunctions at any finite z are regular for $\Delta_\phi = 2\Delta_\Psi + \mathbb{N}$. Let us now give an argument why the coefficient rule can receive modification.The right way to interpret the linear combination $\mathcal{H}_1 + \mathcal{P}_1$ is as a mixing of the two independent operators dual to the fundamental scalar operator and the bilinear (double trace) Cooper pair operator. This suggests that we should think in a similar way about the resonance at $\Delta_\phi = 2\Delta_\Psi + 2$. There should be another Cooper-pair like operator in the theory which mixes with the fundamental scalar, such that the linear combination that constitutes the order parameter is finite.

In AdS/CFT this connection between mixing and resonances is in fact cleanly seen in correlation functions of bilinear operators [28, 29]. These bilinear operators are also known as double trace operators, since in the models where we know the dual CFT, each operator dual to an AdS field is a single trace over an $N \times N$ matrix valued combination of fields. Bilinear operators are thus the normal-ordered product of two single trace operators. Each pair of single trace CFT operators $\mathcal{O}_\Psi$, however, gives rise to an infinite tower of independent primary double trace operators:

$$\begin{aligned}
\mathcal{O}_{(0)} &= \mathcal{O}_{\overline{\Psi^C}}\mathcal{O}_\Psi \\
\mathcal{O}_{(1)} &= \mathcal{O}_{\overline{\Psi^C}}(\overleftarrow{\partial}_\mu - \overrightarrow{\partial}_\mu)(\overleftarrow{\partial}^\mu - \overrightarrow{\partial}^\mu)\mathcal{O}_\Psi - \text{trace} \\
\mathcal{O}_{(2)} &= \mathcal{O}_{\overline{\Psi^C}}(\overleftarrow{\partial}_\mu - \overrightarrow{\partial}_\mu)(\overleftarrow{\partial}^\mu - \overrightarrow{\partial}^\mu)(\overleftarrow{\partial}_\nu - \overrightarrow{\partial}_\nu)(\overleftarrow{\partial}^\nu - \overrightarrow{\partial}^\nu)\mathcal{O}_\Psi - \text{traces} \\
&\vdots
\end{aligned} \tag{2.54}$$

[4] Another putative combination found by chance, $\langle \mathcal{O}_\phi \rangle = \mathcal{H}_1 + \frac{1}{2}e^{-(2\Delta_\Psi - \Delta_\phi)}((2\Delta_\Psi + 2) - \Delta_\phi)\mathcal{P}_1 + \frac{1}{2}e^{-(2\Delta_\Psi + 2 - \Delta_\phi)}(\Delta_\phi - 2\Delta_\Psi)\mathcal{P}_3$ has a remarkable overlap with the scalar condensate in the case $\eta_5 = 0$, see Fig. 2.14(b).

These conformal partial waves are all the higher derivative bilinear operators that cannot be written as a descendant (a derivative) of the a lower order primary. All these operators have the same global quantum numbers as the simple pair operator with scaling dimension $2\Delta_\Psi$, but increase their dimension by two integer units each time. The correlation function study [28, 29] in particular shows that in the case of an interacting purely scalar bulk theory, all these linearly independent double trace primaries mix in as well and cause single-pole Feschbach resonances in s-wave scattering of single trace operators. The correspondence between the $2n$ difference in scaling dimension[5] between each successive primary and the location of the resonance in the leading part of the bulk scalar wavefunction supports that this mixing is the right interpretation of the resonance.[6]

We do not yet have a controlled method to extract the quantative expectation value of these higher order double trace primaries from the constituent single trace fields. The mixing originates in the renormalization of the theory, and this suggests that the proper value of the order parameter results from the introduction of higher order boundary counterterms of the type

$$S_{counter} \sim \int_{z=\epsilon} d^3x \left(-\phi^2 - \phi \bar{\Psi}_+^C \Psi_- - \phi \bar{\Psi}_+^C \overleftrightarrow{\partial}_\mu \overleftrightarrow{\partial}^\mu \Psi_- - \ldots \right) \tag{2.55}$$

where $\Psi_\pm$ are eigenspinors of Γ^5. To construct this correct set of counterterms and deduce the appropriate extraction of the vev in the boundary field theory is an interesting question to pursue.

The conclusion is that the resulting condensate ought to be of the form in Fig. 2.14. Qualitatively this result shows the BCS/BEC crossover as a function of the scalar scaling dimension Δ_ϕ. Though our set up is rather abstract in that scalar field here is an additional degree of freedom introduced by hand, instead of emerging from microscopic dynamics, it

[5] As we mentioned one also expects a resonance at $2\Delta_\Psi + 3$ for high enough chemical potential. This is due to the effect of the electric field on the fermion wave functions. From the boundary perspective this could be a result of mixing with $\mathcal{O}_\psi J_\mu (\overleftarrow{\partial^\mu} - \overrightarrow{\partial^\mu}) \mathcal{O}_\psi$ type operator which has the right scaling dimension ($\Delta_J = 2$).

[6] The conformal partial wave operators share a resemblance with operators relevant for Fulde-Ferrel-Larkin-Ovchinnikov pairing [30, 31]. In the original FFLO set-up one considers the Zeeman splitting of spin-up/spin-down electrons and this causes an offset in their Fermi surfaces of the same form seen here. The discussion about the mixing in of these higher order partial waves does not rely on the split degeneracy of Fermi surfaces. The mixing is therefore not correlated with an FFLO-like phenomenon.

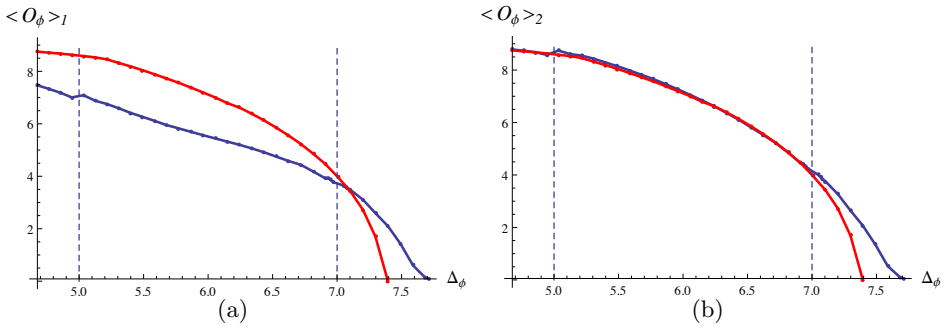

Figure 2.14. (a): The blue curve represents a particular linear combinations of the series expansion coefficients $\langle \mathcal{O}_\phi \rangle_1 = \mathcal{H}_1 + \frac{1}{2}((2\Delta_\Psi + 2) - \Delta_\phi)\mathcal{P}_1 + \frac{1}{2}(\Delta_\phi - 2\Delta_\Psi)\mathcal{P}_3$ such that all the resonances cancel out. The red curve included for comparison represents $\langle \mathcal{O}_\phi \rangle$ at $\eta_5 = 0$. (b): The serendipitous combination $\langle \mathcal{O}_\phi \rangle_2 = \mathcal{H}_1 + \frac{1}{2}e^{-(2\Delta_\Psi - \Delta_\phi)}((2\Delta_\Psi + 2) - \Delta_\phi)\mathcal{P}_1 + \frac{1}{2}e^{-(2\Delta_\Psi + 2 - \Delta_\phi)}(\Delta_\phi - 2\Delta_\Psi)\mathcal{P}_3$ that has a remarkable overlap with the $\eta_5 = 0$ solution at low Δ_ϕ as desired. All parameters are as in Fig.2.10.

captures the BCS/BEC physics. For small scaling dimension the scalar operator $\mathcal{O}_\phi$ dominates the Bose-Fermi competition, whereas at large scalar conformal dimensions corresponding to weak coupling regime, $\eta_5/m_\phi \ll 1$, the dynamics of the boson field are suppressed, and its order parameter expectation value is dominated by fermions as shown on Fig. 2.12. The most interesting region is just to the right of the red curve. Here there is no bosonic contribution to the order parameter, but there is an enhanced Cooper pair contribution (due to the proximity effect). This is the most notable region where we have pairing induced superconductivity in holography. At larger scalar conformal dimension the order parameter exponentially decreases with increasing of Δ_ϕ, although it never vanishes. In the strict $m_\phi \to \infty$ limit we have the standard BCS scenario of section 2.3.4.

Let us finally briefly comment on the dependence on the UV cut off ω_D. In the previous section we discussed that at very large bulk scalar mass all dynamics depends only on two parameters, η_5/ω_D and η_5/m_ϕ. For a dynamical scalar the dependence is more complicated, but we can still qualitatively infer what will happen. We know that most of the contribution to the pairing operator is located near the Fermi surfaces. Increasing

ω_D means taking into account states lying far away from k_F's. The physical picture will therefore only change minimally; to first approximation it can be compensated by adjusting η_5 such that η_5/ω_D stays constant. A non-trivial effect does happen when ω_D becomes so large that the integral becomes sensitive to fermions in the second band (for instance, see Fig. 2.1), but this is beyond the scope of this chapter.

2.5 Conclusions

We have constructed a holographic model of superconductivity which explicitly takes into account fermionic pairing driving the phase transition. In the simplest holographic models, the microscopic mechanism of superconductivity is not addressed. Specific top-down models may shed light on the strong coupling dynamics and a possible pairing mechanism [32, 33], but generic holographic models operate at a Landau-Ginzburg order parameter level.

Even so, the physics of fermionic pairing and condensation should also be explicitly representable in holographic systems. The most straightforward way to do so is to mimic the classic BCS mechanism. This is what we have done here. By introducing an attractive four-fermion interaction in the AdS bulk, we show that this directly reduces to a pairing induced superconducting groundstate both in the bulk and the dual boundary. To cleanly separate the fermion physics, we introduced a hard wall cut-off. This essentially guaranteed this results as the low energy theory in both sides is just a Fermi liquid in the absence of the four-fermion interaction. The one technical difference with textbook BCS is the relativistic nature of the underlying fermion theory.

Next we introduced separately a kinetic term for the AdS dual of the order parameter. Physically the paired operator should become dynamical if the coherence length is much shorter than the scales of interest. One should find a BCS/BEC crossover as one tunes between these regimes. Here that control parameter is the scaling dimension of the order parameter field (relative to the scaling dimension of the Cooper pair operator). For large scaling dimension the kinetics of the dual AdS field is suppressed and we have the BCS physics found earlier. For low scaling dimension the scalar dynamics should be energetically favored compared to pairing condensation, and one should find a regular BEC (holographic) superconductor.

In observing this BCS/BEC crossover we encountered a surprise. At specific values $\Delta_\phi = 2\Delta_\Psi$ and $\Delta_\phi = 2\Delta_\Psi + 2$ of the control parameter the independent scalar $\langle \mathcal{O}_\phi \rangle$ and pairing $\langle \mathcal{O}_{\overline{\Psi^C}} \mathcal{O}_\Psi \rangle$ vevs diverge. In fact the naive order parameter $\langle \mathcal{O}_\phi \rangle + \langle \mathcal{O}_{\overline{\Psi^C}} \mathcal{O}_\Psi \rangle$ remains divergent at $\Delta_\phi = 2\Delta_\Psi + 2$. The mathematics is clear and suggests that these divergences can also occur at higher value of the scaling dimension. Physically, a plausible explanation is that higher order primaries $\mathcal{O}_{\overline{\Psi^C}} (\overleftarrow{\partial}_\mu - \overrightarrow{\partial}_\mu)^n (\overleftarrow{\partial^\mu} - \overrightarrow{\partial^\mu})^n \mathcal{O}_\Psi$, that arise in the OPE of the product of two single fermion operators, mix in with the scalar vev and the lowest order primary $\langle \mathcal{O}_\phi \rangle + \langle \mathcal{O}_{\overline{\Psi^C}} \mathcal{O}_\Psi \rangle$. To establish this concretely requires a more detailed study of single and double trace operator mixing in AdS/CFT. We aim to address this in a future publication. We can nevertheless readily construct an extraction rule for a finite order parameter that interpolates between the BCS and BEC regimes.

In both aspects the physics that holographic system describes is very conventional. It is again an excellent proving ground for AdS/CFT that it does so, but by construction it does not uncover any unconventional or exotic physics. The main reason it does not do so is the presence of the hard wall. It ensures that the groundstate dynamics closely follows standard Fermi liquid and Landau-Ginzburg theory. It would be very interesting, but technically challenging [16, 17], to try to remove the hard wall. This would reintroduce the low energy dynamics that could yield exotic and novel behaviour. In particular, it might be an important step towards a holographic fermionic theory of unconventional superconductivity.

2.A Green's functions and charge densities

In this Appendix we provide a detailed derivation of the formulas for the fermionic bilinears appearing in the bosonic equations. In principle while calculating these objects one needs to be careful because of the renormalization of these composite operators. However, we are just regularizing these object with a cut off and not attempting to perform the renormalization. We can write the fermionic electric charge density as a limit of Feynman Green's function:

$$\langle \psi^+(x)\psi(x) \rangle = \lim_{t,\vec{x}\to t',\vec{x}'} \langle T\psi^+(t,\vec{x})\psi(t',\vec{x}') \rangle = \lim_{t,\vec{x}\to t',\vec{x}'} G_{\psi_i^+\psi_i} \tag{2.56}$$

We would like to express it with the Nambu-Gorkov (NG) Green's

function defined as

$$G_{\chi_i\chi_j^+} = \frac{1}{Z}\int D\chi D\chi^+ \chi_i\chi_j^+ \exp\left(i\int d^4x\chi^+\widetilde{K}\chi\right). \tag{2.57}$$

Using properties of the time ordered product the relations between the original Green's functions and the NG ones are

$$G_{\psi_1^+\psi_1}(t,\vec{x};t',\vec{x}') = -G_{\chi_1\chi_1^+}(t',\vec{x}';t,\vec{x}), \tag{2.58}$$

$$G_{\psi_3^+\psi_3}(t,\vec{x};t',\vec{x}') = G_{\chi_3\chi_3^+}(t,\vec{x};t',\vec{x}'). \tag{2.59}$$

With these the charge densities can be expressed with the components of the NG Green's function

$$\begin{aligned}\langle\psi^+\psi\rangle = \lim_{t,\vec{x}\to t',\vec{x}'}\Big(&-G_{\chi_1\chi_1^+}(t',\vec{x}';t,\vec{x}) - G_{\chi_2\chi_2^+}(t',\vec{x}';t,\vec{x})\\ &+G_{\chi_3\chi_3^+}(t,\vec{x};t',\vec{x}') + G_{\chi_4\chi_4^+}(t,\vec{x};t',\vec{x}')\Big),\\ \langle\overline{\psi^c}\Gamma^5\psi\rangle = \lim_{t,\vec{x}\to t',\vec{x}'}\Big(&G_{\chi_1\chi_4^+}(t,\vec{x};t',\vec{x}') + G_{\chi_2\chi_3^+}(t,\vec{x};t',\vec{x}')\\ &+G_{\chi_2\chi_3^+}(t',\vec{x}';t,\vec{x}) + G_{\chi_1\chi_4^+}(t',\vec{x}';t,\vec{x})\Big).\end{aligned} \tag{2.60}$$

Since the NG Green's function solves (2.20) we can decompose it as

$$G(t,\vec{x};t',\vec{x}') = \int\frac{d\omega}{2\pi}e^{-i\omega(t-t')}\sum_n\int\frac{d^2k}{4\pi^2}\frac{ie^{i\vec{k}\left(\vec{x}_\perp-\vec{x}'_\perp\right)}}{\omega-\omega_{\vec{k},n}+i\mathrm{sgn}(\omega)\epsilon}\chi_{\vec{k},n}(z)\chi^+_{\vec{k},n}(z'), \tag{2.61}$$

where $\chi_{\vec{k},n}(z)$ solves the Dirac equation (2.21) and form an orthonormal basis

$$\int_0^{z_w} dz\chi^+_{\vec{k},n}(z)\chi_{\vec{k},n'}(z) = \delta_{nn'}, \tag{2.62}$$

$$\sum_n \chi_{\vec{k},n}(z)\chi^+_{\vec{k},n}(z') = \delta(z-z'). \tag{2.63}$$

We can immediately perform the ω integral to get (supposing that $t > t'$)

$$G(t,\vec{x};t',\vec{x}') = \sum_n\int\frac{d^2k}{4\pi^2}e^{-i\omega_{\vec{k},n}(t-t')}e^{i\vec{k}\left(\vec{x}_\perp-\vec{x}'_\perp\right)}\chi_{\vec{k},n}(z)\chi^+_{\vec{k},n}(z')\Theta\left(\omega_{\vec{k},n}\right), \tag{2.64}$$

$$G(t',\vec{x}';t,\vec{x}) = -\sum_n\int\frac{d^2k}{4\pi^2}e^{-i\omega_{\vec{k},n}(t'-t)}e^{i\vec{k}\left(\vec{x}'_\perp-\vec{x}_\perp\right)}\chi_{\vec{k},n}(z)\chi^+_{\vec{k},n}(z')\Theta\left(-\omega_{\vec{k},n}\right). \tag{2.65}$$

Substituting this into (2.60) we obtain (2.23) and (2.24).

2.B Perturbative solution

2.B.1 Perturbative fermion spectrum, AdS-gap equation

We will solve the fermionic equation of motion (2.21) perturbatively in the scalar interaction and determine the gap equation. It is convenient for this to write the eigenvalue problem in terms of $(\alpha_1, \alpha_2, \alpha_3, \alpha_4) = (\chi_1, i\chi_2, \chi_3, i\chi_4)$. The redefined Hamiltonian is real (but we will still denote it with H).

Our Hamiltonian can be split as $H = H_0 + V$, where $H_0 = H(\eta_5 = 0)$. The perturbation is coming from the Majorana coupling

$$V = 2\eta_5 \frac{\phi}{z} \begin{pmatrix} 0 & -\epsilon \\ \epsilon & 0 \end{pmatrix}, \tag{2.66}$$

where ϵ is the 2x2 matrix $\epsilon = i\sigma_2$

The solution of the unperturbed problem for a given momentum takes the form

$$\alpha^{(0)}_{k,+,n} = \begin{pmatrix} \xi_{k,n} \\ 0 \end{pmatrix} \quad \omega^{(0)}_{1,k,n} = \omega^{(0)}_{k,n} > 0, \tag{2.67}$$

$$\alpha^{(0)}_{k,-,n} = \begin{pmatrix} 0 \\ \epsilon\xi_{k,n} \end{pmatrix} \quad \omega^{(0)}_{2,k,n} = -\omega^{(0)}_{k,n}. \tag{2.68}$$

We will focus on $n = 1$ and will omit this index.

When doing the perturbation theory we should be careful because near the Fermi-surface different bands are crossing each other. Therefore we start with two modes with unperturbed energy $\omega^{(0)}_k$ and $-\omega^{(0)}_k$ and approximate the solution as $\alpha_k = a\alpha^{(0)}_{k,+} + b\alpha^{(0)}_{k,-}$. Near the Fermi-surface this is a good approximation.

The perturbed energy and wave-functions can be determined by the off-diagonal matrix element of V (the diagonal elements are zero).

$$V_k = \int_0^{z_w} dz \alpha^{(0)+}_{k,+} V \alpha^{(0)}_{k,-} = 2\eta_5 \int_0^{z_w} dz |\xi_k|^2 \frac{\phi}{z}. \tag{2.69}$$

The new energy levels are

$$\omega_\pm = \pm\sqrt{\left(\omega^{(0)}_k\right)^2 + V_k^2}, \tag{2.70}$$

so the size of the gap is V_{k_F}. The normalized wave-functions are

$$\alpha_{k,+} = \begin{pmatrix} \xi_k \cos\frac{1}{2}\beta_k \\ \epsilon\xi_k \sin\frac{1}{2}\beta_k \end{pmatrix}, \quad \alpha_{k,-} = \begin{pmatrix} -\xi_k \sin\frac{1}{2}\beta_k \\ \epsilon\xi_k \cos\frac{1}{2}\beta_k \end{pmatrix}, \tag{2.71}$$

where

$$\tan\beta_k = \frac{V_k}{\omega_k^{(0)}}. \tag{2.72}$$

Using this perturbative result we can express the scalar source with the unperturbed fermion wave functions:

$$\langle\bar{\psi^C}\Gamma^5\psi\rangle = -\frac{i}{4\pi}\int_{-\Lambda(\omega_D)}^{\Lambda(\omega_D)} dk|k|\frac{V_k}{\sqrt{\left(\omega_k^{(0)}\right)^2 + V_k^2}}|\xi_k(z)|^2. \tag{2.73}$$

Here $\Lambda(\omega_D)$ is a momentum cut-off corresponding to the energy scale ω_D. In our numerics we sample discrete number of momenta and sum over it. In order to capture the contribution around k_F accurately we can use the following discretization

$$\begin{aligned}\int_{-\Lambda(\omega_D)}^{\Lambda(\omega_D)} dk|k|\frac{V_k}{\sqrt{\left(\omega_k^{(0)}\right)^2 + V_k^2}}|\xi_k|^2 &\approx \sum_{k_i} V_{k_i}k_i\frac{1}{|\omega'(k_i)|}\int_{\omega(k_i)}^{\omega(k_{i+1})}\frac{d\omega}{\sqrt{\omega^2+V_k^2}} \\ &= \sum_i |\xi_{k_i}|^2\frac{V_{k_i}k_i}{\omega'(k_i)}\log\left(\frac{\omega_{i+1}^{(0)} + \sqrt{\left(\omega_{i+1}^{(0)}\right)^2 + V_{k_i}}}{\omega_i^{(0)} + \sqrt{\left(\omega_i^{(0)}\right)^2 + V_{k_i}}}\right)\end{aligned} \tag{2.74}$$

2.B.2 Simplified Gap equation

The dominant contribution for the scalar charge comes from a region near the Fermi surface where the (unperturbed) spectrum is linear. Since the perturbation matrix element V_k is a slowly varying function of k we can approximate its value with $V_{k_{F,1}} = V_1$ and $V_{k_{F,2}} = V_2$.

We have two Fermi surfaces. Hence the gap-equation is (recall that our scalar is an auxiliary field with no dynamics here)

$$\phi(z) = \frac{z^3}{4\eta_5}\left[\gamma_1 V_1 \log\left(\frac{\omega_D + \sqrt{\omega_D^2 + V_1^2}}{V_1}\right)\rho_1(z) + \right. \tag{2.75}$$

$$\left. \gamma_2 V_2 \log\left(\frac{\omega_D + \sqrt{\omega_D^2 + V_2^2}}{V_2}\right)\rho_2(z)\right], \tag{2.76}$$

where $\rho_1(z) = |\xi_{k_{F,1}}|^2$, $\rho_2(z) = |\xi_{k_{F,2}}|^2$ and $\gamma_{1,2} = \frac{\eta_5^2}{m_\phi^2 \pi} \frac{|k_{F1,2}|}{|\omega'(k_{F1,2})|}$. We make the following ansatz

$$\phi = (C_1\rho_1(z) + C_2\rho_2(z))\, z^3. \tag{2.77}$$

In this case the perturbation matrix element is

$$V_1 = 2\eta_5 \left(C_1 I_{11} + C_2 I_{12}\right) \ , \quad V_2 = 2\eta_5 \left(C_2 I_{22} + C_1 I_{12}\right), \tag{2.78}$$

where

$$I_{11} = \int_0^{z_w} z^2 \rho_1^2 dz, \quad I_{22} = \int_0^{z_w} z^2 \rho_2^2 dz, \quad I_{12} = \int_0^{z_w} z^2 \rho_2 \rho_1 dz. \tag{2.79}$$

In the limit of $\omega_D \gg \eta_5$ our gap-equations take the following form

$$\begin{aligned} aV_1 + bV_2 &= 2\eta_5\gamma_1 V_1 \log\left(\frac{\omega_D}{\eta_5 V_1}\right) \\ bV_1 + cV_2 &= 2\eta_5\gamma_2 V_2 \log\left(\frac{\omega_D}{\eta_5 V_2}\right), \end{aligned} \tag{2.80}$$

with

$$a = \frac{I_{22}}{I_{22}I_{11} - I_{12}^2} \ , \quad b = \frac{I_{12}}{I_{12}^2 - I_{22}I_{11}} \ , \quad c = \frac{I_{11}}{I_{22}I_{11} - I_{12}^2}. \tag{2.81}$$

For the ratio $x = V_1/V_2$ we obtain

$$x^2 + \left(\frac{I_{22}}{I_{12}}\frac{\gamma_2}{\gamma_1} - \frac{I_{11}}{I_{12}}\right) x - \frac{\gamma_2}{\gamma_1} = \frac{\gamma_2}{b} x \log x. \tag{2.82}$$

We can now solve our equations easily to obtain

$$C_1 = (ax+b)\frac{\omega_D}{\eta_5} \exp\left(-\frac{bx+c}{\gamma_2}\right) \ , \quad C_2 = (bx+c)\,\frac{\omega_D}{\eta_5} \exp\left(-\frac{bx+c}{\gamma_2}\right). \tag{2.83}$$

2.C Numerical methods

2.C.1 General strategy

To solve the equations (2.41) numerically, we resort to an iterative Hartree resummation:

- At a constant $A_0 = \mu$ and zero scalar field, we find the unperturbed spectrum of fermions. As a result we get a set of fermionic wavefunctions for a discrete array of energies and momenta $(k_i, \omega_{n,i})$.

- With these wavefunctions we construct the source terms on the right hand side of the first two equations in (2.41) and solve for $A_0(z)$ and $\phi(z)$. Both UV cut offs in both k and ω should be imposed to render the sums in the source terms finite.

- Substitute the new $A_0(z)$ and $\phi(z)$ into the Dirac equation and find the new spectrum.

- Repeat steps 2 – 4 till full convergence.

Once the system converges sufficiently, we can extract the information of the dual theory by a fit to the near boundary behavior of the resulting wavefunctions.

We have optimized our numerics in several ways: The most time-consuming part of the algorithm is the repeated calculation of the Dirac fermion spectrum. A significant improvement is obtained using the perturbative prescription described in a previous section. We exclude the $\phi(z)$ field from the Dirac equation, and instead of four coupled ODE we get for fermions two identical decoupled systems of a second order. Then we construct the corrected wavefunctions. In addition, we do not need to take equally dense sampling in k, because most of the fermionic spectral weight is concentrated around k_F (remember that we have two slighly different Fermi momenta in the theory), and we may take sparser k-sampling away from these points without loss in accuracy.

Empirically we found that different numerical schemes to fermionic and bosonic subsystems was the most efficient. For the fermionic spectrum we use the shooting method: we impose boundary conditions dependent on a free parameter at the boundary cut off $z = \epsilon$, and scan over this parameter to make the resulting solution satisfy physical boundary conditions at the hard wall.

However, the shooting method in the gauge field and scalar sector often leads the system to converge to some higher harmonics instead of the groundstate. The Newton method is much more stable in that case: we impose both AdS-infinity and hardwall boundary conditions at the same time, approximate differential equations by finite differences, and solve the resulting system of linear algebraic equation with a relaxation

algorithm. For our purposes a grid of $N_p = 3000$ points in z-direction (for $z_w = 1$) was chosen, in which case the relaxation algorithm converges after $5 - 6$ iterations.

Once the bulk wave functions are obtained, it is still not a trivial question how to extract the leading boundary behavior from this data. This is what contains the information of the dual field theory. The analytical puzzles related to this problem were discussed in section 2.A. Here we focus on corresponding numerical issues.

We are interested in coefficients $\mathcal{H}_1$, $\mathcal{P}_1$, $\mathcal{P}_3$ defined in (2.51). The function $\phi(z)$ is known in a form of discrete list of values $\{z_i, \phi(z_i)\}$ of the length $N_p = 3000$, therefore our accuracy is limited and naive use of the standard fitting schemes of *Mathematica* leads to large errors.

Instead we first determine the expansion coefficients of the fermionic bilinear sourcing the scalar field

$$-i\eta_5 z^3 \langle \overline{\psi^c} \Gamma^5 \psi \rangle = \mathcal{S}_1 z^5 + \mathcal{S}_3 z^7 + ... \tag{2.84}$$

These can be easily found, as contra to the scalar field profile the fermionic bulk wave functions are derived with a great accuracy due to the use of the shooting method.

Then we use the algebraic relations (2.51) to obtain the "particular" coefficients on the base of $\mathcal{S}_i$.

Knowing $\mathcal{P}_1$ and $\mathcal{P}_3$ we can subtract these from the scalar wave function and run the Newton relaxation scheme one more time for

$$\tilde{\phi}(z) = \phi(z) - \mathcal{P}_1 z^5 - \mathcal{P}_3 z^7. \tag{2.85}$$

We now need to fit only for the single coefficient $\mathcal{H}_1$. This can be easily done even for moderate number of discretized points N_p.

Bibliography

[1] C. P. Herzog, P. Kovtun, S. Sachdev and D. T. Son, "Quantum critical transport, duality, and M-theory," Phys. Rev. D **75**, 085020 (2007) [hep-th/0701036].

[2] S. A. Hartnoll, P. K. Kovtun, M. Muller and S. Sachdev, "Theory of the Nernst effect near quantum phase transitions in condensed matter, and in dyonic black holes," Phys. Rev. B **76**, 144502 (2007) [arXiv:0706.3215 [cond-mat.str-el]].

[3] S. S. Gubser, "Breaking an Abelian gauge symmetry near a black hole horizon," Phys. Rev. D **78**, 065034 (2008) [arXiv:0801.2977 [hep-th]].

[4] S. A. Hartnoll, C. P. Herzog and G. T. Horowitz, "Building a Holographic Superconductor," Phys. Rev. Lett. **101**, 031601 (2008) [arXiv:0803.3295 [hep-th]].

[5] S. A. Hartnoll, C. P. Herzog and G. T. Horowitz, "Holographic Superconductors," JHEP **0812**, 015 (2008) [arXiv:0810.1563 [hep-th]].

[6] H. Liu, J. McGreevy and D. Vegh, "Non-Fermi liquids from holography," Phys. Rev. D **83**, 065029 (2011) [arXiv:0903.2477 [hep-th]].

[7] M. Cubrovic, J. Zaanen and K. Schalm, "String Theory, Quantum Phase Transitions and the Emergent Fermi-Liquid," Science **325**, 439 (2009) [arXiv:0904.1993 [hep-th]].

[8] T. Hartman and S. A. Hartnoll, "Cooper pairing near charged black holes," JHEP **1006**, 005 (2010) [arXiv:1003.1918 [hep-th]].

[9] T. Faulkner, G. T. Horowitz, J. McGreevy, M. M. Roberts and D. Vegh, "Photoemission 'experiments' on holographic superconductors," JHEP **1003**, 121 (2010) [arXiv:0911.3402 [hep-th]].

[10] S. S. Gubser, F. D. Rocha and P. Talavera, "Normalizable fermion modes in a holographic superconductor," JHEP **1010**, 087 (2010) [arXiv:0911.3632 [hep-th]].

[11] J. -W. Chen, Y. -J. Kao and W. -Y. Wen, "Peak-Dip-Hump from Holographic Superconductivity," Phys. Rev. D **82**, 026007 (2010) [arXiv:0911.2821 [hep-th]].

[12] S. Sachdev, "A model of a Fermi liquid using gauge-gravity duality," Phys. Rev. D **84**, 066009 (2011) [arXiv:1107.5321 [hep-th]].

[13] J. de Boer, K. Papadodimas and E. Verlinde, "Holographic Neutron Stars," JHEP **1010**, 020 (2010) [arXiv:0907.2695 [hep-th]].

[14] S. A. Hartnoll and A. Tavanfar, "Electron stars for holographic metallic criticality," Phys. Rev. D **83**, 046003 (2011) [arXiv:1008.2828 [hep-th]].

[15] Y. Liu, K. Schalm, Y. W. Sun and J. Zaanen, "BCS instabilities of electron stars to holographic superconductors," JHEP **1405**, 122 (2014) [arXiv:1404.0571 [hep-th]].

[16] A. Allais, J. McGreevy and S. J. Suh, "A quantum electron star," Phys. Rev. Lett. **108**, 231602 (2012) [arXiv:1202.5308 [hep-th]].

[17] A. Allais and J. McGreevy, "How to construct a gravitating quantum electron star," Phys. Rev. D **88**, 066006 (2013) [arXiv:1306.6075 [hep-th]].

[18] C. P. Herzog and J. Ren, "The Spin of Holographic Electrons at Nonzero Density and Temperature," JHEP **1206**, 078 (2012) [arXiv:1204.0518 [hep-th]].

[19] Y. Seo, S. -J. Sin and Y. Zhou, "Thermal Mass and Plasmino for Strongly Interacting Fermions," JHEP **1306**, 076 (2013) [arXiv:1305.1446 [hep-th]].

[20] D. Bertrand, "A Relativistic BCS Theory of Superconductivity", PhD Thesis, Louvain 2005. [http://cp3.irmp.ucl.ac.be/upload/theses/phd/bertrand.pdf]

[21] S. Bolognesi and D. Tong, "Magnetic Catalysis in AdS4," Class. Quant. Grav. **29**, 194003 (2012) [arXiv:1110.5902 [hep-th]].

[22] S. Bolognesi, J. N. Laia, D. Tong and K. Wong, "A Gapless Hard Wall: Magnetic Catalysis in Bulk and Boundary," JHEP **1207**, 162 (2012) [arXiv:1204.6029 [hep-th]].

[23] T. Nishioka, S. Ryu and T. Takayanagi, "Holographic Superconductor/Insulator Transition at Zero Temperature," JHEP **1003**, 131 (2010) [arXiv:0911.0962 [hep-th]].

[24] G. T. Horowitz and B. Way, "Complete Phase Diagrams for a Holographic Superconductor/Insulator System," JHEP **1011**, 011 (2010) [arXiv:1007.3714 [hep-th]].

[25] S. Caron-Huot, P. Kovtun, G. D. Moore, A. Starinets and L. G. Yaffe, "Photon and dilepton production in supersymmetric Yang-Mills plasma," JHEP **0612**, 015 (2006) [hep-th/0607237].

[26] Y. Liu, K. Schalm, Y. -W. Sun and J. Zaanen, "Bose-Fermi competition in holographic metals," JHEP **1310**, 064 (2013) [arXiv:1307.4572 [hep-th]].

[27] F. Nitti, G. Policastro and T. Vanel, "Dressing the Electron Star in a Holographic Superconductor," JHEP **1310**, 019 (2013) [arXiv:1307.4558 [hep-th]].

[28] A. L. Fitzpatrick, E. Katz, D. Poland and D. Simmons-Duffin, "Effective Conformal Theory and the Flat-Space Limit of AdS," JHEP **1107**, 023 (2011) [arXiv:1007.2412 [hep-th]].

[29] J. Fan, "Effective AdS/renormalized CFT," JHEP **1109**, 136 (2011) [arXiv:1105.0678 [hep-th]].

[30] P. Fulde and R. A. Ferrell, Phys. Rev. **135**, A550 (1964).

[31] A. I. Larkin and Yu. N. Ovchinnikov, Zh. Eksp. Teor. Fiz. **47**, 1136 (1964); translation: Sov. Phys. JETP, **20**, 762 (1965).

[32] M. Ammon, J. Erdmenger, M. Kaminski and P. Kerner, "Flavor Superconductivity from Gauge/Gravity Duality," JHEP **0910**, 067 (2009) [arXiv:0903.1864 [hep-th]].

[33] M. Ammon, J. Erdmenger, M. Kaminski and A. O'Bannon, "Fermionic Operator Mixing in Holographic p-wave Superfluids," JHEP **1005**, 053 (2010) [arXiv:1003.1134 [hep-th]].

Chapter 3

Non-perturbative emergence of non-Fermi liquid behaviour in $d = 2$ quantum critical metals

3.1 Introduction

A complete classification of infrared universality classes for phases of quantum matter at finite density is an open problem in condensed matter theory. Experimentally, a number of fermionic states of matter that exhibit breakdown of the quasiparticle Fermi-liquid paradigm [7] are known to exist, e.g. the strange metallic phase of unconventional superconductors [8] or the non-Fermi liquid phase of graphene [9, 10]. Theoretically, however, they are not understood. These phases are strongly interacting and this prevents the use of most conventional approaches that rely on perturbation theory.

One important scenario which is widely believed to cause the partial destruction of Fermi surfaces and substantial change of transport properties of the electronic state in high-T_c compounds [11], heavy fermion systems [12], and Mott insulators [13, 14] is the interaction of electronic quasiparticles with gapless bosons. The underlying physics is the proximity of a quantum critical point and these bosons are the protected emergent gapless collective degrees of freedom [15, 5, 11]. The nature of the fermion-boson interaction is determined by the precise details of the quantum critical point — ferromagnetic [17] or antiferromagnetic [18] spin density waves, Kondo impurities [19], etc; see [6] for a review.

Qualitatively the simplest model that should already capture the nontrivial physics is the theory of spinless fermions at finite density interacting with a massless scalar through a straightforward Yukawa coupling. The

action of this theory is:

$$S = \int \mathrm{d}x\mathrm{d}y\mathrm{d}\tau \left[\psi^\dagger \left(-\partial_\tau + \frac{\nabla^2}{2m} + \mu \right) \psi + \frac{1}{2} \left(\partial_\tau \phi \right)^2 + \frac{1}{2} \left(\nabla \phi \right)^2 + \lambda \phi \psi^\dagger \psi \right]. \tag{3.1}$$

This model is believed to describe the Ising-nematic transition (see e.g. [11, 20]), observed for example in $YBa_2Cu_3O_y$, There, the meaning of the boson is the fluctuating order parameter related to the $C_4 \to C_2$ symmetry breaking of the electronic correlations. In the ordered phase the mass square of the boson is positive $M^2 > 0$, while in the disordered phase $M^2 < 0$. For non-zero mass we obtain a regular Fermi-liquid at low frequency. By choosing $M = 0$ we tune our theory to criticality where we expect non-Fermi liquid behavior. The model is also closely related to the theory of fermionic spinon excitations in a spin density wave minimally coupled to $U(1)$; at low energies only the transverse component of the gauge field survives and acts as the scalar above (see e.g. [24]).

Eq. (3.1) and related models of finite density fermions coupled to critical bosons were first studied in detail by Hertz [15] and Millis [5], but their results do not apply in 2+1 dimensions. For $d = 2$ the coupling λ is relevant [11], and can drive the system to a qualitatively new groundstate. This novel non-Fermi liquid groundstate is out of range of perturbation theory, and the fermion sign problem prevents us from using efficient numerical techniques.

Our work continues on a recent revival of interest in determining this groundstate. The crucial physics that is thought to control the non-Fermi liquid behavior is the Landau damping: the quantum fermion-loop corrections to the boson two-point correlation function/self-energy. By extending the model to an arbitrary number of fermions N_f and bosons N_b, one can enhance this physics in a limit where the number of fermion flavors N_f is much larger than the number of bosonic degrees of freedom ($N_f \gg N_b$); it is easily seen at the one loop level that this enhances the "Landau-damping" diagram in Fig. 3.1(b) compared to the self-energy Fig. 3.1(a). In this $N_f \gg N_b$ regime the problem of a Fermi surface coupled to the Ising nematic and spin density wave order parameters has been considered in [20, 21] and an extensive perturbative renormalization group analysis has been performed up to three loops (higher order effects are investigated in [22, 23]). However, as pointed out in these papers and [24], in the (vector) large N_f expansion one still needs to sum infinitely many diagrams.

Figure 3.1. One loop corrections to fermion (a) and boson (b) self-energies due to Yukawa interaction. For a gapless boson (b) is the one loop contribution to Landau damping: this contribution to the self-energy can dominate in the IR. This term (b) is clearly proportional to the number of fermions N_f in contrast to the one-loop correction to the fermion self-energy (a). In the limit $N_f \gg N_b$ the boson self-energy/Landau damping therefore dominates, whereas it is suppressed in the opposite limit $N_f \ll N_b$.

(A well-defined expansion can be obtained by introducing an arbitrary dynamical critical exponent for the boson, z_b, as an extra control parameter [25].)

Here, however, we show that Landau damping is not essential to obtain exotic non-Fermi liquid physics in the IR. We will study correlation functions of the theory in the opposite limit $N_f \to 0$; $N_b = 1$. This so-called quenched limit discards all fermion loop contributions. As $N_f \ll N_b$ it shares common ground with recent matrix large N expansions of this model where the boson is taken to transform in the adjoint of an $SU(N)$ and the fermions in the fundamental, see e.g. the studies [26–29], but the strict quenched limit is more comprehensive. In the matrix large N limit where $N_f = N$ and $N_b = N^2$ with $N \gg 1$, not only the diagrams with fermion loops but also diagrams with crossed boson lines are suppressed (Fig. 3.2), whereas these are kept in the quenched approximation. By inspection of the associated momentum integral it is clear, however, that crossed boson corrections are important contributions to the IR physics. The IR of the quenched theory will therefore be different from the large N matrix limit and perhaps closer to that of the full theory.

Physically the quenched approximation we study here means the following: as pointed out in [29] there is a distinct energy scale where Landau damping becomes important. This is the scale where the fermion one-loop correction proportional to N_f becomes comparable to the leading boson dispersion — this happens at $E_{\rm LD} \sim \sqrt{\lambda^2 N_f k_F}$ (see the end of section 3.2.1). By considering small N_f we are suppressing this scale and we are zooming in on the energy regime directly above the Landau damping scale

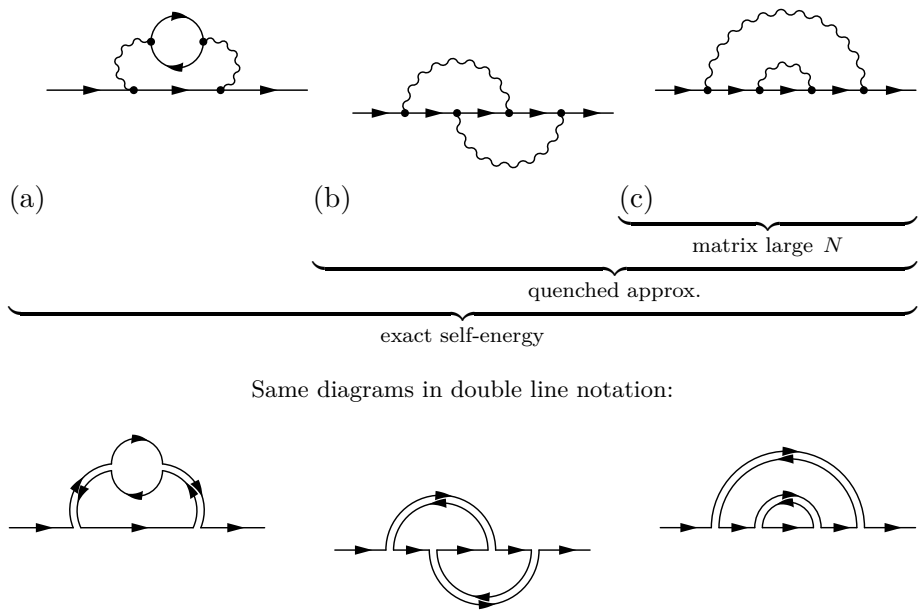

Figure 3.2. The two-loop contributions to the fermion self-energy in theory in Eq. (4.2). The quenched limit where $N_f \to 0$ only suppresses the fermion loop contribution Fig. (a), whereas matrix large N limits, where the boson is a $N \times N$ matrix $\phi_i{}^j$ and the fermion a N-component vector ψ_i also suppress crossed diagrams of type (b). This is evident in double line notation of the same Feynman diagrams where the fermion is written as a single line (it has one index) and the matrix-valued boson as two lines (it has two indices). Indices have to match at interactions; each closed loop therefore corresponds to a sum over this index and gives a weight N to the diagram. We then see that the crossed diagram has no loops and is thus sub-dominant in N to other diagrams at the same order in the coupling constant.

E_{LD} (see Fig. 3.3).[1]

The quenched approximation has an additional benefit. Under the assumption that that the cut-off of the boson is much smaller than the Fermi momentum ($k_F \gg \Lambda_{\mathrm{UV}}$), the small N_f limit also allows us to consistently focus on a small local patch (see Fig. 3.3) around the Fermi surface where the fermionic excitations disperse linearly. The reason the curvature effects are negligible and the global structure of the Fermi surface becomes irrelevant, is that their influence on the IR physics is also through Landau damping. If the Landau damping is not negligible, one does have to either work with the full Fermi surface (i.e. in [26–29] for the case of spherical Fermi surface) or at least consider the antipodal patch since the dominant contribution is coming from there [20, 21]. Specifically, as we discuss below, Landau damping depends both on the Fermi-surface curvature $\kappa \sim \frac{1}{k_F}$ and N_f as N_f/κ. After the quenched approximation $N_f \to 0$ for fixed κ, we may subsequently take κ small as well.

The remarkable fact is that with these approximations the fermion Green's function can be determined exactly (directly in $d = 2$ spatial dimensions). We achieve this by solving the differential equation for the Green's function in a background scalar field and then evaluating the bosonic path integral. Similar functional techniques have been used in high energy physics, for example in the study of high temperature QED plasma [30], lattice QCD [31] or for solving the so-called Bloch-Nordsieck model (which is QED in the quenched approximation) [32–34, 31, 35]. In condensed matter context, the fact that the fermion spectral function is exactly solvable in these limits was also observed for finite density fermions coupled to a transverse gauge field by Khveshchenko and Stamp [36] and independently by Ioffe, Lidsky, Altshuler and Millis [37, 38], though the latter solve the model by bosonization.

At the technical level, the reason the spectral function can be solved exactly in the quenched limit is that propagators of linearly dispersing fermions (the local patch approximation) obey special identities. These allow a rewriting of the loop expansion in such a way that it can be resummed completely, or rather that it can be recast as the solution to a tractable differential equation. We show this in section 3.2. Note, that our method does not rely on renormalization group techniques. When we are to define an RG flow, we have to choose a proper decimation scheme.

[1] There are other ways to suppress the Landau damping physics, e.g. by considering large (UV) Fermi velocity, but we will not be considering these cases here.

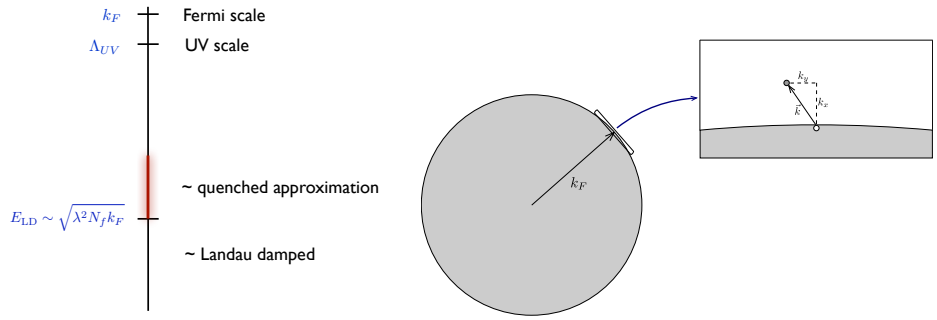

Figure 3.3. Left: The energy scales relevant to 2+1 dim. finite density fermions coupled to a massless boson. We assume the theory is already truncated at a UV cut-off $\Lambda_{\rm UV}$ lower than the Fermi scale k_F. The quenched $N_f \to 0$ limit focuses in on the intermediate energy regime right above the scale $E_{\rm LD} \sim \sqrt{\lambda^2 N_f k_F}$ where Landau damping becomes important.
Right: A small patch of the Fermi surface. In a small region near the Fermi level the surface curvature is negligible. Fermionic excitations can acquire both orthogonal k_x and tangent k_y momenta, but the latter does not contribute to the kinetic energy of the excitation. In the $N_f \to 0$ limit each patch decouples from other parts of the Fermi surface.

In relativistic field theories, it is natural to define the cut-off in a way that maintains the Lorentz invariance, while for the non-relativistic model of critical metals the choice of the cut-off is ambiguous, see e.g. [26].

These exact results in quenched approximation then allow us to establish that the IR fermion physics, even in the absence of Landau damping, is already that of a non-Fermi liquid. Specifically we show in section 3.3 that:

- The naive free Fermi surface breaks apart into three. A thin external shell of it splits apart from the rest, and we effectively have three nested singular surfaces (see Fig. 3.4). This immediately follows from the fact that in a region around the original (free) Fermi level the dispersion of fermion changes sign, $\frac{d\omega}{dk_x} < 0$. This can be interpreted as a topological instability of the Fermi surface [22], as the dispersion curve must cross the Fermi energy two more times

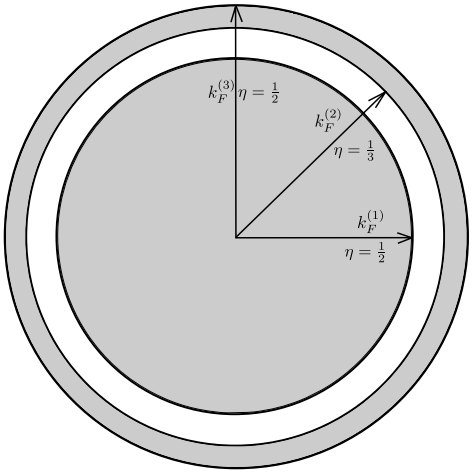

Figure 3.4. The emergent Fermi surface structure at low energy in the 2+1 dimensional quenched planar patch quantum critical metal. Due to the interactions the naive single Fermi surface is topologically unstable. The excitations around the Fermi surfaces are not well-defined quasiparticles, instead they have a continuous spectrum corresponding to a Green's function of the type $G(\omega, k) \sim (\omega - vk)^{-\eta}$ with scaling dimensions η. The different values of η at each of the emergent singular surfaces are mentioned.

to connect to the free UV theory. Luttinger's theorem nevertheless continues to hold.

- The Fermi-liquid quasiparticle pole is destroyed by the interaction with the critical boson. Instead the spectrum is singular everywhere on the dispersion curve. Specifically near the three Fermi surfaces the singular Green's function takes a scaling form with different scaling dimensions. Around the original Fermi momentum the Green's function behaves as $G(\omega, k_x) \sim (\omega + ck_x)^{-1/3}$, where c is the dispersion velocity of the boson; around the two split-off Fermi surfaces behaves as $G(\omega, k) \sim (\omega - v^* k_x)^{-1/2}$ with v^* an emergent dispersion velocity $0 < v^* < v_F$.

We conclude this chapter with a brief outlook in section 4.6.

3.2 2+1 dimensional quantum critical metals in the patch approximation

As stated, the theory we study is that of N_f spinless fermionic flavours at finite density minimally coupled to a critical (relativistically dispersing) boson in $2+1$ dimensions. It has the Euclideanized action

$$S = \int \mathrm{d}x\mathrm{d}y\mathrm{d}\tau \left[\psi_j^\dagger \left(-\partial_\tau + \frac{\nabla^2}{2m} + \mu\right)\psi^j + \frac{1}{2}\left(\partial_\tau\phi\right)^2 + \frac{1}{2}\left(\nabla\phi\right)^2 + \lambda\phi\psi_j^\dagger\psi^j\right] \tag{3.2}$$

with $j = 1 \ldots N_f$; we will show below that the rotation back to real time has no ambiguities. Assuming that the theory is still weakly coupled at scales much below the Fermi momentum k_F, we may make a local approximation around a patch of the Fermi surface and truncate the fermion kinetic term to (Fig. 3.3) [11]

$$S_P = \int \mathrm{d}x\mathrm{d}y\mathrm{d}\tau \left[\psi_j^\dagger(-\partial_\tau + iv\partial_x)\psi^j + \right. \tag{3.3}$$

$$\left. + \frac{1}{2}\left(\partial_\tau\phi\right)^2 + \frac{1}{2}\left(\partial_x\phi\right)^2 + \frac{1}{2}\left(\partial_y\phi\right)^2 + \lambda\phi\psi_j^\dagger\psi^j\right]. \tag{3.4}$$

Two comments are in order. (1) Though it is very well known that the leading "Fermi surface curvature" correction to the kinetic term $\mathcal{L}_{\mathrm{curv}} = -\kappa\psi_j^\dagger\partial_y^2\psi^j/2 + \ldots$ is a dangerously irrelevant operator important for fermion loops even at low energies, in the $N_f \to 0$ limit (where there are no fermion loops) this operator is safely irrelevant and can be consistently neglected for physics below the scale set by $1/\kappa$. We will show here through exact results that the minimal theory in Eq. (4.2) already has a very non-trivial IR. We shall comment on the relevance of $\mathcal{L}_{\mathrm{curv}}$ to our results below. (2) From a Wilsonian point of view, self-interactions of the boson should also be included. We leave the effect of this term for future investigations and take the action S_P as given from here on and study it on its own.[2]

[2]Note that, although the kinetic term is effectively $(1+1)$-dimensional, the properties of fermionic field are still strongly dependent on the dimensionality of the system, because the fermions interact with the $(d+1)$-dimensional boson. An instructive way to think about the fermion dynamics in dimensions parallel to the Fermi surface, is to Fourier transform in those directions. Because the kinetic term does not depend on these directions, the parallel momenta act as additional global quantum numbers. E.g. in $d = 2$, one therefore has an infinite set of one-dimensional fermionic subsystems, labeled by k_y. The Yukawa interaction with the bosons then describes the interactions between these many one-dimensional subsystems.

Throughout this chapter we are mostly interested in the case where the characteristic speed $c = 1$ of the critical bosonic excitations is larger than the Fermi velocity, $c > v$. This need not be the case in the UV. However, as was recently argued [27, 29], the Fermi velocity decreases substantially under the RG flow and because in our analysis we consider energies below a cut-off $\Lambda_{\mathrm{UV}} \ll k_{\mathrm{f}}$, we take this condition for granted as a starting point.

In $d = 2$ spatial dimensions the Yukawa coupling is relevant — λ has scaling dimension $1/2$ — and the theory will flow to a new IR fixed point. Rather than focusing on a complete understanding of the IR of the action Eq. (4.2), we will focus only on understanding a single correlation function: the fermion spectral function. Coupling the fermionic fields to external sources

$$Z[J, J^\dagger] = \int \mathcal{D}\psi^j \mathcal{D}\psi_j^\dagger \mathcal{D}\phi \exp\left(-S_P - J_j^\dagger \psi^j - \psi_j^\dagger J^j\right), \tag{3.5}$$

the fermionic integral is Gaussian and can be easily evaluated yielding

$$Z[J] = \int \mathcal{D}\phi \, \exp\left(-S_b[\phi] - S_{\mathrm{det}}[\phi] - \int d^3z d^3z' J_i^\dagger(z) G_j^i[\phi](z;z') J^j(z')\right), \tag{3.6}$$

with

$$\begin{aligned} S_b &= \int \mathrm{d}x\mathrm{d}y\mathrm{d}\tau \left[\frac{1}{2}\left(\partial_\tau \phi\right)^2 + \frac{1}{2}\left(\partial_x \phi\right)^2 + \frac{1}{2}\left(\partial_y \phi\right)^2\right] \\ S_{\mathrm{det}} &= \int \mathrm{d}x\mathrm{d}y\mathrm{d}\tau \left[-N_f \mathrm{Tr} \ln G^{-1}[\phi]\right] \end{aligned} \tag{3.7}$$

and $G^i{}_j[\phi](z;z') = \delta_j^i G[\phi](\tau, x, y; \tau', x', y')$ is the fermionic propagator in presence of a background bosonic field configuration. By definition it satisfies

$$\begin{aligned} \left(-\partial_\tau + iv\partial_x + \lambda\phi(\tau, x, y)\right) G[\phi](\tau, x, y; \tau', x', y') = \\ = \delta(\tau - \tau')\delta(x - x')\delta(y - y') \end{aligned} \tag{3.8}$$

Taking functional derivatives with respect to the sources, the full fermion Green's function is then given by a path integral over only the bosonic field:

$$\langle \psi_j^\dagger(z)\psi^i(0)\rangle_{\mathrm{exact}} = \delta_j^i G(z, z') = \delta_j^i \frac{\int \mathcal{D}\phi \, G[\phi](z, z') e^{-S_b[\phi] - S_{\mathrm{det}}[\phi]}}{\int \mathcal{D}\phi \, e^{-S_b[\phi] - S_{\mathrm{det}}[\phi]}}. \tag{3.9}$$

3.2.1 The $N_f = 0$ quenched approximation and Landau damping

We will evaluate this integral in the quenched or Bloch-Nordsieck approximation. This is a well known ad hoc approximation in lattice gauge theory [31] and finite temperature QED [32–35] whereby all contributions from S_{det} are ignored: one sets the one-loop (fermion) determinant to one by hand. In our context we can make this approximation precise. Eq. (3.7) shows that S_{det} is directly proportional to N_f, whereas no other terms are. From Eq. (3.9) it is then clear that this approximation computes the leading contribution to the full fermion Green's function in the limit $N_f \to 0$. Note that we consider the N_f limit within correlation functions and not directly in the partition function.

Diagrammatically this means that one considers only contributions to the full Green's functions that do not contain fermion loops. Fermion loop corrections to the bosonic propagator, however, encode the physics of Landau damping. As discussed, this is important in the deep infrared and requires treatment of the dangerously irrelevant quadratic corrections to the kinetic term $\mathcal{L}_{\text{curv}}$ due to Fermi surface curvature. It is its Landau damping contribution that redirects the RG flow. This can be seen from the one-loop "polarization" correction Π to the boson-propagator at finite N_f.

$$G_B^{-1} = G_{B0}^{-1} + \Pi = q_0^2 - q_x^2 - q_y^2 + \Pi \tag{3.10}$$

The form of the polarization depends on the concrete form of the Fermi surface. In case of a spherical Fermi surface with Fermi momentum k_F its form at the one-loop level for large k_F equals

$$\Pi_{1S}\left(q_0, q_x, q_y\right) = \frac{\left(2\pi\right)^2 \lambda^2 k_F N_f}{v} \left(\frac{|q_0|}{\sqrt{q_0^2 + v^2(q_x^2 + q_y^2)}} \right). \tag{3.11}$$

The Fermi surface curvature κ is inversely proportional to the Fermi momentum $\kappa \sim 1/k_F$, therefore the polarization is controlled by the combination N_f/κ. One immediately sees that there is an energy scale $E_{\text{LD}} \sim \sqrt{\lambda^2 N_f/\kappa}$ where the polarization becomes of order of the leading boson dispersion, where perturbation theory must break down and the theory changes qualitatively.[3] On the other hand, as we explained in the introduction, above this scale E_{LD} one ought to be able to neglect

[3] One may worry that at higher loop order a different scale arises. It turns out,

these contributions to the boson propagator [29, 39]. This is therefore the regime captured by the $N_f \to 0$ limit. Since this $N_f \to 0$ limit tames the dangerous nature of irrelevant Fermi surface curvature κ, this also justifies the patch approximation and linearization of the fermion dispersion relation. In this chapter we focus on this regime; we leave the effects of Landau damping captured by the $\mathcal{O}(N_f)$ corrections for Chapter 4.

The remarkable fact is that in this regime $G_{\text{full}}(z; z')$ can be determined exactly, as we will now show. This is because the fermion two-point function in the presence of a background field $G[\phi](z; z')$ depends on the background bosonic field exponentially. The overall path integral over ϕ therefore remains Gaussian even in presence of the Yukawa interaction. This gives us qualitatively new insight in the physics right above E_{LD}.

3.2.2 The exact fermion Green's function

First, we determine the fermion Green's function in the presence of an external boson field $G[\phi]$. Rather then working in momentum space, it will be much more convenient to work in position space. Note that because the background scalar field $\phi(\tau, x, y)$ can be arbitrary, the fermionic Green's function $G[\phi]$ is not translationally symmetric. However, translational invariance will be restored after evaluating the path integral over ϕ.

Rewriting the background dependent Green's function as

$$G[\phi](\tau_1, x_1, y_1; \tau_2, x_2, y_2) = \tilde{G}_0(\tau_1 - \tau_2, x_1 - x_2, y_1 - y_2) \exp\left(-\lambda V[\phi](\tau_1, x_1, y_1; \tau_2, x_2, y_2)\right), \tag{3.12}$$

with $\tilde{G}_0$ the translationally invariant free Green's function in real space

$$\tilde{G}_0(\tau, x, y) = -\frac{i}{2\pi} \frac{\text{sgn}(v)}{x + iv\tau} \delta(y) \equiv G_0(\tau, x)\delta(y), \tag{3.13}$$

it is readily seen that the solution to the defining Eq. (3.8) is given by

$$V[\phi](\tau_1, x_1, y_1; \tau_2, x_2, y_2) = \int \mathrm{d}x\mathrm{d}y\mathrm{d}\tau \left[\tilde{G}_0(\tau_1 - \tau, x_1 - x, y_1 - y) - \tilde{G}_0(\tau_2 - \tau, x_2 - x, y_2 - y)\right] \phi(\tau, x, y), \tag{3.14}$$

however, that at higher order, contributions to Π are subleading in k_F compared to the one-loop result. This is because for linearized fermion dispersion ($\kappa \to 0$) the properly symmetrized closed fermion loops with more than two fermion lines vanishes [54]. In this chapter where we take the $N_f/\kappa \to 0$ limit we therefore use the unmodified boson propagator G_{B0}.

To be more precise, we need to ensure that the background dependent Green's function (3.12) satisfies proper boundary conditions as well. We did so by considering the problem at finite temperature and volume and taking explicitly the continuum limit. The compact analog of (3.12) has to satisfy antiperiodic boundary condition along the imaginary time direction and periodic boundary condition along the spatial direction. This can be achieved by taking the periodic free fermion Green's function ($\tilde{G}_0^P$) in the exponent Eq. 3.14 and the antiperiodic one ($\tilde{G}_0^{AP}$) in Eq. 3.12. In the continuum limit, however, their functional forms are indistinguishable, and we denote them with the same symbol ($\tilde{G}_0$).

The insight is that the only dependence on ϕ in the background dependent Green's function is in the exponential factor $V[\phi]$ and that this dependence is linear. In combination with the quenched $N_f \to 0$ limit, the path-integral over ϕ Eq. (3.9) needed to obtain the full Green's function is therefore Gaussian, and we can straightforwardly evaluate this to (3.9) to obtain

$$G\left(\tau_1, x_1, y_1; 0\right) = G_0\left(\tau_1, x_1\right) \delta(y_1) \exp\left[I(\tau_1, x_1; 0)\right] \tag{3.15}$$

with

$$I(\tau_1, x_1; 0) = \frac{\lambda^2}{2} \int \mathrm{d}x \mathrm{d}\tau \mathrm{d}x' \mathrm{d}\tau' M(\tau_1 - \tau, x_1 - x; -\tau, -x) \cdot \tag{3.16}$$

$$\cdot G_B(\tau - \tau', x - x', 0) M(\tau_1 - \tau', x_1 - x'; -\tau, -x), \tag{3.17}$$

where

$$M(\tau_1, x_1; \tau_2, x_2) = G_0(\tau_1, x_1) - G_0(\tau_2, x_2) \ , \tag{3.18}$$

and $G_B(\tau - \tau', x - x', y - y') = G_B(\tau, x, y; \tau', x', y')$ equal to the translationally invariant free boson propagator defined by

$$\left(\partial_\tau^2 + \nabla^2\right) G_B(\tau, x, y; \tau', x', y') = -\delta(\tau - \tau')\delta(x - x')\delta(y - y') \ . \tag{3.19}$$

Eq. (3.15) is a remarkable result. In the $N_f \to 0$ quenched approximation the full fermion Green's function still consists of a complicated set of Feynman diagrams that are normally not resummable. In particular at the two-loop level there are rainbow diagrams (Fig. 3.2(c)) and vertex-corrections of self-energies (Fig. 3.2(b)) that do not readily combine to a summable series. The reason why in this $N_f \to 0$ planar patch theory

we can do so, is the existence of the following multiplicative identity of fermion propagators in the planar limit where the dynamics is effectively 1+1 dimensional.

$$G_0(\tau_1, x_1)G_0(\tau_2, x_2) = G_0(\tau_1 + \tau_2, x_1 + x_2)\left(G_0(\tau_1, x_1) + G_0(\tau_2, x_2)\right) \tag{3.20}$$

This identity follows directly from trivial equality

$$(G_0(\tau_1, x_1))^{-1} + (G_0(\tau_2, x_2))^{-1} = (G_0(\tau_1 + \tau_2, x_1 + x_2))^{-1}, \tag{3.21}$$

and has many corollary multiplicative identities for products of $n > 2$ planar fermion propagators. The usual perturbative series and the exact result Eq. (3.15) may seem different but their equality can be proven to all orders. We do so in Appendix 3.A, thereby unambiguously establishing that this is the exact fermion two-point function in the planar theory in the quenched approximation.

3.3 The physics of the planar quenched quantum critical metal

We now show that this all order result for the fermion Green's function, albeit in the quenched $N_f \to 0$ approximation, describes very special physics. In this approximation the fermionic excitations constitute a continuous spectrum of excitations with power-law tails analogous to a critical theory; in particular, there are no distinct quasiparticle excitations. Importantly, in the low energy limit this continuous spectrum centers at three distinct momenta with different exponents for the power-law fall-off.

To exhibit this exotic physics from the exact $N_f \to 0$ Green's function (3.15), we substitute the explicit form of the boson and fermion Green's functions and Fourier transform the internal integrals. For the exponent $I(\tau, x; 0)$ we then have:

$$I(\tau, x; 0) = \frac{\lambda^2}{8\pi^3}\int \mathrm{d}\omega \mathrm{d}k_x \mathrm{d}k_y \frac{\cos(\omega\tau - k_x x) - 1}{(i\omega - vk_x)^2(\omega^2 + k_x^2 + k_y^2)} \tag{3.22}$$

This integral can be done analytically to obtain (for $v^2 \neq 1$)

$$I(\tau, x; 0) = \frac{\lambda^2}{8\pi(1-v^2)} \left[\frac{(\tau - ivx)}{\sqrt{1-v^2}} \log \left(\frac{\tau - ivx + \sqrt{(1-v^2)\,(\tau^2+x^2)}}{\tau - ivx - \sqrt{(1-v^2)\,(\tau^2+x^2)}} \right) \right.$$
$$\left. -2\sqrt{\tau^2+x^2} \right]; \tag{3.23}$$

for $v^2 = 1$ one obtains

$$I_{v^2=1}(\tau, x; 0) = \lambda^2 \frac{(\tau + i\,\mathrm{sgn}(v)x)^2}{12\pi\sqrt{\tau^2+x^2}}. \tag{3.24}$$

This gives us the all order $N_f \to 0$ Green's function in real space.

Analytically continuing in τ for $0 < v < 1$ yields the retarded Green's function. The physics follows from Fourier transforming this real time Green's function to momentum space; this is described in Appendix 3.C. The resulting retarded Green's function in momentum space is given by

$$G_R(\omega, k_x) = \frac{1}{\omega - k_x v + \frac{\lambda^2}{4\pi\sqrt{1-v^2}}\sigma(\omega, k_x)}, \tag{3.25}$$

where $\sigma(\omega, k_x)$ is the root, within $0 < \mathrm{Im}(\sigma) < i\pi$, of the equation

$$\frac{\lambda^2}{4\pi\sqrt{1-v^2}}(\sinh(\sigma) - \sigma\cosh(\sigma)) + v\omega - k_x - \cosh(\sigma)(\omega - k_x v + i\epsilon) = 0 \tag{3.26}$$

A small positive parameter ϵ is introduced to identify the correct root when it otherwise would be on the real axis, which is the case for

$$(k_x + \omega)\left(\lambda^2 \sinh\left(\frac{4\pi\sqrt{1-v^2}(vk_x - \omega)}{\lambda^2}\right) + 4\pi\sqrt{1-v^2}(v\omega - k_x)\right) \geq 0. \tag{3.27}$$

Note that the center-combination $v\omega - k_x$ is correct; we are working in units in which the boson-dispersion velocity $c = 1$. The units can be made correct by restoring c.

Expression (4.4) together with (3.26) is the main technical result of the chapter. We can now extract the insights into the spectrum of fermionic

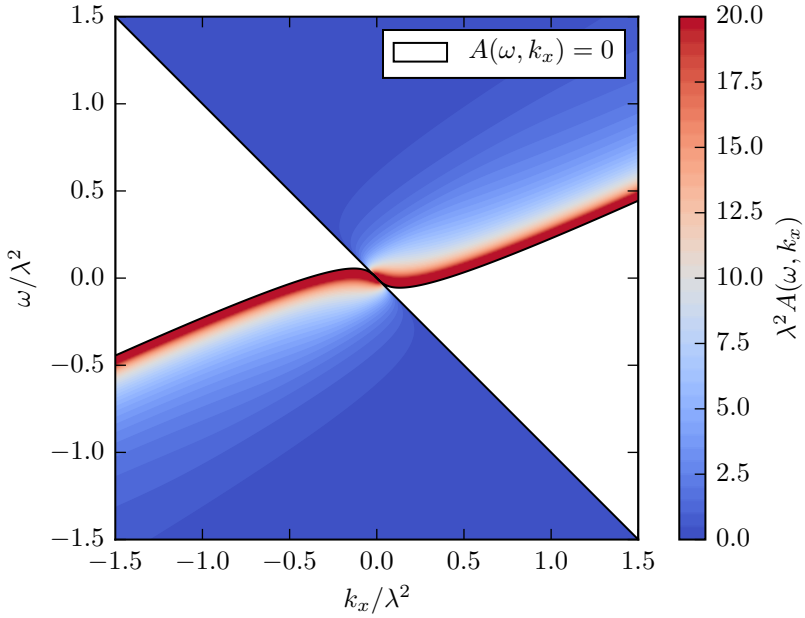

Figure 3.5. Fermionic spectral function for $v = 0.5$. It is identically zero in the white region.

excitations around the ground state of the planar quenched metal. Fig. 3.5 plots the spectral function $A(\omega, k_x) = -2\text{Im}G_R(\omega, k_x)$ as a function of the dimensionless combinations ω/λ^2, k_x/λ^2, as λ is the only scale in the problem. We immediately note that there is an obvious continuous peak, corresponding to a clear excitation in the spectrum. This excitation has the properties that:

- The dispersion relation is S-shaped in the infrared near $k_x = 0$, and now has three intersections with $\omega = 0$. A truncation of the theory to very low energies would therefore indicate three distinct Fermi surfaces. Similar topological Fermi surface instabilities due to electron interaction have been found e.g. in [40]. Curiously the dispersion is nearly identical to the one-loop result.

- As has been demonstrated before by means of a perturbative renormalization group analysis [27], we see the speed of fermions v decreases as we go from high to low frequency/momentum. The dis-

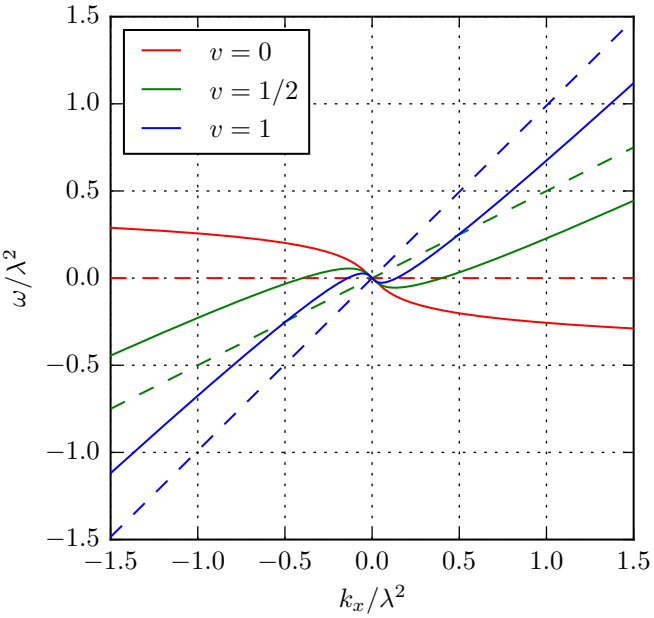

Figure 3.6. The dispersion relation (the zeros of G^{-1}) for different v in the interacting theory (solid line) and the free theory (dashed)

tinct S-shaped curve is outside of the regime of perturbation theory, however. With the exact result we see that the emergent Fermi-velocity at the innermost ($k_x = -k_x^* < 0$) and the outermost ($k_x = k_x^* > 0$) Fermi surfaces is non-universal, but positive and depends on the UV fermionic velocity v. These Fermi-surfaces are therefore particle-like.

However, the reverse of direction due to the S-shape shows that the Fermi velocity at the emergent Fermi-surface at the original Fermi-momentum $k_x = 0$ is now in the opposite direction and the surface is therefore hole-like. Moreover, the value of the emergent Fermi-velocity at $k_x = 0$ is universal: it equals the boson-velocity $v_F = -1$ at $k = 0$ (near the middle Fermi surface), independent of the UV fermionic velocity v (Fig. 3.6). A way to perceive what happens is that the hole-like excitations at $k_x = 0$ become tied to the critical boson which completely dominates the dynamics.

- The three emergent Fermi surfaces are symmetric around $k_x = 0$;

the hole-like one is at $k_x = 0$ and as follows from Eq. (4.4) and (3.26) the two particle-like ones are symmetrically arranged at $\pm k_x^*$. The precise value of k_x^* depends on the initial fermi velocity v. In the planar approximation where the Fermi surface is infinite in extent, this guarantees that Luttinger's theorem holds: the original Fermi surface (the region $-\infty < k_x < 0$) has the same volume as the emergent two regions enclosed by Fermi surfaces ($-\infty < k_x < -k_x^*$ and $0 < k_x < k_x^*$).

- The spectral function, $A(\omega, k_x) = -2\mathrm{Im}G_R(\omega, k_x)$, is identically zero for the range of ω and k_x whenever $\sigma(\omega, k_x)$ is exactly real. This is whenever Inequality (3.27) is satisfied. Such a large range of zero-weight may seem to violate unitarity. As a consistency check, however, it can be demonstrated that the Green's function satisfies the sum rule for all v (Appendix 3.D)

$$\int_{-\infty}^{\infty} \mathrm{d}\omega A(\omega, k_x) = 2\pi, \ \forall k_x \tag{3.28}$$

- Importantly, the weight of the spectral function is infinite at all points of the dispersion relation. Substituting the implicit dispersion relation $\sigma = \frac{4\pi\sqrt{1-v^2}}{\lambda^2}(\omega - vk_x)$ into the constraint Eq. (3.26), one can verify this explicitly. The spectrum is therefore a continuum, and not discrete. The excitation spectrum therefore resembles that of a scale-invariant critical theory, rather than that of interacting particles.

- Focusing on the low-energy regime, i.e. a narrow band in the spectral function around $\omega = 0$, we can determine the spectral weight analytically around the three different Fermi-surfaces — the three different crossings of the dispersion relation with $\omega = 0$. Expanding Eq. (3.26) around $(\omega, k_x) = (0, 0)$ the retarded Greens's function behaves as

$$G_R(\omega, k_x) = C\lambda^{-4/3} |\omega + k_x|^{-1/3}, \tag{3.29}$$

with $C = (1+v)^{1/3} \frac{4\pi}{(12\pi)^{1/3}} \left[i\frac{\sqrt{3}}{2} - \frac{1}{2}\,\mathrm{sgn}(\omega + k) \right]$, whereas near the outer Fermi surfaces $(\omega, k_x) = (0, \pm k_x^*)$ we have

$$G_R(\omega, k_x) \sim \lambda^{-1} (v^* k_x - \omega)^{-1/2}. \tag{3.30}$$

In each case the IR $\omega \simeq 0$ spectral function thus has a clear power-law behavior with a branch-cut singularity, but it has a different exponent depending on the Fermi surface. Furthermore, at the $k_x = 0$ Fermi surface the spectral function is symmetric around ω, while in the other two it is zero for negative (positive) frequencies. This is clearly visible in Fig. 3.5.

Interestingly, in all three cases the power-law scaling conforms with a uniform scaling of energy and momentum corresponding to ground-state with a dynamical critical exponent $z_f = 1$ (consistent with [26, 29]). This is in contrast to the expectation that the 2+1 dimensional quantum critical metal has a $z_f \neq 1$ groundstate [11]. However, the role of Landau damping and Fermi surface curvature is crucial in this expectation, and both are ignored in the planar $N_f = 0$ approximation here.

All these insights are non-perturbative. This can be readily shown by comparing our exact result to the one-loop perturbative answer (Fig. 3.7 and Fig. 3.8). The one-loop result is only a good approximation in the UV, far away from the continuous set of excitations, i.e. the dimensionful Yukawa coupling $\lambda^2 \ll |\omega - v k_x|$. Perturbation theory therefore fails to capture any of the distinct non-Fermi liquid phenomenology of IR of the planar quenched model (with the exception of the shape of the dispersion-curve). Despite the fact that this is not the true IR of the full theory, where Landau damping must also be taken into account, for energies and temperatures slightly above E_{LD} the full physics will resemble this quenched critical non-Fermi-liquid result.

For completeness we can also compute the density of states and the occupation number as a function of momentum. The former gives (see Appendix 3.D)

$$N(\omega) = \int \mathrm{d}k_x \frac{A(\omega, k_x)}{2\pi} = \frac{1}{v}\left[1 + \theta(\lambda^2 \frac{\cosh^{-1}(v^{-1}) - \sqrt{1-v^2}}{4\pi(1-v^2)^{3/2}} - |\omega|)\right]. \tag{3.31}$$

The occupation number can be obtained from the spectral function by using the formula

$$n_{k_x} = \int_{-\infty}^{0} \mathrm{d}\omega \frac{A(\omega, k_x)}{2\pi} \tag{3.32}$$

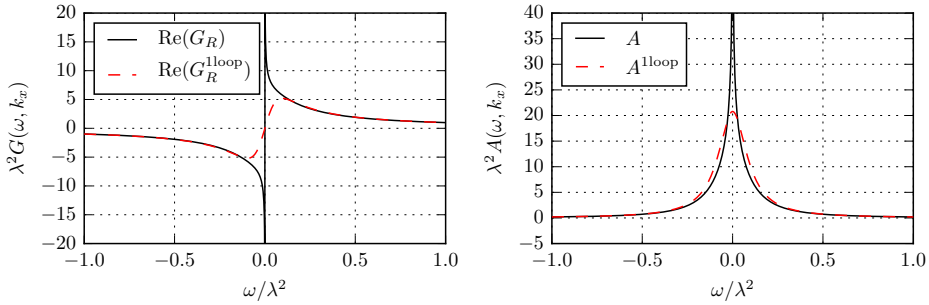

Figure 3.7. The real and the imaginary part of the Green's function at the middle Fermi surface ($k_x = 0$, $v = 0.5$) as a function of ω (solid line), compared with the corresponding one-loop result (dashed)

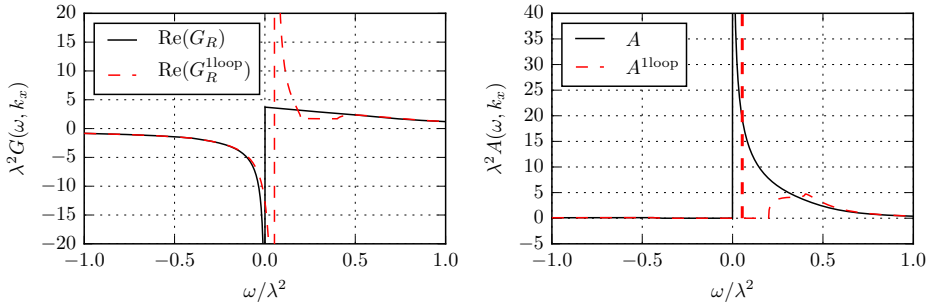

Figure 3.8. The real and the imaginary part Green's function at the outer Fermi surface ($k_x = k_x^* \approx 0.4\lambda^2$, $v = 0.5$) as a function of ω (solid line), and the one-loop truncated result (dashed). The spectral weight of the one-loop approximation is concentrated to a δ-function whereas the spectral weight of the full result is spread in the power-law singularity.

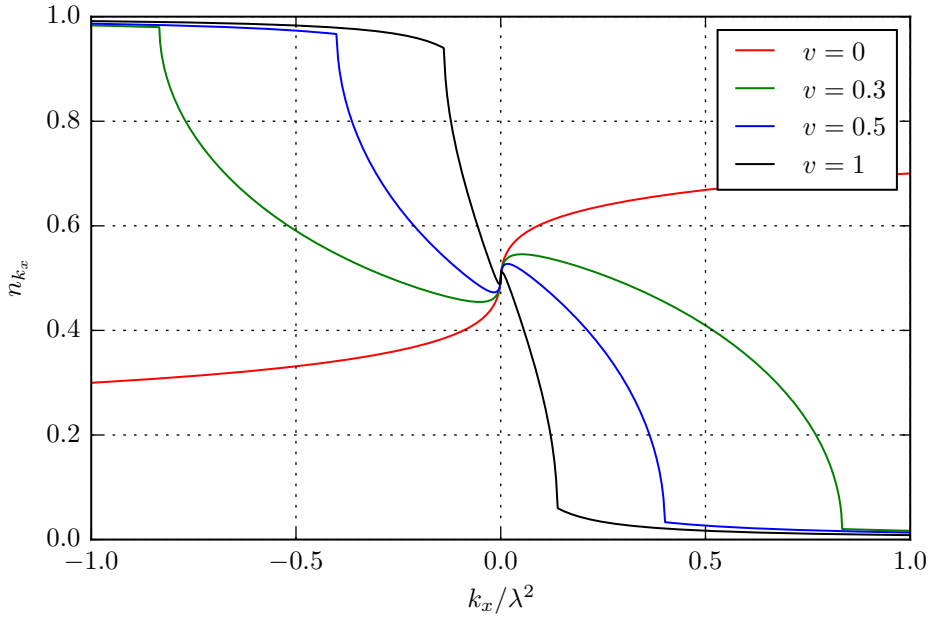

Figure 3.9. The occupation number for different v as a function of momentum. We can see the effect of the multiple sharp fermi surfaces, the non-fermi liquid behaviour is also apparent as a non-monotonic behaviour of the occupation number.

This evaluates to (Appendix 3.D)

$$n_{k_x} = \frac{1}{\pi} \arg \left[\frac{\cosh(\sigma(\omega = 0, k_x/\lambda^2, v)) - v}{v \cosh^{-1}(v) - \sqrt{1 - v^2}(i - 4\pi(1 - v^2)k_x/\lambda^2)} \right], \qquad (3.33)$$

where $\sigma(\omega, k_x)$ is defined by (3.26). It is plotted in Fig. 3.9. We can see the effect of the multiple Fermi surfaces as discontinuities in the derivative of the occupation number, even though the occupation number itself is continuous. This is another way to see that the fermionic excitation spectrum is that of a non-Fermi liquid. (Note that in the singular case of vanishing UV Fermi velocity $v = 0$, the occupation number has different asymptotics as $k_x \to \pm\infty$ than for any small but non-zero v. For $v \neq 0$ the occupation number approaches $n_{k_x} = 1$ at $k_x = -\infty$ and $n_{k_x} = 0$ at $k_x = \infty$, as it should.)

3.4 Conclusions

In this chapter we have shown that in the quenched $N_f \to 0$ limit the fermion Green's function in a 2+1 dimensional quantum critical metal can be determined exactly. The quenched limit neuters the dangerous nature of dimensionally irrelevant Fermi surface corrections and allows us to truncate to a linear dispersion relation for the fermions. This reduction to an effective one-dimensional system allows an explicit solution to the fermion Green's function in the presence of a background scalar field. The quenched $N_f \to 0$ limit further allows us to compute the full background scalar field path-integral when coupled minimally to the fermion.

Even though the quenched limit discards the physics of Landau damping, our result shows that the resulting physics is already very non-trivial. There are three distinct low-energy excitations as opposed to the excitations around a single Fermi surface of the free theory. Most importantly, the sharp excitations of the free theory broaden into a power-law singularity of the spectral function of the form $G \sim (\omega - \epsilon(k_x))^{-\eta}$, with either $\eta = 1/2$ or $\eta = 1/3$. The groundstate is a non-Fermi-liquid.

Beyond the quenched limit and including N_f corrections, i.e. fermion loops, Landau damping effects become important. These effects will show up below some energy scale E_{LD} set by both N_f and the Fermi surface curvature κ. Our model breaks down below this scale, but it is expected to describe the physics above E_{LD}. What our results show is that, qualitatively, the physics is that of a non-Fermi-liquid both above E_{LD} and below E_{LD} [38], but in detail it will differ.

In order to access IR physics below E_{LD}, the corrections in the Fermi surface curvature and the number of fermionic flavours must be treated systematically, but a (possible) shortcut deserves to be mentioned. Our analytic determination of the exact fermionic Green's analytically hinged on the free fermion dispersion being linear, but the approach taken in this chapter does not put any restrictions on the allowed form of the bosonic propagator. This opens up the possibility to implement the Landau-damping effects phenomenologically, just by modifying the background bosonic Green's function, and staying within the Gaussian approximation. This is the approach taken by Khveshchenko and Stamp [36] and Altshuler, Lidsky, Ioffe and Millis [37, 38]. Comparing to vector large N_f approaches [20, 21], it is not clear that this is sufficient to reliably capture the IR. The Landau damping is not the only important effect. Interactions of the boson field with itself beyond the Gaussian approximation

must also be taken into account, e.g. our model needs to be enhanced by a ϕ^4 interaction to describe the Ising-nematic critical point [39].

The interesting question will be which non-Fermi liquid features are retained and which change. The dynamical critical exponent z_f below the Landau damping scale is likely different from 1. Also, the splitting of the Fermi surface seems to be a subtle phenomenon, and whether it remains stable upon including fermionic loop corrections or going beyond the local patch approximation requires a careful investigation. On the other hand, the destruction of the quasi-particle poles and the fact that the spectrum is singular along the full dispersion curve is expected to be a robust effect that resembles that of a critical state. This is thought to be enhanced by the Landau damping.

3.A Comparison with perturbation theory

We can expand (3.15) in the coupling constant. Although at first sight this expansion seems different from the usual perturbative expansion, we will show that in the case of zero fermi surface curvature they match at any order if we do not include fermion loops.

The λ^{2n} term in (3.15) is

$$G_n(z) = \frac{G_0(z)}{2^n n!}\Big(\int dx' dx'' d\tau' d\tau'' \left[G_0\left(z-z'\right)+G_0\left(z'\right)\right] G_B\left(z'-z''\right) \left[G_0\left(z-z''\right)+G_0\left(z''\right)\right] \Big)^n, \tag{3.34}$$

where $z = x + iv\tau$. The usual perturbative expansion result can be obtained by expanding

$$\langle \psi(z)\psi(0)^\dagger \exp(\lambda\phi\psi^\dagger\psi)\rangle \tag{3.35}$$

and evaluating by Wick contraction

$$G_n^{\text{pert}}(z) = \frac{(2n-1)!!}{(2n)!}\int dx_1 ... dx_{2n} d\tau_1 ... d\tau_{2n} I \cdot G_B(x_1-x_2,\tau_1-\tau_2)...\cdot \cdot G_B(x_{2n-1}-x_{2n},\tau_{2n-1}-\tau_{2n}), \tag{3.36}$$

$$I = \sum_{(i_1,..,i_{2n})\in S_{2n}} G_0\left(z - z_{i_1}\right) G_0\left(z_{i_1} - z_{i_2}\right) ... G_0\left(z_{i_{2n-1}} - z_{i_{2n}}\right) G_0\left(z_{i_{2n}}\right) \tag{3.37}$$

Here S_n is the set of permutations of the numbers 1 through n. The factor $1/(2n!)$ comes from the Taylor expansion of the exponential. By summing over the different assignments of internal points we are explicitly counting the different contractions of the fermion fields. There are however still $(2n-1)!!$ possibilities to pair the boson fields (each pairing gives rise to the same contribution after a change of variable in the integral). Since $(2n)!/(2n-1)!! = n! \cdot 2^n$ the identity which remains to be proved, once we have used our simple form of the free fermion Green's function, is

$$\sum_{(i_1,..,i_m)\in S_m} \frac{1}{z - z_{i_1}} \frac{1}{z_{i_1} - z_{i_2}} ... \frac{1}{z_{i_{m-1}} - z_{i_m}} \frac{1}{z_{i_m}} = \tag{3.38}$$

$$= \frac{z^{m-1}}{\left(z - z_1\right)\left(z - z_2\right) ... \left(z - z_m\right) z_1 ... z_m}. \tag{3.39}$$

We need this for $m = 2n$, but the statement is true for odd m as well.

The identity can be proven by induction. The $m = 1$ case is easily checked and given that the equality holds for $m - 1$ we have

$$\sum_{(i_1,..,i_m)\in S_m} \frac{1}{z - z_{i_1}} \frac{1}{z_{i_1} - z_{i_2}} ... \frac{1}{z_{i_{m-1}} - z_{i_m}} \frac{1}{z_{i_m}} = \tag{3.40}$$

$$= \frac{1}{z_1 ... z_m} \sum_{k=1}^{m} \frac{1}{z - z_k} \frac{z_k^{m-1}}{\left(z_k - z_1\right)\left(z_k - z_2\right) ... \left(z_k - z_m\right)}.$$

where the product in the last denominator excludes $(z_k - z_k)$. The right hand side of (3.39) and (3.40) are the same since they are both meromorphic functions of z with the same pole locations and residues and they both approach 0 at ∞.

3.B Calculating the real-space fermion Green's function

To find the real-space Euclidean fermionic Green's function we have to evaluate the integral (3.22). In order to do that, it is convenient to firstly

make a coordinate transformation of the following form

$$\begin{aligned}\omega &= \frac{xk_1 + \tau k_2}{\sqrt{x^2+\tau^2}},\\ k_x &= \frac{xk_1 - \tau k_2}{\sqrt{x^2+\tau^2}}.\end{aligned} \tag{3.41}$$

The integral in k_2 can be then explicitly evaluated, giving

$$\int \mathrm{d}k_1 \mathrm{d}k_y \frac{\lambda^2\left(\tau^2+x^2\right)\left(\cos\left(k_1\sqrt{\tau^2+x^2}\right)-1\right)}{8\pi^2\sqrt{k_1^2+k_y^2}\left(x\left(\sqrt{k_1^2+k_y^2}+|k_1|v\right)-i\tau\left(v\sqrt{k_1^2+k_y^2}+|k_1|\right)\right)^2}. \tag{3.42}$$

Now switching to polar coordinates, $k_1 = k\cos\theta$, $k_y = k\sin\theta$, and performing the radial integral in k we obtain

$$I = \int_0^{2\pi} \mathrm{d}\theta \frac{\lambda^2|\sin(\theta)|\left(\tau^2+x^2\right)^{3/2}}{16\pi(\tau v + ix + |\sin(\theta)|(ivx+\tau))^2}. \tag{3.43}$$

Finally, integrating over θ for $v^2 \neq 1$ we derive

$$I = \frac{\lambda^2}{8\pi(1-v^2)}\left(\frac{(\tau+ivx)}{\sqrt{1-v^2}}\log\left(\frac{\tau+ivx+\sqrt{(1-v^2)\left(\tau^2+x^2\right)}}{\tau+ivx-\sqrt{(1-v^2)\left(\tau^2+x^2\right)}}\right) - 2\sqrt{\tau^2+x^2}\right). \tag{3.44}$$

For the specific case $v^2 = 1$ the integration should be done independently and gives a simpler result

$$I = \lambda^2\frac{(\tau - i\,\mathrm{sgn}(v)x)^2}{12\pi\sqrt{\tau^2+x^2}}. \tag{3.45}$$

To Fourier transform the corresponding Green's function to momentum space, we will need an analytical continuation. For $0 < v < 1$, (3.15) with exponent (3.44) can be analytically continued in τ to the complex plane with two branch-cuts along parts of the imaginary axis

$$G_E(x,\tau) = -\frac{i}{2\pi}\frac{\mathrm{sgn}(v)}{x+iv\tau}\cdot \\ \cdot e^{\frac{\lambda^2}{8\pi(1-v^2)}\left(\frac{(\tau+ivx)}{\sqrt{1-v^2}}\left(i\pi\mathrm{sgn}(x)+2\tanh^{-1}\left(\frac{\tau+ivx}{\sqrt{(1-v^2)(\tau^2+x^2)}}\right)\right)-2\sqrt{\tau^2+x^2}\right)} \tag{3.46}$$

3.C Fourier transforming the fermion Green's function

The next step is to calculate the retarded fermionic Green's function in momentum space. We know that the time-ordered momentum space Green's function of the Lorentzian signature theory, $G_T(\omega)$, is related to the Green's function of the Euclidean theory, $G_E(\omega)$, by analytical continuation

$$G_T(\omega, k_x) = G_E(\omega(-i+\epsilon), k_x). \tag{3.47}$$

$G_T(\omega, k_x)$ is analytic below the real line in the left half plane and above the real line in the right half plane. $G_E(\omega, k_x)$ is the Fourier transform in a generalized sense of (3.46). The (rather severe) divergence at infinity has to be regularized. Since the expression we found in Appendix 3.B permitted an analytic continuation to all of the first and third quadrants, we can continuously rotate the integration contour in the Fourier transform, $\tau = t(i+\delta)$, if additionally there is a regulator analytic in the first and third quadrant. We thus have

$$G_T(\omega, k_x) = \int \mathrm{d}t(i+\delta)\mathrm{d}x \mathrm{e}^{i(\omega(-i+\epsilon)(i+\delta)t - k_x x)} G_E(t(i+\delta), x). \tag{3.48}$$

From this we see that the real-space time-ordered Green's function is given by analytically continuing the real-space Green's function of the Euclidean theory

$$G_T(t, x) = iG_E(t(i+\delta), x). \tag{3.49}$$

This slightly heuristic argument of analytical continuation in real space has been verified to give the correct Green's function up to one loop perturbation theory. The retarded Green's function is given by

$$G_R(\omega, k_x) = \int \mathrm{d}t\mathrm{d}x \mathrm{e}^{i(\omega t - k_x x)} \theta(t)(G_T(t, x) + G_T^*(-t, -x)). \tag{3.50}$$

$G_T(t, x)$ is of the form $t^{-1} f_1(x/t) \exp(\lambda^2 t f_2(x/t))$. By performing a change of variable from x to $u = x/t$ we can perform the t integral. For this we need a regulator $\exp(-\epsilon t)$. The integrand of the remaining u integral has compact support, $u \in [-1, 1]$. We can perform a further change of variables

$$\sigma = \tanh^{-1}\left(\frac{\sqrt{(1-v^2)(1-u^2)}}{1-uv}\right). \tag{3.51}$$

This function maps $[-1, v) \to \mathbb{R}^+$ and $(v, 1] \to \mathbb{R}^+$, both bijectively. The inverse thus has two branches that we need to integrate over, one for $u < v$ and one for $u > v$, and both integrals will be over $\mathbb{R}^+$. This change of variable is consistent with the principal value integral required for the singularity at $u = v$ if the $\sigma \to \infty$ limits are performed at the same time. The integrand obtained with this change of variable can be written as a sum of four pieces

$$G_R(\omega, k_x) = \int_0^\infty \mathrm{d}\sigma \Big[F(\sigma) + F(-\sigma) - F(\sigma + i\pi) - F(-\sigma + i\pi) \Big], \quad (3.52)$$

where $F(\sigma)$ is defined as

$$F(\sigma) = \frac{i}{2\pi} \frac{\sinh(\sigma)}{\frac{\lambda^2(\sinh(\sigma) - \sigma\cosh(\sigma))}{4\pi\sqrt{1-v^2}} + v\omega - k_x - \cosh(\sigma)(\omega - k_x v + i\epsilon)}. \quad (3.53)$$

Since $F(\sigma)$ is a meromorphic function and it approaches 0 as $\mathrm{Re}(\sigma) \to \pm\infty$, we can close the contour at $\pm\infty$ and obtain the integral as the residue of $F(\sigma)$'s single pole in the strip $0 < \mathrm{Im}(\sigma) < i\pi$,

$$G_R(\omega, k_x) = \frac{1}{\omega - k_x v + \frac{\lambda^2}{4\pi\sqrt{1-v^2}}\sigma(\omega, k_x)} \quad (3.54)$$

where $\sigma(\omega, k_x)$ is the solution, within $0 < \mathrm{Im}(\sigma) < i\pi$, of the equation

$$0 = \frac{\lambda^2}{4\pi\sqrt{1-v^2}}(\sinh(\sigma) - \sigma\cosh(\sigma)) + v\omega - k_x - \cosh(\sigma)(\omega - vk_x + i\epsilon). \quad (3.55)$$

The dispersion, $\omega(k_x)$, given by the location of the singularity of $G(\omega, k_x)$ is no longer monotonic as in the free case. The singularity occurs when the roots of (3.55) leave the real line. The dispersion can not be found analytically in general but for the two points where $\mathrm{d}\omega/\mathrm{d}k_x = 0$ we have,

$$\begin{aligned} \omega &= \pm\lambda^2 \frac{\sqrt{1-v^2} - \cosh^{-1}(v^{-1})}{4\pi(1-v^2)^{3/2}}, \\ k_x &= \pm\lambda^2 \frac{\sqrt{1-v^2} - v^2\cosh^{-1}(v^{-1})}{4\pi v(1-v^2)^{3/2}}. \end{aligned} \quad (3.56)$$

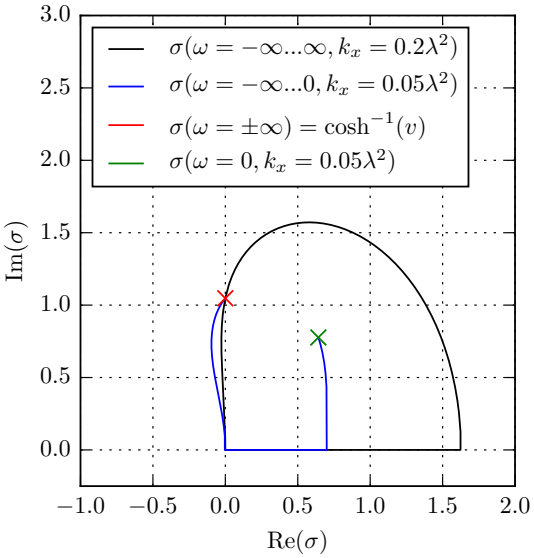

Figure 3.10. This figure shows a closed contour of integration for the sum rule and an open contour for calculating the occupation number integral. $v = .5$.

3.D Integrals of the spectral function

Several important observables like the density of states or the occupation number are defined by momentum space integrals of the spectral function $A(\omega, k) = -2\text{Im}G_R(\omega, k)$. Despite the fact that we have only an implicit expression for the Green's function (3.54), these integrals can be relatively easily evaluated by bringing the imaginary axis projection outside the integral and then changing integration variable to σ. We then do not have a closed form expression for the (now complex) contour of integration but the integrand is greatly simplified.

For a fixed k_x we have ω as a closed form function of σ. Making this change of variable in integrals over ω gives the integrand

$$\int_C \mathrm{d}\omega A(\omega, k_x) = -2\text{Im}\left(\int_{\sigma(C)} \mathrm{d}\sigma \frac{\sinh(\sigma)}{v - \cosh(\sigma)}\right). \tag{3.57}$$

The curve of integration, $\sigma(C)$, is now defined through the implicit expression for σ in (3.55).

First of all we check that the sum rule $\int \mathrm{d}\omega A(\omega, k_x) = 2\pi$ is satisfied. Taking the $\omega \to \pm\infty$ limits in (3.55) we see that σ approaches $\cosh^{-1}(v)$ in both limits and the curve is thus closed. See Fig. 3.10. To solve the integral we thus just have to figure out what poles are within the contour. It turns out that the single pole is the one at $\sigma = \cosh^{-1}(v)$, which is on the contour. This gives divergences but since the residue is real they are in the real part and do not matter for the spectral density. The contribution to the imaginary part is just $2\pi i$ times half the residue since the contour is smooth at the pole. The result of the integral is then 2π as expected, for all values of k_x/λ^2 and v.

The occupation number at zero temperature is given by

$$\rho(k_x) = \int_{-\infty}^{0} \frac{\mathrm{d}\omega}{2\pi} A(\omega, k_x). \tag{3.58}$$

Since this contour is not closed we find a primitive function defined along the whole contour. The contribution from the point $\omega = 0$ depends on $\sigma(\omega = 0, k_x, v)$ so we can not get a closed form expression in this case. The contribution from $\omega \to -\infty$ now depends on the direction of the limit in the complex σ-plane since the point is only approached from one side. Summing the contributions from the two endpoints of the integral gives

$$\rho(k_x) = \frac{1}{\pi} \arg\left[\frac{\cosh(\sigma(\omega = 0, k_x/\lambda^2, v)) - v}{v\cosh^{-1}(v) - \sqrt{1-v^2}(i - 4\pi(1-v^2)k_x/\lambda^2)} \right]. \tag{3.59}$$

From this we see that in the region where σ is real we actually have a closed form expression for the occupation number.

The density of states, $N(\omega) = \int \mathrm{d}k_x A(\omega, k_x)$ is similarly calculated by changing variables to σ. For any ω there is a K_x such that $\sigma(k_x)$ is real for all $|k_x| > K_x$. The limits $k_x \to \pm\infty$ give $\sigma \to \pm\cosh^{-1}(1/v)$ and these are thus approached along the real line. Once again the integrand has poles (residue 1/v) at these points and since we are only interested in the imaginary part of the integral of the retarded Green's function we will only need to know the direction we approach these poles from. Finding a primitive function is again trivial and in the end the result only depends on the direction the poles are approached from. Since σ is real in the limits, each pole is approached from either the left or the right. There are three different cases, for

$$\omega < -\lambda^2 \frac{\cosh^{-1}\left(v^{-1}\right) - \sqrt{1-v^2}}{4\pi(1-v^2)^{3/2}} \tag{3.60}$$

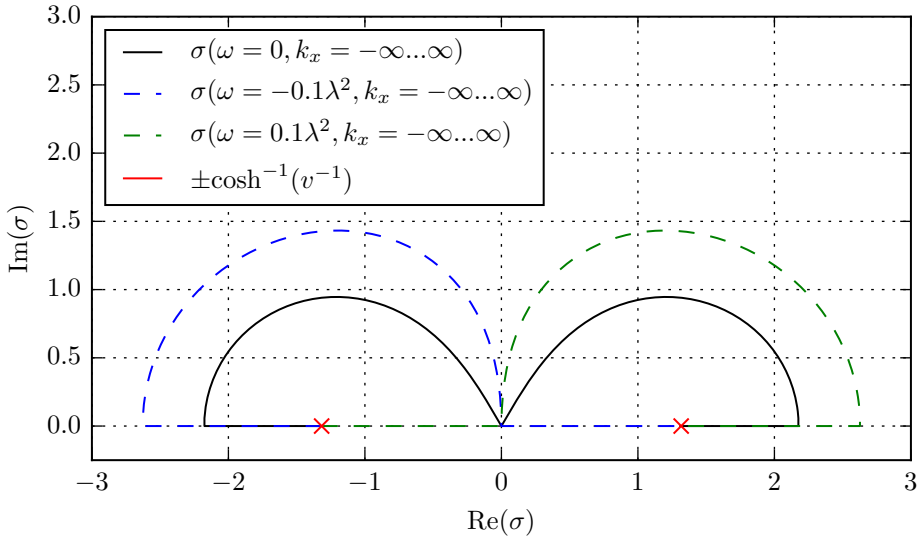

Figure 3.11. Integration contours for calculating density of states. The integrand and locations of the endpoints are independent of ω but since the integrand has poles at the endpoints the direction of approach matters. The poles are always approached along the real axis and this figure shows the three possible configurations. $v = .5$.

both poles are approached from the left. For

$$\omega > \lambda^2 \frac{\cosh^{-1}\left(v^{-1}\right) - \sqrt{1-v^2}}{4\pi(1-v^2)^{3/2}} \tag{3.61}$$

both poles are approached from the right and for ω between these two values the left pole is approached from the left and the right pole from the right. See Fig. 3.11. Taking these different limits of the primitive function gives

$$N(\omega) = \frac{1}{v}\left[1 + \theta(\lambda^2 \frac{\cosh^{-1}\left(v^{-1}\right) - \sqrt{1-v^2}}{4\pi(1-v^2)^{3/2}} - |\omega|)\right]. \tag{3.62}$$

The density of state takes two different values and we see that the ω where it changes are exactly the points where there are two instead of one solution in k_x to the equation $G^{-1}(\omega, k_x) = 0$.

Bibliography

[1] L. D. Landau, "The theory of a Fermi liquid," Sov. Phys. Jetp-Ussr **3(6)**, 920-925 (1957)

[2] C. M. Varma, P. B. Littlewood, S. Schmitt-Rink, E. Abrahams and A. E. Ruckenstein, "Phenomenology of the normal state of Cu-O high-temperature superconductors," Phys. Rev. Lett. **63** (1989) 1996

[3] Y. Barlas and K. Yang, "Non-Fermi-liquid behavior in neutral bilayer graphene," Phys. Rev. B **80** (2009) 161408(R); arXiv:0908.1238 [cond-mat.mes-hall]

[4] F. Guinea and M. I. Katsnelson, "Many-Body Renormalization of the Minimal Conductivity in Graphene," Phys. Rev. Lett. **112** (2014) 116604; arXiv:1307.6221 [cond-mat.mes-hall]

[5] D. van der Marel, H. J. A. Molegraaf, J. Zaanen, Z. Nussinov, F. Carbone1, A. Damascelli, H. Eisaki, M. Greven, P. H. Kes, M. Li "Quantum critical behaviour in a high-Tc superconductor," Nature 425, 271-274 (2003); arXiv:cond-mat/0309172

[6] P. Gegenwart, Q. Si, F. Steglich, "Quantum criticality in heavy-fermion metals," Nature Physics 4, 186 - 197 (2008); arXiv:0712.2045 [cond-mat.str-el]

[7] T. Senthil, "Theory of a continuous Mott transition in two dimensions," Phys. Rev. B **78** (2008) 045109; arXiv:0804.1555 [cond-mat.str-el]

[8] T. Misawa and M. Imada, "Quantum criticality around metal–insulator transitions of strongly correlated electron systems," Phys. Rev. B **75** (2007) 115121; arXiv:cond-mat/0612632

[9] J. A. Hertz, "Quantum critical phenomena," Phys. Rev. B **14** (1976) 1165

[10] A. .J. Millis, "Effect of a nonzero temperature on quantum critical points in itinerant fermion systems", Phys. Rev. B **48**, 7183 (1993).

[11] S. Sachdev, "Quantum phase transitions," 2nd Edition, Cambridge University Press 2011 (Chapter 18 especially).

[12] J. Rech, C. Pepin, A. V. Chubukov, "Quantum critical behavior in itinerant electron systems: Eliashberg theory and instability of a ferromagnetic quantum critical point," Phys. Rev. B, f74(19) (2006) 195126; arXiv:cond-mat/0605306

[13] S. Chakravarty, B. I. Halperin and D. R. Nelson, "Two-dimensional quantum Heisenberg antiferromagnet at low temperatures," Phys. Rev. B **39** (1989) 2344

[14] Q. Si, J. L. Smith, K. Ingersent, "Quantum critical behavior in Kondo systems," Int. J. Mod. Phys. B **13** (1999) 2331; arXiv:cond-mat/9905006

[15] H. v. Löhneysen, A. Rosch, M. Vojta, P. Wölfle, "Fermi-liquid instabilities at magnetic quantum phase transitions" Rev. Mod. Phys. **79**, 1015 (2007).

[16] M. A. Metlitski and S. Sachdev, "Quantum phase transitions of metals in two spatial dimensions: I. Ising-nematic order," Phys. Rev. B **82** (2010) 075127 arXiv:1001.1153 [cond-mat.str-el]

[17] M. A. Metlitski and S. Sachdev, "Quantum phase transitions of metals in two spatial dimensions: II. Spin density wave order," Phys. Rev. B **82** (2010) 075128 arXiv:1005.1288 [cond-mat.str-el]

[18] T. Holder and W. Metzner, "Anomalous dynamical scaling from nematic and U(1)-gauge field fluctuations in two dimensional metals," Phys. Rev. B **92** (2015) 4, 041112 arXiv:1503.05089 [cond-mat.str-el]

[19] T. Holder and W. Metzner, "Fermion loops and improved power-counting in two-dimensional critical metals with singular forward scattering," arXiv:1509.07783 [cond-mat.str-el]

[20] S. S. Lee, "Low-energy effective theory of Fermi surface coupled with U(1) gauge field in 2+1 dimensions," Phys. Rev. B **80** (2009) 165102; arXiv:0905.4532 [cond-mat.str-el]

[21] D. F. Mross, J. McGreevy, H. Liu and T. Senthil, "A controlled expansion for certain non-Fermi liquid metals," Phys. Rev. B **82** (2010) 045121; arXiv:1003.0894 [cond-mat.str-el]

[22] A. L. Fitzpatrick, S. Kachru, J. Kaplan and S. Raghu, "Non-Fermi liquid fixed point in a Wilsonian theory of quantum critical metals," Phys. Rev. B **88** (2013) 125116 arXiv:1307.0004 [cond-mat.str-el]

[23] A. L. Fitzpatrick, S. Kachru, J. Kaplan and S. Raghu, "Non-Fermi-liquid behavior of large-N_B quantum critical metals," Phys. Rev. B **89** (2014) 16, 165114 arXiv:1312.3321 [cond-mat.str-el]

[24] R. Mahajan, D. M. Ramirez, S. Kachru and S. Raghu, "Quantum critical metals in $d = 3 + 1$ dimensions," Phys. Rev. B **88** (2013) 11, 115116 arXiv:1303.1587 [cond-mat.str-el]

[25] G. Torroba and H. Wang, "Quantum critical metals in $4 - \epsilon$ dimensions," Phys. Rev. B **90** (2014) 16, 165144 arXiv:1406.3029 [cond-mat.str-el]

[26] J. P. Blaizot and E. Iancu, "The Bloch-Nordsieck propagator at finite temperature," Phys. Rev. D **56** (1997) 7877 arXiv:hep-ph/9706397

[27] M. F. L. Golterman, "Chiral perturbation theory and the quenched approximation of QCD," Acta Phys. Polon. B **25**, 1731 (1994) arXiv:hep-lat/9411005

[28] A. Jakovac and P. Mati, "Resummations in the Bloch-Nordsieck model," Phys. Rev. D **85** (2012) 085006 arXiv:1112.3476 [hep-ph]

[29] A. Kernemann and N. G. Stefanis, "Exact Solutions for Fermionic Green's Functions in the Bloch-nordsieck Approximation of QED," Phys. Rev. D **40** (1989) 2103

[30] A. Jakovác and P. Mati, "Spectral function of the Bloch-Nordsieck model at finite temperature," Phys. Rev. D **87** (2013) 12, 125007 arXiv:1301.1803 [hep-th]

[31] A. Jakovác and P. Mati, "Validating the 2PI resummation: the Bloch-Nordsieck example," Phys. Rev. D **90** (2014) 4, 045038 arXiv:1405.6576 [hep-th]

[32] A. I. Karanikas, C. N. Ktorides and N. G. Stefanis, "On the infrared structure of the one fermion Green's function in QED," Phys. Lett. B **289** (1992) 176

[33] D. V. Khveshchenko and P. C. E. Stamp, "Low-energy properties of two-dimensional fermions with long-range current-current interactions", Phys. Rev. Lett. **71** (1993) 2118

[34] L. B. Ioffe, D. Lidsky, B. L. Altshuler, "Effective lowering of the dimensionality in strongly correlated two dimensional electron gas", arXiv:cond-mat/9403023.

[35] B. L. Altshuler, L. B. Ioffe, A. J. Millis, "On the low energy properies of fermions with singular interactions", Phys. Rev. **B50**, 14048. arXiv:cond-mat/9406024.

[36] A. Allais and S. Sachdev, "Spectral function of a localized fermion coupled to the Wilson-Fisher conformal field theory," Phys. Rev. B **90** (2014) 3, 035131 arXiv:1406.3022 [cond-mat.str-el]

[37] J. Quintanilla and A. J. Schofield, "Pomeranchuk and topological Fermi surface instabilities from central interactions," Phys. Rev. B **74** (2006) 115126; arXiv:cond-mat/0601103 [cond-mat.str-el]

[38] A. Neumayr and W. U. Metzner, "Fermion loops, loop cancellation and density correlations in two-dimensional Fermi systems,' Phys. Rev. B **58** (1998) 15449 doi:10.1103/PhysRevB.58.15449 [cond-mat/9805207]

Chapter 4

The Green's function of a $d = 2$ quantum critical metal at large k_F and small N_f

4.1 Introduction

The robustness of Landau's Fermi liquid theory relies on the protected gapless nature of quasiparticle excitations around the Fermi surface. Wilsonian effective field theory then guarantees that these protected excitations determine the macroscopic features of the theory in generic circumstances [2, 3]. Aside from ordering instabilities, there is a poignant exception to this general rule. These are special situations where the quasiparticle excitations interact with other protected gapless states. This is notably so near a symmetry breaking quantum critical point. The associated Goldstone modes should also contribute to the macroscopic physics. In $d \geq 3$ dimensions this interaction between Fermi surface excitations and gapless bosons is marginal/irrelevant and quantum critical metals can be addressed in perturbation theory as first discussed by Hertz and Millis [15, 5, 6, 16]. In 2+1 dimensions, however, the interaction is relevant and the theory is presumed to flow to a new interacting fixed point [51–53, 16]. This unknown fixed point has been offered as a putative explanation of exotic physics in layered electronic materials such as the Ising-nematic transition. As a consequence, the deciphering of this fixed point theory is one of the major open problems in theoretical condensed matter physics.

In this chapter we show that the fermionic and bosonic spectrum of the most elementary $d = 2$ quantum critical metal can be computed for small N_f in the limit that $k_F \to \infty$ is the largest scale in the problem (but the combination $N_f k_F$ is arbitrary). This strong forward scattering limit provides controlled insights into the properties of the postulated strongly interacting fixed point theory. All the results here refer to the

most elementary quantum critical metal. This is a set of N_f free spinless fermions at finite density interacting with a free massless (Goldstone) scalar through a simple Yukawa coupling. Its action reads (in Euclidean time)

$$S = \int \mathrm{d}x\mathrm{d}y\mathrm{d}\tau \left[\psi_j^\dagger \left(-\partial_\tau + \frac{\nabla^2}{2m} + \mu \right) \psi^j + \frac{1}{2} \left(\partial_\tau \phi \right)^2 + \frac{1}{2} \left(\nabla \phi \right)^2 + \lambda \phi \psi_j^\dagger \psi^j \right], \tag{4.1}$$

where $j = 1 \ldots N_f$ sums over the N_f flavors of fermions and $\mu = \frac{k_F^2}{2m}$. We will assume a spherical Fermi surface to start and consider excitations with momentum close to the Fermi momentum (as in [43]). In other words we often approximate the fermion action with

$$\begin{aligned} S &= \int \mathrm{d}x\mathrm{d}y\mathrm{d}\tau \left[\psi_j^\dagger \left(-\partial_\tau + \frac{\nabla^2}{2m} + \mu \right) \psi^j + \ldots \right] \\ &= \int_{-\Lambda_k}^{\Lambda_k} \frac{(k_F + k)\mathrm{d}k\mathrm{d}\theta}{(2\pi)^2} \mathrm{d}\tau \left[\psi_j^\dagger \left(-\partial_\tau - \frac{k_F}{m} \cdot k + \frac{k^2}{2m} \right) \psi^j + \ldots \right] \\ &= \int_{-\Lambda_k}^{\Lambda_k} \frac{(k_F)\mathrm{d}k\mathrm{d}\theta}{(2\pi)^2} \mathrm{d}\tau \left[\psi_j^\dagger \left(-\partial_\tau - \frac{k_F}{m} \cdot k \right) \psi^j + \ldots \right] \end{aligned} \tag{4.2}$$

with $k \equiv \left| \vec{k} \right| - k_F$ the momentum measured from the Fermi surface, and $\Lambda_k \ll k_F$ in accordance with our assumption that k_F is the largest scale. Note that this is subtly different from the so-called patch model where one splits the Fermi surface into subregions. We will still include the angle-dependence and the quadratic term at crucial points. Ignoring the angle dependence would ignore the leading correction to the boson propagator at low frequencies. This so-called Landau damping contribution becomes strong in the IR and the angle dependence can no longer be neglected (see e.g. [16]). The strong forward scattering limit $k_F \to \infty$ we consider here takes the leading Landau damping contribution into account.

The two features that allow us to compute the fermionic and bosonic spectrum at small N_f and large k_F (with $N_f k_F$ fixed) are:

1. Our earlier finding [48] that in the limit $N_f k_F \to 0$ (which we will refer to as $N_f \to 0$ for simplicity) — which self-consistently suppresses Landau damping and is closely related to the strong forward

scattering limit [49] — the exact fermion retarded Green's function of this model is given by an exponentially "dressed" free Green's function

$$G_{R,N_f\to 0}(r,t) = G_{R,\text{free}}(r,t)e^{I(r,t)} \tag{4.3}$$

with the exponent $I(r,t)$ a closed function in terms of the free boson and fermion Green's function. Due to this simple dressed expression the retarded Green's function and therefore the fermionic spectrum of this model can be determined exactly in the limit $N_f \to 0$. The retarded Green's function in momentum space reads

$$G_{R,N_f\to 0}(\omega,k) = \frac{1}{\omega - kv + \frac{\lambda^2}{4\pi\sqrt{1-v^2}}\sigma(\omega,k)}, \tag{4.4}$$

where σ is the solution of the equation

$$\frac{\lambda^2}{4\pi\sqrt{1-v^2}}(\sinh(\sigma) - \sigma\cosh(\sigma)) + v\omega - k - \cosh(\sigma)(\omega - kv + i\epsilon) = 0, \tag{4.5}$$

with k the distance from the Fermi surface, $v = k_F/m$ is the Fermi velocity, and $\epsilon \to 0^+$ is an $i\epsilon$ prescription that selects the correct root. This quenched $N_f \to 0$ limit ought to reliably capture the physics in the non-perturbative regime $\omega < \lambda^2$ but still above the Landau damping scale $\omega > \omega_{LD} \equiv \sqrt{\lambda^2 N_f k_F}$. This regime already describes interesting singular fixed point behavior: the spectrum exhibits non-Fermi liquid scaling behavior with multiple Fermi surfaces [48]. Eq. (4.4) is obtained by solving the non-linear defining equation for the fermionic Green's function directly. Formally this solution can also be obtained by summing up all diagrams without fermion loops (including the crossed-diagrams). The $N_f \to 0$ limit means that the boson propagator is not corrected by loops.

2. If one inspects the infinite series of corrections to the boson propogator diagram by diagram, one can show that for fermions with a linearized dispersion (strong forward scattering or equivalently $k_F \to \infty$) there is a cancellation among diagrams beyond one-loop [49]. In this limit the bosonic sector is therefore perturbatively determined, at small N_f (but arbitrary value of $N_f k_F$) even for finite

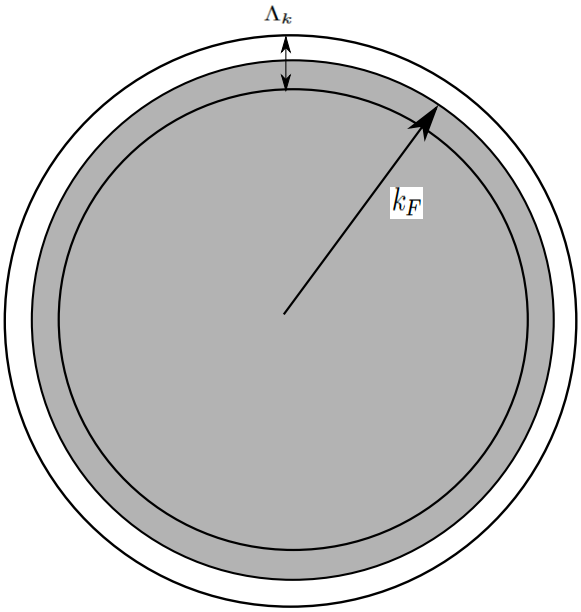

Figure 4.1. We are considering spherical surface and assume that the Fermi momentum k_F is the largest scale. The fermions have a cutoff in momentum space $k_F \gg \Lambda_k$

.

coupling. To put it another way, in the limit $k_F \to \infty$ the one-loop RPA approximation to the boson propagator becomes exact, and all bosonic higher order correlation functions vanish. The latter specifically means that the bosonic action remains quadratic and as a result one can deduce an expression of the form Eq.(4.3) with the free boson propagator replaced by the RPA summed one-loop expression.

The strong forward scattering limit has been related to an effective simplification of the fermion number Ward-identity. We review in Section 4.2 why this simplified Ward identity renders the system solvable. Using the simplified Ward-identity one can deduce a set of non-linear Schwinger-Dyson equations for the fermion and boson two-point functions alone. The vertex function drops out. As a check we recover the real space formula for the non-perturbative in λ, $N_f \to 0$ fermion propagator (in the $k_F \to \infty$ limit) we derived in our earlier paper via path integral

methods [48]. In Section 4.3 we show that the one-loop result of the boson propagator is exact in the limit $k_F \to \infty$, that higher order moments of the boson vanish, and that this also follows from the large k_F non-linear Schwinger-Dyson equations. In Section 4.4 we then show that this implies that the non-perturbative fermion propagator is given by a generalization of the quenched result where the effect of the one-loop corrected boson propagator is taken into account. With these preliminaries in hand we use the bulk of Section 4.4 to solve the non-linear large k_F equation for the fermion spectral function for small N_f —- analytically in real space and numerically in momentum space. In Section 4.5 we collect our results for the 2+1 dimensional quantum critical metal. We conclude with an outlook in Section 4.6.

4.2 A closed system of Schwinger-Dyson equations and large k_F Ward identities for the elementary quantum critical metal

The Schwinger-Dyson equations of a field theory are in general an infinite set of coupled integral equations that together determine the correlations functions exactly. Here we review that using the Ward identity associated with the $U(1)$ symmetry $\psi \to \psi \exp(i\alpha)$ the integral equations describing the relation between the fermionic Green's function G and the bosonic Green's function G_B form a closed system in the limit $k_F \to \infty$.

The Schwinger-Dyson equation which describes the fermionic propagator reads

$$G(K) = G_0(K) + \lambda G_0(K) G(K) \int \mathrm{d}Q \, G_B(Q) G(K-Q) \Gamma(K, K-Q), \tag{4.6}$$

where Q and K are shorthand notation for the collection of momentum and euclidean frequency variables $Q = (iq_0, \vec{q})$, $\mathrm{d}Q = \frac{\mathrm{d}q_0 \mathrm{d}^2\vec{q}}{(2\pi)^3}$; $\Gamma(K, K-Q)$ is the 1PI 3-point vertex and

$$G_0(K) = \frac{1}{ik_0 - \frac{1}{2m}\left(\vec{k}^2 - k_F^2\right)} \tag{4.7}$$

is the free fermion propagator. For completeness we give its derivation in Appendix 4.A.

The analogous boson Schwinger-Dyson equation[1]

$$G_B(Q) = G_{B,0}(Q) - \lambda N_f G_{B,0}(Q) G_B(Q) \int \mathrm{d}K\, G(K) G(K-Q) \Gamma(K, K-Q) \tag{4.8}$$

can be recast in terms of the boson polarization (self-energy) $\Pi \equiv G_B^{-1} - G_{B,0}^{-1}$.

$$\Pi\left(Q\right) = \lambda N_f \int \mathrm{d}K\, G\left(K+Q/2\right) G(K-Q/2) \Gamma(K+Q/2, K-Q/2), \tag{4.9}$$

with

$$G_{B,0} = \frac{1}{q_0^2 + \vec{q}^2}. \tag{4.10}$$

the free boson propagator. This polarization term captures the non-trivial physics of Landau damping.

Usually the system of Schwinger-Dyson equations does not close because the equation for the three-point vertex Γ contains higher point vertices $\Gamma^{(n)}$. For finite k_F the same is true in the model of the elementary quantum critical metal. However, the fermion number symmetry implies a Ward identity between G and Γ. At finite k_F this identity also includes other components Γ^i of the fermion number current. What has been noted for this and similar theories is that for large k_F the current components are proportional to Γ (see e.g. [38, 49, 56]) and the Ward identity collapses to

$$\Gamma\left(P, Q\right) = \lambda \frac{G^{-1}\left(P\right) - G^{-1}\left(Q\right)}{i(p_0 - q_0) - \left(\frac{\vec{p}^2}{2m} - \frac{\vec{q}^2}{2m}\right)} + \ldots. \tag{4.11}$$

We have modified the result obtained there slightly by terms that also vanish as $k_F \to \infty$ such that at lowest order $\Gamma = \lambda + \ldots$ as it should.

Using the large k_F form of the Ward identity (4.11), where we drop the $\ldots$ terms, the Schwinger-Dyson equations (4.6) and (4.9) become a

[1] The extra minus sign is from the fermion loop.

closed set of equations for G_B and G

$$G(K) = G_0(K) + \lambda^2 G_0(K) \int \mathrm{d}Q\, G_B(Q) \frac{G(K-Q) - G(K)}{iq_0 + v\frac{\vec{q}^2}{2k_F} - v|\vec{q}|\cos\theta - v\frac{k}{k_F}|\vec{q}|\cos\theta}, \tag{4.12}$$

$$\Pi(Q) = \lambda^2 N_f \int \mathrm{d}K \frac{G(K-Q/2) - G(K+Q/2)}{iq_0 - v|\vec{q}|\cos\theta - v\frac{k}{k_F}|\vec{q}|\cos\theta}, \tag{4.13}$$

which should become exact in the limit $k_F \to 0$. Here θ is the angle between $\vec{k}$ (measured from the origin) and $\vec{q}$.

Note that the large k_F limit of the Ward identity is crucial to derive this closed set. Therefore, we will drop the subleading terms from the denominators such as k/k_F and $\vec{q}^2/k_F$. The solutions to this closed set of integral equations determine the two-point functions at large k_F and hence the spectrum of the elementary quantum critical metal. We now proceed to study and solve this closed set of equations in the limit $k_F \to \infty$.

4.2.1 The $k_F \to \infty$ limit of the Schwinger-Dyson equations and the fermion two-point function: formal connection with the quenched result

Let us study the consequences of the large k_F limit of the fermion SD-equation (4.12). In this approximation it can be written as

$$\frac{G(k_0,k)}{G_0(k_0,k)} = 1 + \lambda^2 \int \frac{\mathrm{d}q_0 \mathrm{d}q_x}{(2\pi)^2} \mathcal{K}(q_0,q_x) \left[G(k_0-q_0,k-q_x) - G(k_0,k)\right], \tag{4.14}$$

with the kernel

$$\mathcal{K}(q_0,q_x) = \int \frac{\mathrm{d}q_y}{2\pi} \frac{G_B(Q)}{iq_0 - vq_x} \tag{4.15}$$

where $q_x = |\vec{q}|\cos\theta$, $q_y = |\vec{q}|\sin\theta$, i.e. we have aligned the $\vec{q}$-integral with the external momentum $\vec{k}$. In the arguments of the full Green's function $G(k_0,k)$ in Eq. (4.14) we have used the fact that because of spherical symmetry $G(k_0,k)$ can only depend on the distance to the Fermi surface $k = |\vec{k}| - k_F$. In addition, for the spatial argument of $G(K-Q)$ we

have used that $|\vec{k}-\vec{q}|-k_F \approx k-q_x+\mathcal{O}\left(\vec{q}^2/k_F\right)$. The same argument applied to the free fermion propagator $G_0=\frac{1}{iq_0-vq_x}+\ldots$ shows that the denominator in the definition of the kernel in Eq.(4.15) becomes equivalent to G_0. In other words

$$\mathcal{K}(q_0,q_x)=G_0(q_0,q_x)\int\frac{\mathrm{d}q_y}{2\pi}G_B(Q) \tag{4.16}$$

Note that using the notation $G_0(q_0,q_x)$ in the definition of the kernel is somewhat formal. Of course as we mentioned the fermion Green's function is spherically symmetric. To analyze Eq.(4.14) we assume that parity remains unbroken and $G_B\left(Q\right)=G_B\left(-Q\right)$ holds non-perturbatively. Then the term $\int\frac{\mathrm{d}q_0\mathrm{d}q_x}{(2\pi)^2}\mathcal{K}\left(q_0,q_x\right)G\left(k_0,k\right)$ vanishes. We can then solve this integral equation by converting to a differential equation. For this we note that the remaining term on the right-hand side of Eq.(4.14) is a convolution of $\mathcal{K}$ and G, therefore it is advantegeous to write the equation in position space. In position space the term $G_0^{-1}\left(k_0,k\right)=ik_0-vk$ on the left-hand side turns into a differential operator. The position space version of equation (4.14) is

$$\left(\partial_\tau-iv\partial_r\right)G\left(\tau,r\right)=\delta^2(\tau,r)+\lambda^2\mathcal{K}\left(\tau,r\right)G\left(\tau,r\right). \tag{4.17}$$

where we have used the Fourier transform convention

$$G(\tau,r)=\int\frac{\mathrm{d}k_0\mathrm{d}k}{(2\pi)^2}G\left(k_0,k\right)\exp\left(-ik_0\tau+ik\cdot r\right), \tag{4.18}$$

The solution to Eq. (4.17) can be found by using the ansatz $G\left(\tau,r\right)=G_0\left(\tau,r\right)\exp\left(I(\tau,r)\right)$ with the exponent $I(\tau,r)$ satisfying

$$\left(\partial_\tau-iv\partial_r\right)I(\tau,r)=\lambda^2\mathcal{K}\left(\tau,r\right), \tag{4.19}$$

with the boundary condition $I(0,0)=0$.

Since $G_0(\tau,r)$ is the Green's function of the differential operator in Eq. (4.19), the solution for $I(\tau,r)$ is formally given by

$$I(\tau,r)=\lambda^2\int\mathrm{d}r'\mathrm{d}\tau'\left[G_0\left(\tau-\tau',r-r'\right)-G_0\left(-\tau',-r'\right)\right]\mathcal{K}\left(\tau',r'\right). \tag{4.20}$$

By transforming $G_0(\tau,r)$ and $\mathcal{K}(\tau,r)$ back to momentum space we arrive at the expression for the exponent

$$I\left(\tau,r\right)=\lambda^2\int\frac{\mathrm{d}k_0\mathrm{d}k\mathrm{d}k_y}{(2\pi)^3}G_0^2\left(k_0,k\right)G_B\left(k_0,k,k_y\right)\left[\cos\left(ik_0\tau-ikr\right)-1\right]. \tag{4.21}$$

We have used the fact that $G_0^2(K)\,G_B(K)$ is symmetric in K.

We now see the drastic simplification that occurs in the limit $k_F \to \infty$. The solution to the exact fermion Green's function in this limit only depends on the exact boson Green's function $G_B(K)$. Once the latter is known, the fermion Green's function G follows and it in turn determines the exact 1PI three-point vertex Γ.

We noted this exponential form of the fully non-perturbative solution already in the previous chapter [48] that discussed the elementary quantum critical metal in the quenched limit $N_f \to 0$ (see also [36]). In that limit $N_f \to 0$, the polarization Π vanishes and the exact boson propagator $G_B(K)$ in Eq. (4.21) can be replaced by the free one $G_{B,0}(K)$. The explicit expression for the exponent $I(\tau, r)$ and thus the non-perturbative fermion two-point function is then formally known, up to the remaining momentum integrals. These have been evaluated for the quenched $N_f \to 0$ case in [48] with the interesting result that even in the absence of corrections to the boson propagator — the absence of Landau damping — the system already resembles that of a non-trivial fixed point. We now proceed by considering the finite N_f polarization corrections in $I(\tau, r)$. Of course we do so in the same limit $k_F \to \infty$.

4.3 The $k_F \to \infty$ limit of the Schwinger-Dyson equations and the exact boson two-point function

We now turn to the study of the boson two-point function. Diagrammatic studies in perturbation theory have shown that the theory simplifies in the limit $k_F \to \infty$ [49]. In particular, as we shall derive below in section 4.3.3, all n-point scalar correlation functions with $n > 2$ vanish. As a corollary the 1PI boson 2-point function is only corrected at one-loop. This suggests that the solution to the Schwinger-Dyson equations should be more readily obtainable in this limit as well.

We show in this section that the large k_F approximation has such an important simplifying consequence for the bosonic equation. The important physics we refer to is the physics of Landau damping — fermionic corrections to the boson propagator — discussed in the introduction. In this elememtary quantum critical metal, where the boson has no self-interactions, this physics is contained in the polarization $\Pi = G_B^{-1} - G_{B,0}^{-1}$.

Generically the calculation of the polarization Π corresponds to summing up infinitely many diagrams as the Schwinger-Dyson equation (4.13) contains the exact fermion propagator G. However, in the limit $k_F \to \infty$ only the one-loop contribution Π_1 survives (for small N_f at least). The realization that in this strong forward scattering limit many diagrams vanish and only the boson two-point function gets corrected is not new; it has been noted earlier in e.g. [49]. We independently rederive it here. First, however, we will give the one-loop result. Based on that one can give a proof why all higher order corrections vanish.

4.3.1 Polarization/Landau damping contribution at one-loop

The $k_F \to \infty$ one-loop contribution to the polarization that captures the leading order physics of Landau damping is obtained by substituting the $k_F \to \infty$ limit of the free fermion propagator $G_0(k_0, k) = \frac{1}{ik_0 - vk} + \ldots$ into the Schwinger-Dyson equation (4.13) and also taking $k_F \to \infty$ in the remaining terms. The result is

$$\Pi_1(Q) = \lambda^2 N_f k_F \int \frac{\mathrm{d}k_0 \mathrm{d}k d\theta}{(2\pi)^2} \frac{1}{(ik_0 - vk)\left(i\left(k_0 + q_0\right) - v\left(k + |\vec{q}|\cos\theta\right)\right)}. \tag{4.22}$$

The result of these integrals is finite but depends on the order of integration. The difference is a constant C

$$\Pi_1(Q) = \frac{\lambda^2 k_F N_f}{v}\left(\frac{|q_0|}{\sqrt{q_0^2 + v^2\vec{q}^2}} + C\right). \tag{4.23}$$

As pointed out for instance for the 3+1 dimensional quantum critical metal in [29], the way to think about this ordering ambiguity is that one should strictly speaking first regularize the theory and introduce a one-loop counterterm. This counterterm has a finite ambiguity that needs to be fixed by a renormalization condition. Even though the loop momentum integral happens to be finite in this case, the finite counterterm ambiguity remains. The correct renormalization condition is the choice $C = 0$. This choice corresponds to the case when the boson is tuned to criticality since a non-zero C would mean the presence of an effective mass generated by quantum effects.

A more physical way to think of the ordering ambiguity is as the relation between the frequency (Λ_0) and momentum (Λ_k) cutoff. We will assume that $\Lambda_k \gg \Lambda_0$ — which means that we evaluate the k integral first and then the frequency k_0 integral. In this case $C = 0$ directly follows.

4.3.2 The solution to the $k_F \to \infty$ Schwinger-Dyson equation: Robustness of the one-loop result

We will now give a heuristic derivation that the one-loop result is in fact the exact answer in the limit $k_F \to \infty$. The full polarization Schwinger-Dyson equation (4.13) in the limit $k_F \to \infty$ can be written as

$$\Pi(q_0, q) = \lambda^2 k_F N_f \int \frac{\mathrm{d}k_0 \mathrm{d}k \mathrm{d}\theta}{(2\pi)^2} \frac{G(k_0 - q_0/2, k) - G(k_0 + q_0/2, k)}{iq_0 - vq\cos\theta} = \frac{-2\pi i \operatorname{sgn} q_0}{\sqrt{q_0^2 + v^2 q^2}} \lambda^2 k_F N_f \int \frac{\mathrm{d}k_0 \mathrm{d}k}{(2\pi)^2} \left[G(k_0 - q_0/2, k) - G(k_0 + q_0/2, k)\right], \tag{4.24}$$

where $q = |\vec{q}|$. Following our discussion above that regularizing and renormalizing with a counterterm is the same as the prescription to perform the momentum integral first, we may shift the momentum integral so that in the difference both Green's functions have the same momentum in their argument. We are not allowed to do this subsequently again for the frequency integral, since $\int dk_0 dk G(k_0, k) = \infty$. One needs to evaluate the frequency integral with an explicit cutoff Λ_0 which can be removed in the end.

The integrand of the frequency integration:
$\int \mathrm{d}k \left[G(k_0 - q_0/2, k) - G(k_0 + q_0/2, k)\right]$, clearly vanishes as $q_0 \to 0$. Expanding around q_0 (in units of the cut-off Λ_0) one has

$$\begin{aligned} \int_{-\Lambda_0}^{\Lambda_0} \mathrm{d}k_0 \int \mathrm{d}k \left[G(k_0 - q_0/2, k) - G(k_0 + q_0/2, k)\right] \\ = -\frac{q_0}{2} \int \mathrm{d}k_0 \frac{d}{dk_0} \left[G(k_0, k) + G(k_0, k)\right] + \mathcal{O}\left(\frac{q_0^2}{\Lambda_0^2}\right) \\ = -q_0 \int \mathrm{d}k \left[G(\Lambda_0, k) - G(-\Lambda_0, k)\right] + \ldots \end{aligned} \tag{4.25}$$

Because the coupling constant of the theory is relevant we can replace the exact, interacting fermion propagator evaluated at $k_0 = \pm\Lambda_0$ with the

free one $G(\Lambda_0, k) \approx G_0(\Lambda_0, k)$. Doing so we arrive to the result of (4.23). This heuristically shows the robustness of the one-loop result. The one caveat is the value of Π for large external momenta q_0 near the cut-off. We now show by an different method that the one-loop result is in fact exact to all orders.

4.3.3 Multiloop cancellation

The robustness of the one-loop result in case of linear fermionic dispersion was recognized before under the name of multiloop cancellation [49]. The technical result is that for a theory with a simple Yukawa coupling and linear dispersion around a Fermi surface, a symmetrized fermion loop with more than two fermion lines vanishes. In our context the linear dispersion is a consequence of the large k_F limit. In other words all higher loop contributions to the polarization Π should be subleading in $1/k_F$. This was explicitly demonstrated at two loops in [55].

Note that there still can be diagrams which contain a subpiece which is subleading in the above sense but the rest of the diagram renders the whole finite. However, in this case multiple fermions running around in the diagram. Therefore, it scales with positive power of N_f (without k_F multiplier) and it is not included in the first order small N_f result.

We will give here a short derivation of this multiloop cancellation in the limit $k_F \to \infty$. As before (below Eq. (4.15)) we may assume in this limit that the momentum transfer at any fermion interaction is always much smaller than the size of the initial ($\vec{k}$) and final momenta ($\vec{k}'$) which are of the order of the Fermi momentum, i.e. $|\vec{k}' - \vec{k}| \ll k_F$ with $|\vec{k}|, |\vec{k}'| \sim k_F$. The free fermion Green's function then reflects a linear dispersion

$$G_0(\omega, k) = \frac{1}{i\omega - vk} \tag{4.26}$$

We now Fourier transform back to real space, as multiloop cancellation is most easily shown in this basis. The real space transform of the "linear" free fermion propagator above is

$$G_0(\tau, r) = -\frac{i}{2\pi} \frac{\mathrm{sgn}(v)}{r + iv\tau}, \tag{4.27}$$

where as before r is the conjugate variable to $k = |\vec{k}| - k_F$. The essential step in the proof is that real space Green's function manifestly obeys the

identity [48]

$$G_0(z_1)\,G_0(z_2) = G_0(z_1+z_2)\,(G_0(z_1)+G_0(z_2)) \tag{4.28}$$

with $z \equiv r + iv\tau$. Consider then (the subpart of any correlation function/Feynman diagram containing) a fermion loop with $n \geq 2$ vertices along the loop connected to indistinguishable scalars (i.e. no derivative interactions and all interactions are symmetrized). The corresponding algebraic expression in a real space basis will then contain the expression

$$F(z_1,...,z_n) = \sum_{(i_1,..,i_n)\in S_n} G_0(z_{i_1}-z_{i_2})\,G_0(z_{i_2}-z_{i_3})\,...G_0(z_{i_{n-1}}-z_{i_n}) \cdot G_0(z_{i_n}-z_{i_1})\,, \tag{4.29}$$

where S_n is the set of permutations of the numbers 1 through n. Using the "linear dispersion" identity Eq. (4.28) and the shorthand notation $G_0(z_{i_1}-z_{i_2}) = G_{12}$ we obtain

$$F(z_1,...,z_n) = \sum_{(i_1,..,i_n)\in S_n} G_{12}G_{23}...G_{n-1,1}\,(G_{n-1,n}+G_{n,1})\,. \tag{4.30}$$

Next we cyclically permute the indices from 1 to $n-1$: $1\to 2$, $2\to 3$, ..., $n-1\to 1$ in the sum

$$\sum_{(i_1,..,i_n)\in S_n} G_{12}G_{23}...G_{n-1,1}G_{n-1,n} = \sum_{(i_1,..,i_n)\in S_n} G_{23}G_{34}...G_{12}G_{1,n}. \tag{4.31}$$

This gives us

$$F(z_1,...,z_n) = \sum_{(i_1,..,i_n)\in S_n} G_{12}G_{23}...G_{n-1,1}\,(G_{1,n}+G_{n,1})\,. \tag{4.32}$$

Then since $G_{i,j}$ corresponds to a (spinless) fermionic Green's function, it is antisymmetric $G_{i,j} = -G_{j,i}$, and we can conclude that F vanishes for $n \geq 3$. For $n = 2$ it is not possible to use the identity Eq. (4.28) since we would need to evaluate $G(0)$ which is infinite.

4.4 The fermion two-point function in the limit $k_F \to \infty$ at small N_f

4.4.1 The exact fermionic two-point function in real space: an analytical form

We have thus established that the exact boson two-point function including Landau-damping is completely given by the Dyson-summed one-loop expression in the limit $k_F \to \infty$, and that this one-loop polarization arguably faithfully captures the low-energy physics. We can now use this exact boson two-point function to determine the exact fermion two-function from the formal solution to the large k_F Ward-Schwinger-Dyson equations (in real space)

$$G(\tau, r) = G_0(\tau, r) e^{I(\tau, r)} \tag{4.33}$$

with (see Eq. (4.21))

$$I(\tau, r) = \lambda^2 \int \frac{\mathrm{d}\omega \mathrm{d}k_x \mathrm{d}k_y}{(2\pi)^3} G_0^2(\omega, k_x) G_B(\omega, k_x, k_y) \left[\cos(\omega\tau - k_x r) - 1\right]. \tag{4.34}$$

Substituting in the exact boson two-point function $G_B = 1/(G_{B,0}^{-1} + \Pi)$, we thus need to calculate the integral

$$I(\tau, r) = \lambda^2 \int \frac{\mathrm{d}\omega \mathrm{d}k_x \mathrm{d}k_y}{(2\pi)^3} \frac{\cos(\tau\omega - r k_x) - 1}{(i\omega - k_x v)^2 \left(\omega^2 + k_x^2 + k_y^2 + \frac{4\pi^2 \lambda^2 N_f k_F |\omega|}{v\sqrt{v^2(k_x^2 + k_y^2) + \omega^2}}\right)}. \tag{4.35}$$

In this expression and the following sections we have rescaled $N_f k_F$ to $(2\pi)^2 N_f k_F$. That is where the factor $4\pi^2$ comes from.

Intermezzo — The large-$N_f k_F$ limit: a comparison to previous approaches

An often used approximation in the literature is to take the IR limit of the boson propagator, see e.g [38, 16]. In this limit the polarisation term will dominate over the kinetic terms, but since the rest of the integrand in (4.35) has no k_y dependence, it is necessary to keep the k_y term in the boson propagator. This simplification is expected to be better with

increasing $N_f k_F$. We therefore refer to the simplified boson two-point function as the large $N_f k_F$ propagator

$$G_{B,N_f k_F\to\infty}(\omega,k_x,k_y)=\frac{1}{k_y^2+\frac{4\pi^2\lambda^2 N_f k_F|\omega|}{v^2|k_y|}}. \tag{4.36}$$

This Landau-damped propagator has been used extensively, for instance [16, 38]. In [38] this propagator was used for the type of non-perturbative calculation we are proposing here. We discuss this here, as we will now show that using this simplified propagator for our method has a problematic feature. In short, this propagator only captures the leading large $N_f k_F$ contribution but the non-perturbative exponential form of the exact Green's function sums up powers of the propagator which then are subleading in $N_f k_F$. We will use therefore the full bosonic propagator which will also enable us to compare our results with our previous quenched calculation. Let us, however, first show explicitly the problems that arise with the simplified propagator.

In the large $N_f k_F$ limit the integral $I(\tau,r)$ to be evaluated simplifies to

$$I_{N_f k_F\to\infty}=\lambda^2\int\frac{\mathrm{d}\omega\mathrm{d}k_x\mathrm{d}k_y}{(2\pi)^3}\frac{\cos(\tau\omega-xk_x)-1}{(i\omega-k_x v)^2\left(k_y^2+\frac{4\pi^2\lambda^2 N_f k_F|\omega|}{v^2|k_y|}\right)}. \tag{4.37}$$

After evaluating the k_x integral:

$$I_{N_f k_F\to\infty}=-\lambda^2\int\frac{\mathrm{d}\omega\mathrm{d}k_y}{(2\pi)^3}\frac{\pi k_y^2|r|e^{-|\omega|\left(\frac{|r|}{v}+i\,\mathrm{sgn}(r)\tau\right)}}{4\pi^2\lambda^2 N_f k_F\,|\omega k_y|+k_y^4 v^2}. \tag{4.38}$$

The k_y integral can be performed next to yield

$$I_{N_f k_F\to\infty}=-\lambda^2\int\mathrm{d}\omega\frac{(2\pi)^{-5/3}\,|r|\,e^{-|\omega|\left(\frac{|r|}{v}+i\,\mathrm{sgn}(r)\tau\right)}}{3\sqrt{3}v^{4/3}(\lambda^2 N_f k_F\,|\omega|)^{1/3}}. \tag{4.39}$$

The primitive function to this ω integral is the upper incomplete gamma function, with argument $2/3$. Evaluating this incomplete gamma function in the appropriate limits and substituting the final expression for $\underset{N_f k_F\to\infty}{I}(\tau,r)$ into the expression for the fermion two-point function gives us:

$$\underset{Nfk_F\to\infty}{G_f}(\tau,r)=\frac{1}{2\pi(ir-v\tau)}\exp\left(-\frac{|r|}{l_0^{1/3}\left(|r|+iv\,\mathrm{sgn}(r)\tau\right)^{2/3}}\right) \tag{4.40}$$

where the length scale l_0 is given by

$$l_0^{1/3} = \frac{3\sqrt{3}(2\pi)^{5/3}v^{2/3}(N_f k_F)^{1/3}}{2\Gamma\left(\frac{2}{3}\right)\lambda^{4/3}}. \tag{4.41}$$

This result has been found earlier in [37] (see also [49]). It is much more instructive to study, however, the momentum space version of the propagator. The Fourier transform of the real space Green's function

$$\underset{N_f k_F\to\infty}{G_f}(\omega,k) = \int \mathrm{d}\tau\mathrm{d}r \frac{\mathrm{e}^{i(\omega\tau-kr)}}{2\pi(ir-v\tau)} \exp\left(-\frac{|r|}{l_0^{1/3}\left(|r|+iv\,\mathrm{sgn}(r)\tau\right)^{2/3}}\right) \tag{4.42}$$

is tricky, but remarkably can be done exactly. We do so in appendix 4.B. The result is

$$\begin{aligned}\underset{N_f k_F\to\infty}{G_f}(\omega,k) =& \frac{1}{i\omega-kv}\cos\left(\frac{\omega}{v l_0^{1/2}(\omega/v+ik)^{3/2}}\right)\\ &+\frac{6\sqrt{3}i\Gamma\left(\frac{1}{3}\right)\omega^{2/3}}{8\pi l_0^{1/3}v^{5/3}(\omega/v+ik)^2}\,{}_1F_2\left(1;\frac{5}{6},\frac{4}{3};-\frac{\omega^2}{4l_0v^2(\omega/v+ik)^3}\right)+\\ &+\frac{3\sqrt{3}i\Gamma\left(-\frac{1}{3}\right)\omega^{4/3}}{8\pi l_0^{2/3}v^{7/3}(\omega/v+ik)^3}\,{}_1F_2\left(1;\frac{7}{6},\frac{5}{3};-\frac{\omega^2}{4l_0v^2(\omega/v+ik)^3}\right).\end{aligned} \tag{4.43}$$

This expression has been compared with numerics to verify its correctness; see Fig. 4.2.

Recall that Eq. (4.43) is the Green's function in Euclidean signature. Continuing to the imaginary line, $\omega = -i\omega_R$, this becomes the proper retarded Greens function, $G_R(\omega_R,k)$, and from this we can obtain the spectral function $A(\omega_R,k) = -2\mathrm{Im}\ G_R(\omega_R,k)$. As it encodes the excitation spectrum, the spectral function ought to be a positive function that moreover equals 2π when integrated over all energies ω_R, for any momentum k. This large $N_f k_F$ spectral function contains an oscillating singularity at $\omega_R = vk$. We are free to move the contour into complex ω_R-plane by deforming $\omega_R \to \omega_R + i\Omega$ where Ω is positive but otherwise arbitrary. Upon doing this it is easy to numerically verify that indeed the integral over ω_R gives 2π. However, if we look at the behaviour close to the essential singularity the function oscillates rapidly and does not stay positive as one approaches the singularity; see Fig. 4.3. This reflects that

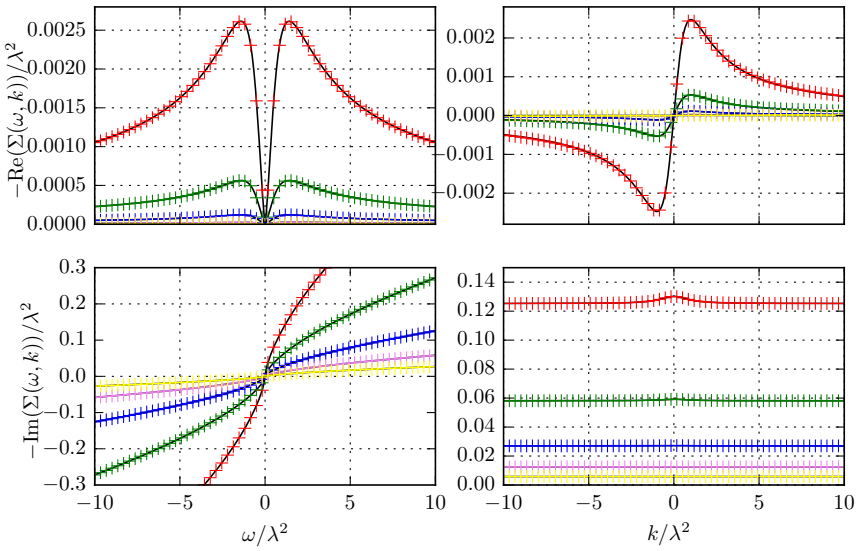

Figure 4.2. Real and imaginary parts of the self energy obtained using the large-$N_f k_F$ Landau-damped propagator. This plot shows the agreement between the numerics and the analytical solution, verifying that both solutions are correct. Notice the difference in magnitude between the real and imaginary part. The agreement of the real parts shows that the numerical procedure has a very small relative error. All plots are for the $k, \omega = \lambda^2$ slice with $v = 1$.

the large $N_f k_F$ approximation done in this way is not consistent. Even though the approximation for the exponent $I(\tau, r) \equiv \frac{\tilde{I}(\tau,r)}{(N_f k_F)^{1/3}}$ is valid to leading order in $1/(N_f k_F)$, this is not systematic after exponentiation to obtain the fermion two-point function

$$\underset{N_f k_F \to \infty}{G_f}(\tau, r) = \frac{1}{2\pi(ir - v\tau)} \exp\left(\frac{\tilde{I}(\tau, r)}{(N_f k_F)^{1/3}} + \mathcal{O}\left(\frac{1}{(N_f k_F)^{2/3}} \right) \right). \tag{4.44}$$

Reexpanding the exponent one immediately sees that keeping only the leading term in $I(\tau, r)$ mixes at higher order with the subleading terms at lower order in $1/N_f k_F$

$$\underset{N_f k_F \to \infty}{G_f}(\tau, x) = \frac{1}{2\pi(ir - v\tau)} \left(1 + \frac{\tilde{I}(\tau, r)}{(N_f k_F)^{1/3}} + \mathcal{O}\left(\frac{1}{(N_f k_F)^{2/3}} \right) + \frac{1}{2}\left(\frac{\tilde{I}(\tau, r)}{(N_f k_F)^{1/3}} + \dots \right)^2 \right). \tag{4.45}$$

Nevertheless, we will see that in the IR $\underset{N_f k_F \to \infty}{G_f}$ (with a small modification) capture the physics very well.

Exact large k_F fermion two-point function; $v = 1$

To get the general $N_f k_F$ answer we return to the full integral Eq.(4.35) needed to determine the real space fermion two-point function. Solving this in general is difficult, and to simplify mildly we consider the special case $v = 1$. In our previous studies of the quenched $N_f k_F = 0$ limit we saw that this case is actually not very special. In fact, nothing abruptly happens as $v \to 1$, except that the quenched $N_f k_F = 0$ solution can be written in closed form for this value of $v = 1$. Nor for the case of large $N_f k_F$ is the choice $v = 1$ in any way special. As can be seen above in Eq. (4.40) for large $N_f k_F$ all v are equivalent up to a rescaling of τ versus r and a rescaling of the single length scale l_0. We may therefore expect that for a finite N_f, the physics of $0 < v < 1$ is qualitatively the same as the (not-so-) special case $v = 1$.

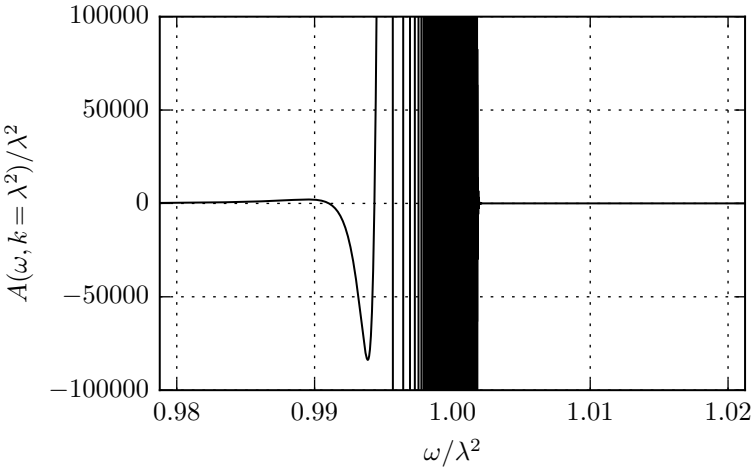

Figure 4.3. Exact fermion spectral function based on the large-$N_f k_F$ approximation for the exact boson propagator. Notice that the function is not positive everywhere. Here $k = \lambda^2$, $v = 1$ and $N_f k_F = \lambda^2$.

After setting $v = 1$ and changing to spherical coordinates we have

$$I = \int \mathrm{d}\tilde{r}\mathrm{d}\phi\mathrm{d}\theta \mathrm{e}^{2i\phi} \frac{\cos\Big(\tilde{r}\sin(\theta)(\tau\sin(\phi) - r\cos(\phi))\Big) - 1}{8\pi^3 \sin(\theta)^2 \Big(N_f k_F \pi^2 |\sin(\phi)| + \lambda^{-2}\tilde{r}^2/\sin(\theta)\Big)} \,. \tag{4.46}$$

Performing the $\tilde{r}$ integral gives us

$$I = \lambda \int \mathrm{d}\phi\mathrm{d}\theta \mathrm{e}^{2i\phi} \frac{\mathrm{e}^{-2\pi\lambda|\tau\sin(\phi) - r\cos(\phi)|\sqrt{N_f k_F |\sin(\phi)| \sin(\theta)^3}} - 1}{32\pi^3 \sqrt{N_f k_F |\sin(\phi)| \sin(\theta)^3}} \,. \tag{4.47}$$

Note that if the signs of both τ and r are flipped, then this is invariant. Changing the sign of only τ, and simultaneously making the change of variable $\phi \to -\phi$, then the (real) fraction is invariant but the exponent in the prefactor changes sign. Thus, I goes to I^* as the sign of either τ or r is changed. Without loss of generality, we can assume that both of them are positive from now on. We further see that the integrand is invariant under $\phi \to \phi + \pi$, so we may limit the range of ϕ to $(0, \pi)$ by doubling the value of integrand. Similarly we limit θ to $(0, \pi/2)$ and multiply by

another factor of 2. We then make the changes of variables:

$$\begin{aligned}\phi &= \tan^{-1}(s) + \pi/2 \\ \theta &= \sin^{-1}(u^{2/3})\end{aligned} \tag{4.48}$$

with $s \in \mathbb{R}$ and u is integrated over the range $(0, 1)$. For convenience we introduce the function

$$z(s) = \frac{\pi}{2}\lambda\sqrt{N_f k_F}|sr + \tau|(1+s^2)^{-3/4} \tag{4.49}$$

Now the two remaining integrals can be written as

$$I = \lambda \int \mathrm{d}s\mathrm{d}u \frac{(\mathrm{e}^{-4uz(s)} - 1)(s-i)}{12\pi^3(s+i)(1+s^2)^{3/4}u^{4/3}\sqrt{N_f k_F(1-u^{4/3})}} \tag{4.50}$$

After expanding the exponential we can perform the u integral term by term. We are left with

$$I = \lambda \int \mathrm{d}s \sum_{n=1}^{\infty} \frac{4^{n-2}(1+s^2)^{1/4}(-z(s))^n}{\pi^{5/2} n! \sqrt{N_f k_F}(i+s)^2} \frac{\Gamma\left(\frac{3n-1}{4}\right)}{\Gamma\left(\frac{3n+1}{4}\right)} \tag{4.51}$$

This can be resummed into a sum of generalized hypergeometric functions, but this is not useful at this stage. Instead we once again integrate term by term. Collecting the prefactors and introducing the constant $a = \tau/r$, the n-th term can be written as

$$I = \sum_{n=1}^{\infty} c_n \int \mathrm{d}s\, (s-i)^2 |s+a|^n (1+s^2)^{-(7+3n)/4} \tag{4.52}$$

This can be written as

$$I = \sum_{n=1}^{\infty} c_n \int \mathrm{d}s\mathrm{d}w\, (s-i)^2 |s+a|^n \frac{\mathrm{e}^{-w(s^2+1)} w^{3(1+n)/4}}{(3(1+n)/4)!} \tag{4.53}$$

where w is integrated on $(0, \infty)$. After splitting the integral at $s = -a$ to get rid of the absolute value we can calculate the s integrals in terms of confluent hypergeometric functions ${}_1F_1(a, b; z)$. Adding the two halves

$s < -a$ and $s > -a$ of the integral we have

$$I = \sum_{n=1}^{\infty} c_n \int \mathrm{d}w \frac{\Gamma\left(\frac{1+n}{2}\right)\mathrm{e}^{-(1+a^2)w}}{2(3(1+n)/4)!} \left(2w(i+a)^2 \ {}_1F_1\left(\frac{2+n}{2}, \frac{1}{2}; a^2 w\right) \right.$$
$$\left. + (2+n) \ {}_1F_1\left(\frac{4+n}{2}, \frac{1}{2}; a^2 w\right) - 4aw(2+n)(i+a) \ {}_1F_1\left(\frac{4+n}{2}, \frac{3}{2}; a^2 w\right) \right). \tag{4.54}$$

It may look like we have just exchanged the s-integral for the w-integral, but by writing the hypergeometric functions in series form,

$$I = \sum_{n=1}^{\infty} c_n \int \mathrm{d}w \sum_{m=0}^{\infty} \frac{2^{2m-1} a^{2m} \mathrm{e}^{-(1+a^2)w} w^{\frac{n-3}{4}+m} \Gamma\left(\frac{1+n}{2}+m\right)}{\Gamma\left(\frac{7+3n}{4}\right)\Gamma\left(2+2m\right)} \cdot$$
$$\cdot \left(n(1+2m-4a(i+a)w) + (1+2m)(1+2m-2(1+a^2)w)\right) , \tag{4.55}$$

the w integral can now be performed. The result is

$$I = \sum_{n=1,m=0}^{\infty} c_n \frac{(a+i)4^{m-1} a^{2m} \left(a^2+1\right)^{-\frac{1}{4}(4m+n+5)} \Gamma\left(m+\frac{n+1}{4}\right)\Gamma\left(m+\frac{n+1}{2}\right)}{\Gamma(2m+2)\Gamma\left(\frac{7+3n}{4}\right)} \cdot$$
$$\cdot \left(a\left(2m-6mn-2n^2-n+1\right) - i(2m+1)(n+1)\right) \tag{4.56}$$

The sum over m can be expressed in terms of the ordinary hypergeometric function, ${}_2F_1(a_1, a_2; b; z)$:

$$I = \sum_{n=1}^{\infty} c_n \frac{(n+1)\left(a^2+1\right)^{-\frac{n}{4}-\frac{1}{4}} \Gamma\left(\frac{n+1}{4}\right)\Gamma\left(\frac{n+1}{2}\right)}{24(a-i)^2(a+i)\Gamma\left(\frac{3n}{4}+\frac{7}{4}\right)} \cdot$$
$$\cdot \left(a^2(n+1)(-3an+a-i(n+1)) \, {}_2F_1\left(\frac{n+3}{2}, \frac{n+5}{4}; \frac{5}{2}; \frac{a^2}{a^2+1}\right) + \right.$$
$$\left. - 6\left(a^2+1\right)(a(2n-1)+i) \, {}_2F_1\left(\frac{n+1}{4}, \frac{n+1}{2}; \frac{3}{2}; \frac{a^2}{a^2+1}\right) \right) \tag{4.57}$$

The space-time dependence in this expression is implicit in $a = \tau/r$ and with additional r-dependence in the coefficients c_n The result above is the value for both τ and r positive. Using the known symmetries presented above the solution can be extended to all values of τ and r by appropriate absolute value signs. Then changing variables to

$$\begin{aligned} \tau &= R\cos(\Phi) \\ r &= R\sin(\Phi) \end{aligned} \tag{4.58}$$

we have

$$I = \frac{\lambda f\left(R\lambda\sqrt{N_f k_F}, \Phi\right)}{\sqrt{N_f k_F}} \tag{4.59}$$

with the function $f(\tilde{R}, \Phi)$ given by

$$\begin{aligned} f(\tilde{R}, \Phi) =& \sum_{n=1}^{\infty} f_n \tilde{R}^n \\ f_n =& \frac{\pi^{n-2} e^{i\Phi}(-1)^n \Gamma\left(\frac{n+1}{4}\right) |\sin(\Phi)|^{\frac{1+3n}{2}}}{72(3n-1)\Gamma\left(\frac{n}{2}+1\right)\Gamma\left(\frac{1+3n}{4}\right)} \cdot \\ & \cdot \Bigg({}_2F_1\left(\frac{n+3}{2}, \frac{n+5}{4}; \frac{5}{2}; \cos^2(\Phi)\right)(n+1) \cdot \\ & \quad \cdot \cos^2(\Phi)((1-3n)\cos(\Phi) - i(n+1)\sin(\Phi)) \\ & + {}_2F_1\left(\frac{n+1}{4}, \frac{n+1}{2}; \frac{3}{2}; \cos^2(\Phi)\right) 6((1-2n)\cos(\Phi) - i\sin(\Phi)) \Bigg) \end{aligned} \tag{4.60}$$

This exact infinite series expression for the exponent $I(r, \phi)$ gives us the exact fermion two-point function in real (Euclidean) space (time). We have not been able to find a closed form expression for this final series. Note that $f_n \sim 1/n!$ for large n, and the series therefore converges rapidly. Moreover, numerically the hypergeometric functions are readily evaluated to arbitrary precision (e.g. with Mathematica), and therefore the value of f can be robustly evaluated to any required precision.

As a check on this result, we can compare it to the exact result in the quenched $N_f k_F = 0$ limit in [48], where the exact answer was found in a different way. In the limit where $N_f k_F \to 0$ we see that only the first

term of this series gives a contribution and the expression for the exponent collapses to

$$\lim_{N_f \to 0} I(R, \Phi) = \lambda^2 f_1 R = \lambda^2 \frac{e^{2i\Phi}}{12\pi} R \tag{4.61}$$

In Cartesian coordinates this equals

$$\lim_{N_f \to 0} I(\tau, r) = \lambda^2 \frac{(\tau + ir)^2}{12\pi\sqrt{\tau^2 + r^2}} \tag{4.62}$$

This is the exact same expression as found in [48] for $v = 1$.

There is one value of the argument for which f drastically simplifies. For $r = 0$ ($\Phi = 0, \pi$) we have

$$f_n(\Phi = 0) = -\frac{(-2\pi)^{n-2}}{3\Gamma(n+2)} \tag{4.63}$$

and thus

$$f(\tilde{R}, \Phi = 0) = \frac{1}{12\pi^2} + \frac{e^{-2\pi\tilde{R}} - 1}{24\pi^3 \tilde{R}} \tag{4.64}$$

Further numerical analysis shows that the real part of $f(\tau, r)$ is maximal for $r = 0$. Eq. (4.64) can be seen to give a good qualitative description.

The IR limit of the exact fermion two-point function compared to the large-$N_f k_F$ limit

Before turning to the numerical Fourier transform of the exact real space answer, we derive the IR approximation more systematically. The expression obtained above, Eq. (4.60), is not very useful for extracting the IR Greens function or at a large $N_f k_F$ as the expression is organized in an expansion around $R\lambda\sqrt{N_f k_F} = 0$. To study the limit where $R\lambda\sqrt{N_f k_F} \gg 1$ we can go back to Eq. (4.50). With this expression we see that the exponential in the integrand, $e^{-4uz(s)}$ with $z \sim \sqrt{N_f k_F}|sr + \tau| \sim \tilde{r}$, is generically suppressed for large $\tilde{R} = \lambda R\sqrt{N_f k_F}$. The exceptions are when either $sr + \tau$ is small, s is large, or u is small. The first two cases are also unimportant in the $\tilde{R} \gg 1$ limit. In the first case we restrict the s integral to a small range of order $1/\tilde{R}$ around $-\tau/r$; this contribution therefore becomes more and more negligible in the limit $\tilde{R} \gg 1$. In the second case we will have a remaining large denominator in s outside the exponent that

also suppresses the overall integral. Thus for large $\tilde{R}$, the only appreciable contribution of the exponential term to the integral in $I(\tau, r)$ arises when u is small. To use this, we first write the integral as

$$I_{\rm IR} = I_{\rm IR,exp} + I_{\rm IR,-1}, \tag{4.65}$$

with

$$\begin{aligned} I_{\rm IR,exp}(\tau, r) = \lambda \int_{-\infty}^{\infty} {\rm d}s \frac{s-i}{12\pi^3 (s+i)(1+s^2)^{3/4}\sqrt{N_f k_F}} \cdot \\ \cdot \left(\int_0^1 {\rm d}u \frac{{\rm e}^{-4uz(s)}}{u^{4/3}\sqrt{1-u^{4/3}}} - \int_0^{\infty} {\rm d}u \frac{1}{u^{4/3}} \right) \simeq \\ \lambda \int_{-\infty}^{\infty} {\rm d}s \frac{s-i}{12\pi^3 (s+i)(1+s^2)^{3/4}\sqrt{N_f k_F}} \left(\int_0^1 {\rm d}u \frac{{\rm e}^{-4uz(s)}}{u^{4/3}} - \int_0^{\infty} {\rm d}u \frac{1}{u^{4/3}} \right) \end{aligned} \tag{4.66}$$

and

$$\begin{aligned} I_{\rm IR,-1}(\tau, r) = \lambda \int_{-\infty}^{\infty} {\rm d}s \frac{(s-i)}{12\pi^3 (s+i)(1+s^2)^{3/4}\sqrt{N_f k_F}} \cdot \\ \cdot \left(\int_0^{\infty} {\rm d}u \frac{1}{u^{4/3}} + \int_0^1 {\rm d}u \frac{-1}{u^{4/3}\sqrt{1-u^{4/3}}} \right) \end{aligned}$$

We have added and subtracted an extra term to each to ensure convergence of each of the separate terms. Since the important contribution to $I_{\rm IR,exp}$ is from the small u region we can extend its range from (0,1) to $(0, \infty)$. This way, the integrals can then be done

$$\begin{aligned} I_{\rm exp} &= \int_{-\infty}^{\infty} {\rm d}s \frac{-\lambda^{4/3} \left| sr + \tau \right|^{1/3}}{2^{2/3} 3^{3/2} \pi^{5/3} (N_f k_F)^{1/3} (s+i)^2 \Gamma\left(\frac{4}{3}\right)} \\ &= -\frac{\Gamma\left(\frac{2}{3}\right) \lambda^{4/3} \left| r \right|^{1/3}}{2^{2/3} 3^{3/2} \pi^{5/3} (N_f k_F)^{1/3} \left(1 + \frac{i\tau}{r}\right)^{2/3}}, \end{aligned} \tag{4.67}$$

$$\begin{aligned} I_{\rm IR,-1} = \int_{-\infty}^{\infty} {\rm d}s \frac{\lambda (s-i)}{12\pi^3 (s+i)(1+s^2)^{3/4}\sqrt{N_f k_F}} \cdot \\ \cdot \left(\int_0^{\infty} {\rm d}u \left(\frac{1}{u^{4/3}} - \frac{\theta(1-u)}{u^{4/3}\sqrt{1-u^{4/3}}} \right) \right) = \frac{\lambda}{12\pi^2 \sqrt{N_f k_F}} \end{aligned} \tag{4.68}$$

In total we have for large $\tilde{R}$:

$$I = -\frac{\Gamma\left(\frac{2}{3}\right)\lambda^{4/3}\,|r|}{2^{2/3}3^{3/2}\pi^{5/3}(N_f k_F)^{1/3}\left(|r| + i\,\mathrm{sgn}(r)\tau\right)^{2/3}} + \frac{\lambda}{12\pi^2\sqrt{N_f k_F}} + \\ + \mathcal{O}(\lambda^{2/3}(N_f k_F)^{-4/6} r^{-1/3}) \tag{4.69}$$

We see that the leading order term in R is the same as was obtained from the large $N_f k_F$ approximation of the exponent. The first subleading term is just a constant. This is good news because we already have the Fourier transform of this expression. This result is valid for length scales larger than $1/\lambda\sqrt{N_f k_F}$ with a bounded error of the order $R^{-1/3}$. This readily seen. Defining this approximation as G_{IR}, i.e.

$$G_{\mathrm{IR}} = G_0 \exp\left(-\frac{\Gamma\left(\frac{2}{3}\right)\lambda^{4/3}\,|r|}{2^{2/3}3^{3/2}\pi^{5/3}(N_f k_F)^{1/3}\left(|r| + i\,\mathrm{sgn}(r)\tau\right)^{2/3}} + \right. \\ \left. + \frac{\lambda}{12\pi^2\sqrt{N_f k_F}}\right) , \tag{4.70}$$

the error of this approximation follows from:

$$\Delta G_{\mathrm{IR}} = G - G_{\mathrm{IR}} = G_{\mathrm{IR}}\left(\exp\left(\mathcal{O}(\tilde{R}^{-1/3})\right) - 1\right) \tag{4.71}$$

Since the exponential in G_{IR} is bounded we have that $\Delta G_{\mathrm{IR}} = \mathcal{O}(R^{-4/3})$. After Fourier transforming this translates to an error of order $\mathcal{O}(k^{-2/3})$.

4.4.2 The exact fermion two-point function in momentum space: Numerical method

We now turn to the evaluation of the Fourier transformation. As our exact answer is in the form of an infinite sum, this is not feasible analytically. We therefore resort to a straightforward numerical Fourier analysis.

To do so we first numerically determine the real space value of the exact Green's functions. To do so accurately, several observations are relevant

- The coefficients f_n in the infinite sum for $I(\tau, r)$ decay factorially in n so once n is of order $\tilde{R}$, convergence is very rapid.

- The hypergeometric functions for each n are costly to compute with high precision, but with the above choice of polar coordinates the arguments of the hypergeometric functions are independent of R and $N_f k_F$. We therefore numerically evaluate the series over a grid in $\tilde{R}$ and Φ. We can then reuse the hypergeometric function evaluations many times and greatly decrease computing time.

- The real space polar grid will be limited to a finite size. The IR expansion from Eq. (4.70) can be used instead of the exact series for large enough $R\sqrt{N_f k_F}$. To do so, we have to ensure an overlapping regime of validity. It turns out that a rather large value of $r\sqrt{N_f k_F}$ is necessary to obtain numerical agreement between these two expansions, i.e. one needs to evaluate a comparably large number of terms in the expansion. For the results presented in this chapter it has been necessary to compute coefficients up to order 16 000 in $R\sqrt{N_f k_F}$, for many different angles Φ. The function is bounded for large τ and r but each term grows quickly. This means that there are large cancellations between the terms that in the end give us a small value. We therefore need to calculate these coefficients to very high precision in evaluating the polynomial. For these high precision calculations, we have used the Gnu Multiprecision Library.

- On this polar grid we computed the exact answer for $\tilde{R} < \tilde{R}_0 \approx 1000$ and used cubic interpolation for intermediate values. For larger $\tilde{R}$ we use the asymptotic expansion in Eq. (4.70).

- Finally we represent the function values using normal 128 bit complex numbers.

We then use a standard discrete numerical Fourier transform (DFT) to obtain the momentum space two-point function from this numeric prescription for $G(R, \Phi)$. Sampling $G(R, \Phi)$ at a finite number of discrete points, the size of the sampling grid will introduce an IR cut-off at the largest scales we sample and a UV-cut off set by the smallest spacing between points. These errors in the final result can be minimized by using the known asymptotic values analytically. Rather than Fourier transforming $G(\tau, r)$ as a whole, we Fourier transform $G_{\text{diff}}(\tau, r) = G(\tau, r) - G_{\text{IR}}(\tau, r)$ instead. Since both these functions approach the free propagator in the UV, the Fourier transform of its difference will decay faster for large ω and k. This greatly reduces the UV artefacts inherent in a discrete fourier

transform (DFT). These two functions also approach each other for large τ and x. In fact, with the numerical method we use to approximate f described above, they will be identical for $\tilde{R}_0 < \sqrt{N_f k_F(\tau^2 + r^2)}$. This means that we only need to sample the DFT within that area. With a DFT we will always get some of the UV tails of the function giving folding aliasing artefacts. Now our function decays rapidly so one could do a DFT to very high frequencies and discard the high frequency part. This unfortunately takes up a lot of memory so we have gone with a more CPU intensive but memory friendly approach. We instead first perform a convolution with a Gaussian kernel, perform the DFT, keep the lowest 1/3 of the frequencies and then divide by the Fourier transform of the kernel used. This gives us a good numeric value for $G_{\text{diff}}(\omega, k)$. To this we add our analytic expression for $G_{\text{IR}}(\omega, k)$.

4.5 The physics of 2+1 quantum critical metals at large k_F

With the exact analytical real space expression and numerical momentum space expression for the full non-perturbative fermion Green's function, we can now start to discuss the physics of the elementaray quantum critical metal in the limit of large k_F and small N_f. Let us emphasize right away that all our results are in Euclidean space. Although we suspect that a good Lorentzian continuation with a well-defined and consistent spectral function exists of the Euclidean momentum space Green's function, this function is not easily obtainable from our numerical Euclidean result. We leave this for future work. The Euclidean signature Green's function does not visually encode the spectrum directly, but for very low energies/frequencies the Euclidean and the Lorentzian expressions are nearly identical, and we can extract much of the IR physics already from the Euclidean correlation function.

In Figure 4.4 we show density plots of the imaginary part of $G(\omega, k)$ for different values of $N_f k_F$ as well as cross-sections at fixed low ω. For the formal limit $N_f k_F = 0$ we detect three singularities near $\omega = 0$ corresponding with the three Fermi surfaces found in Lorentzian signature in our earlier work [48]. However, for any appreciable value of the dimensionless ratio $N_f k_F/\lambda^2$ one only sees a single singularity. As the plots for $G(\omega, k)$ at low frequency show, its shape approaches that of the strongly Landau-damped RPA result as one increases $N_f k_F/\lambda^2$, though for low

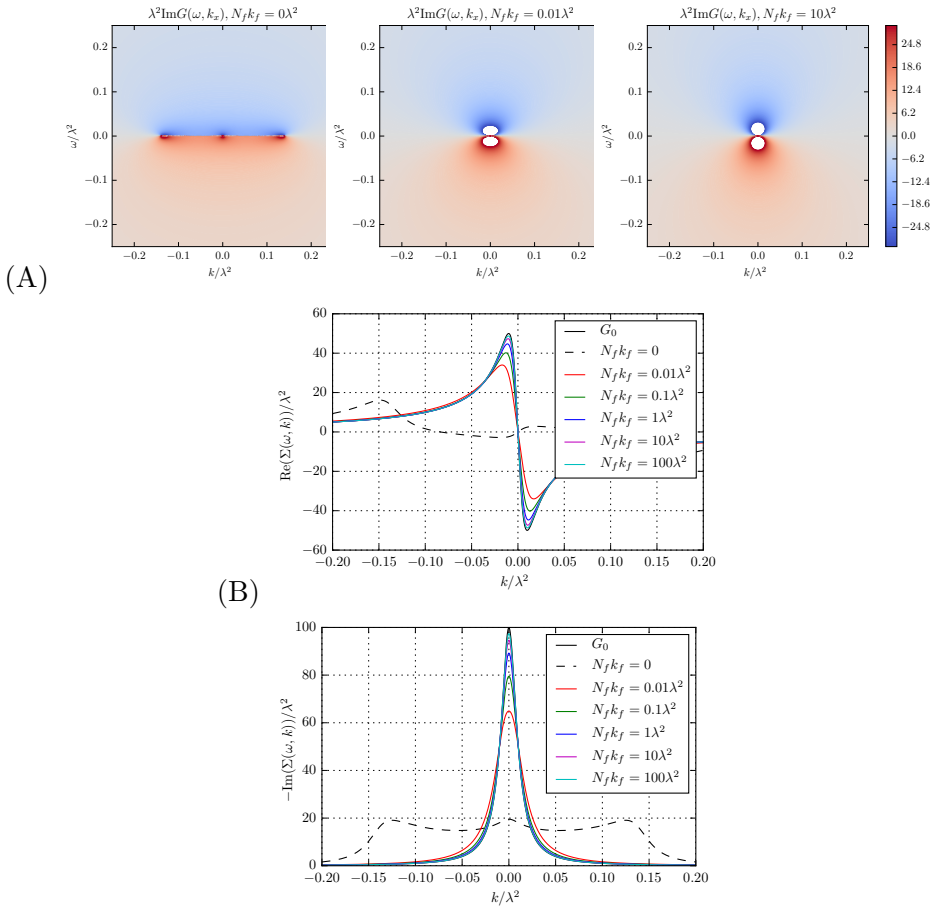

Figure 4.4. (A) Density plots of the imaginary part of the exact (Euclidean) fermion Green's function $G(\omega, k)$ for various values of $N_f k_F$. In the quenched limit $N_f k_F = 0$ the three Fermi surface singularities are visible. For any appreciable finite $N_f k_F$ the Euclidean Green's function behaves as a single Fermi surface non-Fermi liquid. (B) Real and imaginary parts of $G(\omega, k)$ for very small $\omega = 0.01\lambda^2$.

$N_f k_F$ it is still distinguishably different.

This result is in contradistinction to what happens to the bosons. When the bosons are not affected in the IR, i.e. the quenched limit, it is evident that the fermions are greatly affected by the boson: there is a topological Fermi surface transition and the low-energy spectrum behaves as critical excitations [48]. However, once we increase $N_f k_F$, the bosonic

excitations are rapidly dominated in the IR by Landau damping but we now see that this reduces the corrections to the fermions. As $N_f k_F$ is increased, the deep IR fermion two-point function approaches more and more that of the RPA result with self-energy $\Sigma \sim i\omega^{2/3}$.

We can illustrate this more clearly by studying the self-energy of the fermion $\Sigma(\omega, k) = G(\omega, k)^{-1} - G_0(\omega, k)^{-1}$. It is shown that the naive large N_f RPA result (dotted lines) does agree at $\omega = 0, k = 0$ and the leading ω dependence of the imaginary part is captured. The leading k dependence are not captured by RPA. On the other hand, our improved approximation for the low energy regime G_{IR} (dashed lines) captures these higher order terms in the low energy expansion of G very well.

We can calculate the occupation number and check whether it is consistent with the non-Fermi liquid nature of the Green's function. For a Fermi liquid there is a discontinuity in the zero-temperature momentum distribution function $n_k = \int_{-\infty}^{0} \mathrm{d}\omega_R A(\omega_R, k)/2\pi$ with $A(\omega_R, k)$ the spectral function. As the spectral function is the imaginary part of the retarded Green's functions and the latter is analytic in the upper half plane of ω_R we can move this contour to Euclidean ω and use the fact that G approaches G_0 in the UV to calculate the momentum distribution function from our Euclidean results. In detail

$$n_k = -\int_{-\infty}^{0} \mathrm{d}\omega_R \mathrm{Im} \frac{G_R(\omega_R, k)}{\pi} = \mathrm{Im}\left[\int_0^{\Lambda} \mathrm{d}\omega i \frac{G(\omega, k)}{\pi} + \int_C \mathrm{d}z i \frac{G(z, k)}{\pi}\right]; \tag{4.72}$$

the first integral can be done with the numerics developed in the preceding section. The contour C goes from $i\Lambda$ to $-\infty$ and for large enough Λ this is in the UV and can well be approximated by the free propagator. The resulting momentum distribution $n(k)$ is shown in Figure 4.6. Within our numerical resolution, these curves are continuous as opposed to a Fermi liquid. This is of course expected; the continuity reflects the absence of a clear pole in the IR expansions in the preceding subsection. Note also that as $N_f k_F$ is lowered, the finite $N_f k_F$ curves approach the quenched result for $|k| > k^*$ where k^* is the point of the discontinuity of the derivative of the quenched occupation number. At k^* the (derivative) of the quenched momentum distribution number does have a discontinuity (reflecting the branch cut found in [48]).

Our result highlights how various approximations that have been made in the past hang together. In units of the bare coupling λ the $k_F \to \infty$ theory is characterized by two parameters ω/λ^2 and N_f — the latter al-

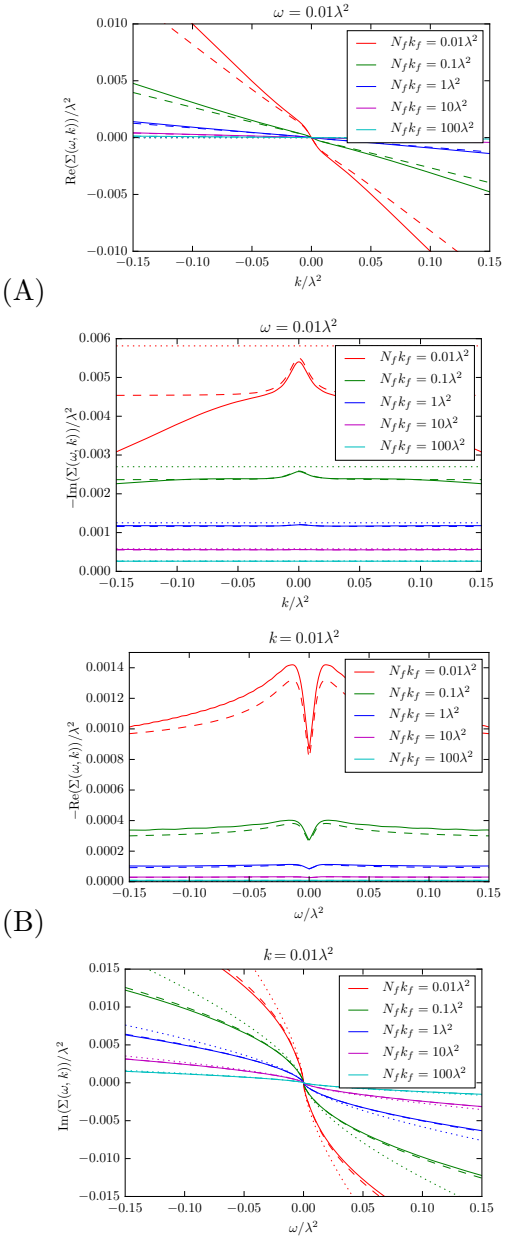

Figure 4.5. Real and imaginary parts of the fermion self-energy for (A) $\omega = 0.01\lambda^2$ and for (B) $k = 0.01\lambda^2$. Dashed lines show the G_{IR}-approximation; dotted lines show the RPA result.

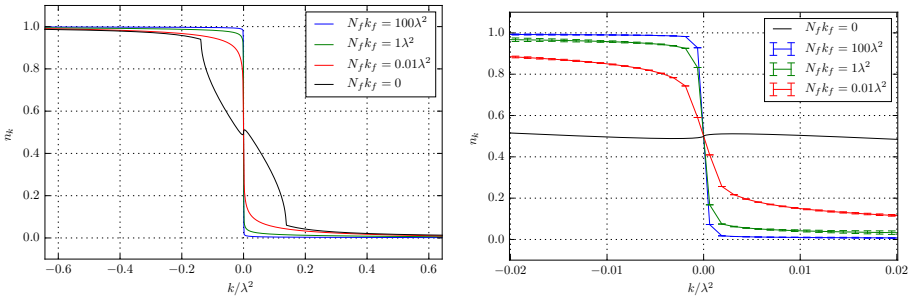

Figure 4.6. Momentum distribution function. The two plots show the same function for different ranges. The error bars of the lower figure show an estimate of the error due to using the free Green's function close to the UV. The error-bars are exaggerated by a factor 100.

ways appears in the combination $N_f k_F/\lambda^2$, and as we explained in section 4.4 we considered this finite even when $k_F/\lambda^2 \to \infty$. For very large ω/λ^2 one can use perturbation theory in λ to understand the theory. This is the perturbation around the UV-fixed point of a free fermion plus a free boson.

For small ω/λ^2 and small $N_f k_F/\lambda^2$ the quenched result we obtained earlier [48] captures the right physics. As the momentum occupation number $n(k)$ indicates, its precise regime of applicability depends discontinuously on the momentum k/λ^2. The discontinuity is surprising, but it can be explained analytically as an order of limits ambiguity. Although it is hard to capture the deep IR region for very small $N_f k_F$ in the full numerics we suspect that in the ω-k plane there is a region where the limit $N_f k_F \to 0$ and $\omega, k \to 0$ do not commute. We show an indication of this in appendix 4.C. Physically this is the scale where Landau damping becomes important.

For small ω/λ^2 the IR approximation presented here captures the physics independently of the value of $N_f k_F/\lambda^2$. For large $N_f k_F/\lambda^2$ the spectrum it predicts closely approximates the known result [38], but improves on it for larger frequencies. We have presented a pictorial overview of how the various approximations are related in Fig.4.7.

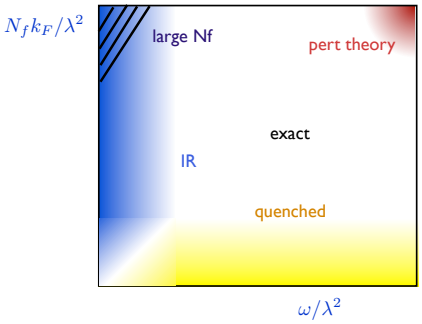

Figure 4.7. A sketch of the regimes of applicability of various approximations to the exact fermion Green's function of the elementary quantum critical metal.

4.6 Conclusion

We have presented a non-perturbative answer for the (Euclidean) fermion and boson two-point functions of the elementary quantum critical metal in the limit of large k_F and small N_f. This non-perturbative answer follows from tracing of the role of the Fermi momentum in the Schwinger-Dyson equations and the fermion number Ward identity. In the limit of large k_F they form a closed set on the boson and fermion two-point functions with the subtle point that the leading one-loop contribution to the boson two-point function (formally divergent as $k_F \to \infty$) needs to be kept. We have presented an analytic expression for the direct IR limit of the Green's functions.

It would be enlightening to have our results in Lorentzian signature (as in the quenced limit); at the technical level this is an obvious next step. At the physics level, an obvious next step is to explore the model without relying on the smallness of N_f and the $k_F \to \infty$ limit. Since this necessarily involves higher-point boson correlations, the role of the self-interactions of the boson needs to be considered. These are also revelant in the IR and may therefore give rise to qualitatively very different physics than found here.

4.A Derivation of the Schwinger-Dyson equations and the Ward Identity

The Schwinger-Dyson equation for the fermion two-point function can be derived from its defining equation in the presence of a background field $\phi(x)$.

$$\left(-\partial_\tau + \frac{\nabla^2}{2m} + \mu + \lambda\phi(x)\right) G[\phi](x,y) = \delta^3(x-y) \tag{4.73}$$

Here $x = \{\tau, \mathbf{x}\}$ etc. In the full theory $\phi(x)$ is a dynamical field and performing the path-integral one obtains

$$\frac{1}{Z_\phi(J)} \int \mathcal{D}\phi \left[(-\partial_\tau + \frac{\nabla^2}{2m} + \mu + \lambda\phi) G[\phi](x,y) - \delta^3(x-y)\right]$$
$$e^{-\int\left[\frac{1}{2}(\partial_\tau\phi)^2 + \frac{1}{2}(\nabla\phi)^2 - J\phi\right]} = \left(-\partial_\tau + \frac{\nabla^2}{2m} + \mu + \lambda\frac{\partial}{\partial J}\right) G_J(x,y) - \delta^3(x-y) = 0 \tag{4.74}$$

with $G_J(x,y)$ the exact fermion two-point function in the presence of a scalar source $J(x)$ and $Z_\phi(J)$ being the partition function of a free scalar. The functional derivative $\dfrac{\partial}{\partial J(x)}$ of the two-point function can be computed using the identity that the two-point function is the inverse of double derivative of the 1PI action $\Gamma[\phi_c, \psi_c, \psi_c^\dagger] = \ln Z(J, J_\psi) - \phi_c J - ...$ with respect to the conjugate fields $\psi_c(y),\ \psi_c^\dagger(x)$

$$\frac{\partial}{\partial J(u)} G_J(x,y) = \frac{\partial}{\partial J(u)} \left(\frac{\partial^2\Gamma}{\partial\psi_c(y)\partial\psi_c^\dagger(x)}\right)^{-1} \tag{4.75}$$

Also for the scalar, the 1PI action depends on the classical Legendre conjugate field $\phi_c(x)$ rather than the source $J(x)$. Using the chain rule, one has

$$\begin{aligned}
\frac{\partial}{\partial J(u)} G_J(x,y) &= \int d^3z \frac{\partial\phi_c(z)}{\partial J(u)} \frac{\partial}{\partial\phi_c(z)} \left(\frac{\partial^2\Gamma}{\partial\psi_c(y)\partial\psi_c^\dagger(x)}\right)^{-1} \\
&= -\int d^3z_1 d^3z_2 d^3z_3 \frac{\partial\phi_c(z_1)}{\partial J(u)} \left(\frac{\partial^2\Gamma}{\partial\psi_c(y)\partial\psi_c^\dagger(z_2)}\right)^{-1} \cdot \\
&\quad \cdot \left(\frac{\partial^3\Gamma}{\partial\phi_c(z_1)\partial\psi_c(z_2)\partial\psi_c^\dagger(z_3)}\right) \left(\frac{\partial^2\Gamma}{\partial\psi_c(z_3)\partial\psi_c^\dagger(x)}\right)^{-1}.
\end{aligned} \tag{4.76}$$

From its definition the conjugate field $\phi_c(z) = \frac{\partial \ln Z}{\partial J(z)}$, we see that $\frac{\partial \phi_c(z)}{\partial J(u)}$ equals the scalar two-point function in the presence of a source J.

$$\frac{\partial \phi_c(z)}{\partial J(u)} = \frac{\partial^2 \ln Z}{\partial J(u) \partial J(z)} = G_{B,J}(z,u) \tag{4.77}$$

Substituting these relations into Eq. (4.76) and the result into (4.74) together with the relation between the double derivative of the 1PI action and the Green's function one obtains

$$\begin{aligned} 0 = -\delta^3(x-y) + \left(-\partial_\tau + \frac{\nabla^2}{2m} + \mu\right) G(x,y) - \\ \lambda G_B(x,z) G(y,z_2) \Lambda(z,z_2,z_3) G(z_3,x) \end{aligned} \tag{4.78}$$

with $\Lambda(z,z_2,z_3) \equiv \frac{\partial^3 \Gamma}{\partial \phi_c(z_1) \partial \psi_c(z_2) \partial \psi_c^\dagger(z_3)}$ equal to the 1PI three-point vertex and we have set the source $J = 0$ at the end. Multiplying by the free fermion Green's function $G_0(x,y)$, the inverse of the free kinetic operator $(-\partial_\tau + \frac{\nabla^2}{2m} + \mu)$ and Fourier transforming we arrive at the equation (4.6) quoted in the main text

$$\begin{aligned} 0 &= -G_0(x,y) + G(x,y) - G_0(x,y) \lambda G_B(x,z) G(y,z_2) \Gamma(z,z_2,z_3) G(z_3,x) \\ &= -G_0(K) + G(K) - \lambda G_0(K) G(K) \int dQ G_B(Q) \Lambda(K, K-Q) G(K-Q) \end{aligned} \tag{4.79}$$

In the main text we use Γ to denote the 1PI three-point vertex, as is conventional. By definition $dQ = \frac{dq_0 d^2 q}{(2\pi)^3}$.

4.B The Fourier transform of the fermion Green's function in the large $N_f k_F$ approximation

We will now show how to perform this Fourier transform. We need to calculate the following integral:

$$\underset{N_f k_F \to \infty}{G_f}(\omega, k) = \int \mathrm{d}\tau \mathrm{d}x \frac{\mathrm{e}^{i(\omega\tau - kx)}}{2\pi(ix - v\tau)} \exp\left(-\frac{|x|}{l_0^{1/3}\left(|x| + iv\,\mathrm{sgn}(x)\tau\right)^{2/3}}\right) \tag{4.80}$$

First we note that integrand is τ-analytic in the region $\{\tau \in \mathbb{C} : \min(0, vx) < \mathrm{Im}(\tau) < \max(0, vx)\}$. Since the integrand necessarily goes to 0 at ∞ we can thus shift the τ contour, $\tau \to \tau + ix/v$. We now have

$$\underset{N_f k_F \to \infty}{G_f}(\omega, k) = -\int \frac{\mathrm{d}\tau \mathrm{d}x}{2\pi v\tau} \exp\left(i\omega\tau - x\left(ik + \omega/v + \frac{\mathrm{sgn}(x)}{l_0^{1/3}\left(iv\,\mathrm{sgn}(x)\tau\right)^{2/3}}\right)\right) \tag{4.81}$$

We have allowed ourselves to choose the order of integration, shift the contour, and then change the order. We see that the x integral now is trivial but only converges for

$$-\frac{v^{1/3}}{2l_0^{1/3}|\tau|^{2/3}} < \mathrm{Re}(\omega) < \frac{v^{1/3}}{2l_0^{1/3}|\tau|^{2/3}} \tag{4.82}$$

This is fine since we know that the final result is ω-analytic in both the right and left open half-planes. As long as we can obtain an answer valid within open subsets of both of these sets we can analytically continue the found solution to the whole half planes. We thus proceed assuming $\mathrm{Re}(\omega)$ is in this range. One can further use symmetries of our expression to relate the left and right ω-half-planes, so to simplify matters, from now on we additionally assume ω to be positive. Let us now consider a negative x, we then see that the τ integral can be closed in the upper half plane and since it is holomorphic there the result will be 0. We can thus limit the x integrals to $\mathbb{R}^+$. We then have

$$\underset{`N_f k_F \to \infty}{G_f}(\omega, k) = \int \mathrm{d}\tau \frac{\mathrm{e}^{i\omega\tau}}{2\pi v\tau} \frac{-1}{a + \frac{1}{l_0^{1/3}(iv\tau)^{2/3}}} \tag{4.83}$$

where $a = ik + \omega/v$. The integrand has a pole at $(i\tau)^{2/3} = -1/(al_0^{1/3}v^{2/3})$. Now break the integral in positive and negative τ and write it as

$$\underset{N_f k_F \to \infty}{G_f}(\omega, k) = \frac{h((-i)^{2/3}u_0^*)^* - h((-i)^{2/3}u_0)}{2\pi v a} \tag{4.84}$$

where

$$\begin{aligned} h(u) &= \int_0^\infty \mathrm{d}\tau \frac{\mathrm{e}^{i\tau}}{\tau + u\tau^{1/3}}, \\ u_0 &= \frac{\omega^{2/3}}{al_0^{1/3}v^{2/3}}. \end{aligned} \tag{4.85}$$

Usng Morera's theorem we can prove that h is holomorphic on $\mathbb{C}/\mathbb{R}^-$. Consider any closed curve C in $\mathbb{C}/\mathbb{R}^-$. We need to show that

$$\int_C \mathrm{d}u h(u) = 0 \tag{4.86}$$

We do this by rotating the contour slightly counter clockwise. For any curve C there is clearly a small $\epsilon > 0$ such that we will still not hit the pole $\tau + u\tau^{1/3} = 0$.

$$\int_C \mathrm{d}u \int_0^{(1+i\epsilon)\infty} \mathrm{d}\tau \frac{\mathrm{e}^{i\tau}}{\tau + u\tau^{1/3}}, \tag{4.87}$$

The piece at ∞ converges without the denominator and thus goes to 0. Since the integral now converges absolutely we can use Fubini's theorem to change the orders of integration

$$\int_0^{(1+i\epsilon)\infty} \mathrm{d}\tau \int_C \mathrm{d}u \frac{\mathrm{e}^{i\tau}}{\tau + u\tau^{1/3}} = 0 \tag{4.88}$$

And since also the integrand is holomorphic on a connected open set containing C the proof is finished.

The function h can for $0 < \arg(u) < 2\pi/3$ be expressed as a Meijer G-function:

$$h(u) = \frac{3}{8\pi^{5/2}} G^{5,3}_{3,5}\left(\begin{matrix} 0, \frac{1}{3}, \frac{2}{3} \\ 0, 0, \frac{1}{3}, \frac{1}{2}, \frac{2}{3} \end{matrix} \middle| -\frac{u^3}{4} \right) \tag{4.89}$$

The G-function has a branch cut at $\mathbb{R}^-$ and because of that we can not easily write $h(u)$ in terms of it since the argument u appears cubed in the argument of the G-function and we know that h is holomorphic on all of $\mathbb{C}/\mathbb{R}-$. We can however express h as an analytic continuation of the G-function past this branch cut, onto the further sheets of its Riemann surface. We will write the G-function as a function with two real arguments, first the absolute value and second the phase of its otherwise complex argument. We will allow the phase to be any real number and when outside the range $[-\pi, \pi]$, we let the function be defined by its analytical continuation to the corresponding sheet. We hereafter omit the

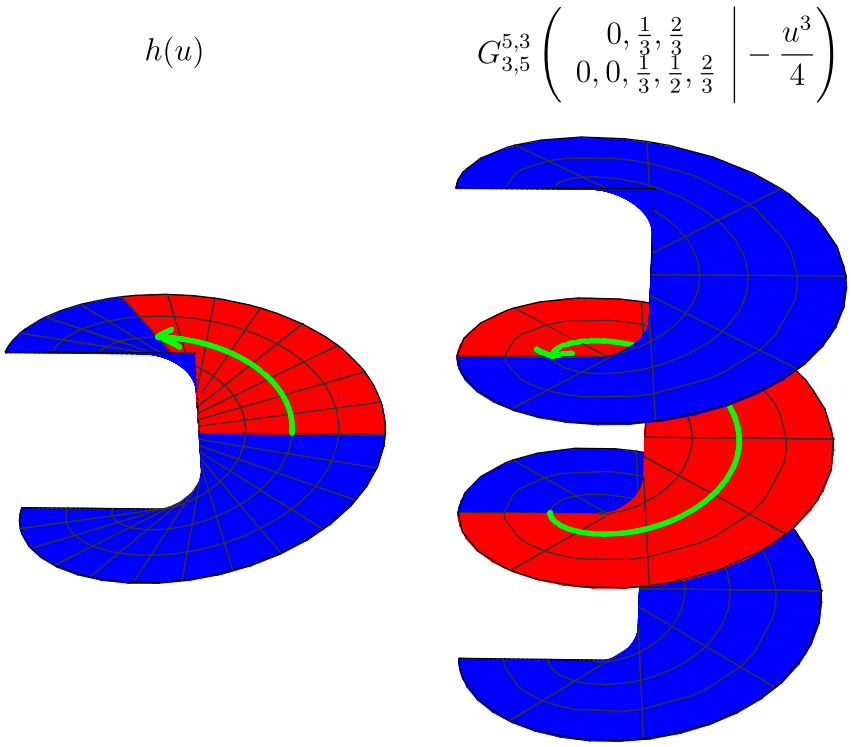

Figure 4.8. The left image shows part of the Riemann surface of the function h and the right image shows part of the Riemann surface of the G-function. The part in red of the left image can be expressed as the G-function evaluated on its first sheet, the red part of the right image. The green arrow shows how points are mapped from one Riemann surface to the other by the mapping $u \mapsto -u^3/4$

constant parameters of the G-function. We then have:

$$\begin{aligned}\underset{N_f k_F \to \infty}{G_f}(\omega, k) &= 3\frac{G_{3,5}^{5,3}\left(\frac{|u_0|^3}{4}, -2\pi - 3\arg(u_0)\right)^* - G_{3,5}^{5,3}\left(\frac{|u_0|^3}{4}, -2\pi + 3\arg(u_0)\right)}{16\pi^{7/2}va} \\ &= 3\frac{G_{3,5}^{5,3}\left(\frac{|u_0|^3}{4}, 3\arg(u_0) + 2\pi\right) - G_{3,5}^{5,3}\left(\frac{|u_0|^3}{4}, 3\arg(u_0) - 2\pi\right)}{16\pi^{7/2}va}\end{aligned} \tag{4.90}$$

In the last step we used the fact that the G-function commutes with complex conjugation. We see that the Green's function is given by a certain monodromy of the G-function. It is given by the difference in its value starting at a point $u_0^3/4$ on the sheet above the standard one and then analytically continuing clockwise around the origin twice to the sheet below the standard one and there return to $u_0^3/4$. Since we only need this difference, we might expect this to be a, in some sense, simpler function as would happen for e.g. monodromies of the logarithm. To see how to simplify this we look at the definition of the G-function. It is defined as an integral along L:

$$G_{p,q}^{m,n}\left(\begin{matrix} a_1, \ldots, a_p \\ b_1, \ldots, b_q \end{matrix} \middle| \, z\right) = \frac{1}{2\pi i}\int_L \frac{\prod_{j=1}^m \Gamma(b_j - s)\prod_{j=1}^n \Gamma(1 - a_j + s)}{\prod_{j=m+1}^q \Gamma(1 - b_j + s)\prod_{j=n+1}^p \Gamma(a_j - s)} z^s \, ds, \tag{4.91}$$

There are a few different options for L and which one to use depends on the arguments. In our case L starts and ends at $+\infty$ and circles all the poles of $\Gamma(b_i - s)$ in the negative direction. Using the residue theorem we can recast the integral to a series. We have double poles at all negative integers and some simple poles in between. The calculation to figure out the residues of all these single and double poles is a bit too technical to present here but in the end the series can be written as

$$G_{3,5}^{5,3}(z) = \sum_{n=0}^{\infty}\left(a_n z^n + b_n z^n \log(z) + c_n z^{n+1/3} + d_n z^{n+1/2} + e_n z^{n+2/3}\right) \tag{4.92}$$

Now we perform the monodromy term by term and a lot of these terms

cancel out.

$$G^{5,3}_{3,5}\Big(|z|,\arg(z)+2\pi\Big)-G^{5,3}_{3,5}\Big(|z|,\arg(z)-2\pi\Big)= \sum_{n=0}^{\infty}\left(4\pi i b_n z^n+i\sqrt{3}c_n z^{n+1/3}-i\sqrt{3}e_n z^{n+2/3}\right) \tag{4.93}$$

The coefficients a_i contain both the harmonic numbers and the polygamma function whereas the other coefficients are just simple products of gamma functions. This simplification now lets us sum this series to a couple of hypergeometric functions. Inserting the expressions for a and u_0 we have

$$\begin{aligned} \underset{N_f k_F\to\infty}{G_f}(\omega,k) &= \frac{1}{i\omega-kv}\cos\left(\frac{\omega}{v l_0^{1/2}(\omega/v+ik)^{3/2}}\right) \\ &+\frac{6\sqrt{3}i\Gamma\left(\frac{1}{3}\right)\omega^{2/3}}{8\pi l_0^{1/3}v^{5/3}(\omega/v+ik)^2}\,{}_1F_2\left(1;\frac{5}{6},\frac{4}{3};-\frac{\omega^2}{4l_0v^2(\omega/v+ik)^3}\right)+ \\ &+\frac{3\sqrt{3}i\Gamma\left(-\frac{1}{3}\right)\omega^{4/3}}{8\pi l_0^{2/3}v^{7/3}(\omega/v+ik)^3}\,{}_1F_2\left(1;\frac{7}{6},\frac{5}{3};-\frac{\omega^2}{4l_0v^2(\omega/v+ik)^3}\right). \end{aligned} \tag{4.94}$$

Note that this expression is ω-holomorphic for ω in the right half plane so our previous assumptions on ω can be relaxed as long as ω is in the right half plane. We note from expression (4.80) that if we change sign on both ω and k and do the changes of variables $\tau\to-\tau$ and $x\to-x$ we end up with the same integral up to an overall minus sign. We can thus get the left half plane result using the relation

$$\underset{N_f k_F\to\infty}{G_f}(-\omega,k)=-\underset{N_f k_F\to\infty}{G_f}(\omega,-k). \tag{4.95}$$

As mentioned in the main text, this expression has been compared with numerics to verify that we have not made any mistakes. See Fig. 4.2. We have also done the two integrals for the Fourier transform in the opposite order, first obtaining a different Meijer G-function then using the G-function convolution theorem to do the second integral. In the end one obtains the same monodromy of the G-function as above.

4.C The discontinuous transition from the quenched to the Landau-damped regime

We show here why the including Landau damping finite N_f physics starting from the quenched $N_f\to 0$ result, is discontinuous in the IR. To do

so we calculate the Green's function by imposing the $N_f \to 0$ limit from the begining. We need to evaluate the Fourier transform integral:

$$G_L(\omega, k) = \int_{-\infty}^{\infty} dx \int_{-L}^{L} d\tau G_0 \exp\left(I_0 + i\omega \cdot \tau - ik \cdot x\right), \tag{4.96}$$

where as before the free propagator is

$$G_0(\tau, x) = -\frac{i}{2\pi} \frac{1}{x + i \cdot \tau} \tag{4.97}$$

and the $N_f \to 0$ limit of the exponent of the real space Green's function:

$$I_0 = \frac{(\tau + i \cdot x)^2}{12\pi\sqrt{\tau^2 + x^2}}. \tag{4.98}$$

Note however that the τ integral is divergent in this limit. Therefore in (4.96) we have introduced a cutoff L in this direction. By looking at the full expansion of I we can see that the natural value of L is of the order $1/\sqrt{N_f}$. For larger values of τ the asymptotic expansion describes I better. We expect that for large enough momenta and frequencies the asymptotic region does not contribute to the Fourier transform and therefore the cutoff can be removed. This naive epxectation however is only partly true. We will shortly see that the region in the $\omega - k$ plane where the cutoff can be removed is more complicated and asymmetric in term of the momenta and frequency.

Let us turn now to the evaluation of (4.96). After making the coordinate change $\tau \to \tau$, $x \to u \cdot \tau$ one of the integral (τ) can be evaluated analytically:

$$G_L(\omega, k) = \int_{-\infty}^{\infty} du \left(I_1(u) + I_2(u) + I_3(u)\right), \tag{4.99}$$

where

$$I_1(u) = \frac{6 \exp\left(ikLu\sqrt{u^2+1} - iL \cdot \omega \cdot \sqrt{u^2+1} - \frac{L(u-i)^2}{12\pi}\right)}{12\pi(u+i)(ku-\omega) + i\sqrt{u^2+1}u + \sqrt{u^2+1}}, \tag{4.100}$$

$$I_2(u) = \frac{6i \exp\left(-ikLu\sqrt{u^2+1} + iL \cdot \omega \cdot \sqrt{u^2+1} - \frac{L(u-i)^2}{12\pi}\right)}{12i\pi k(u+i)u + \sqrt{u^2+1}u - i\sqrt{u^2+1} + 12\pi(1-iu)\omega}, \tag{4.101}$$

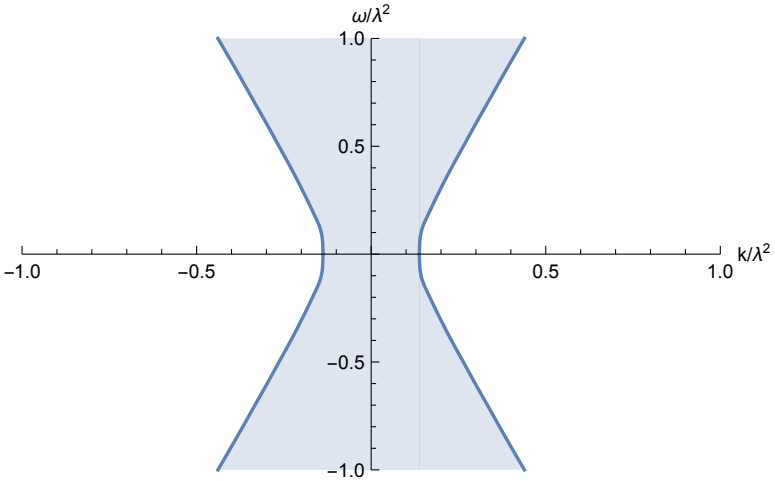

Figure 4.9. The region of convergence. In the shaded area the $L \to \infty$ ($N_f \to 0$) limit is not convergent while outside this area $\lim_{L\to\infty} G_L = G_{quenched}$.

$$I_3(u) = -\frac{144\pi(ku-\omega)}{D(u)}, \tag{4.102}$$

with

$$\begin{aligned} D(u) = u\left(-3 + u\left(144\pi^2 k^2(u+i) + u - 3i\right)\right) \\ -288\pi^2 ku(u+i)\omega + 144\pi^2(u+i)\omega^2 + i. \end{aligned} \tag{4.103}$$

By numerically performing the single integral u we can obtain $G_{N_f\to 0}$. Since it is easier than evaluating the Fourier transform of the true real-space version of the Green's function it is worth to understand how the $L \to \infty$ (which is equivalent to $N_f \to 0$) works. The result is depicted on Fig. 4.9. In the shaded region (which corresponds to small k) the limit is not well defined while outside of this region the limit is equal to the quenched result. The numerics shows that for zero frequency, the edge of this region is at k^*, where the Green's function is singular.

We can qualitatively determine the line separating the convergent and divergent region. For this we assume that when L is large one can expand the exponent in u

$$I_1(u) \sim \exp\left[u^2\left(-\frac{1}{12\pi} - \frac{1}{2}i\omega\right)L + \frac{iu(6\pi k+1)}{6\pi}L - iL\omega + \frac{L}{12\pi} + \mathcal{O}\left(Lu^3\right)\right]. \tag{4.104}$$

We see that because of the term $-L \cdot u^2/(12\pi)$, the integrand is non-zero only in a narrow region around $u = 0$. For the same reason we approximate the denominator of (4.100) by replace u by zero there. With these simplifications we arrive to a gaussian integral which can be evaluated analytically:

$$\int_{-\infty}^{\infty} I_1(u)du \approx \frac{12i\sqrt{3}\pi \exp\left(\frac{iL\left(6\pi k^2+2k+\omega(-12\pi\omega+i)\right)}{12\pi\omega-2i}\right)}{(12\pi\omega+i)\sqrt{L(1+6i\pi\omega)}}. \tag{4.105}$$

The real part of (4.105) is

$$L\frac{3\left(\omega^2-k^2\right)\pi-k}{36\pi^2\omega^2+1}. \tag{4.106}$$

It is clear that if this value is positive (i.e. $3\left(\omega^2-k^2\right)\pi-k>0$) than the $L\to\infty$ limit is divergent. Looking at the numerical result in Fig. 4.9 we indeed see that the boundary of the shaded region is indeed a hyperbola. Note, however, that the exact location of this hyperbola obtained from expanding the exponent is slightly off.

It is interesting to note that if we are in the divergent region G_L is not convergent for large L but for some intermediate values it can still get close to the quenched result $G_{quenched}$. To quantify this let us introduce a relative "error" function

$$error(L) = \left|\frac{G_L - G_{quenched}}{G_{quenched}}\right|. \tag{4.107}$$

In Fig. 4.10 we shows the behavior of this function for various points in the $\omega - k$ plane. For a point which is outside the shaded region the error approaches zero when L is large. For $\omega = 1$, $k = 0$ which is inside the divergent region the error is oscillating but there is an interval of L where the amplitude of this oscillation has a minimum. If the frequency is small ($\omega = 0.1$), this amplitude is larger and there is minimum in that.

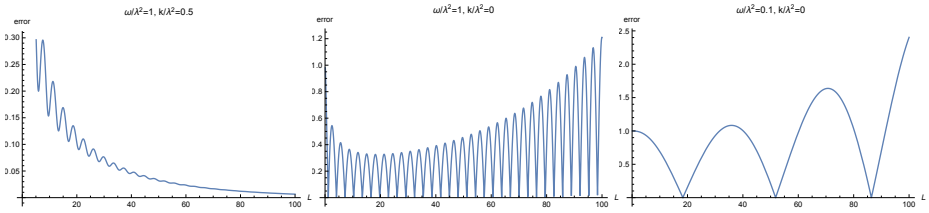

Figure 4.10. The relative difference between G_L and the quenched result as a function of L for different frequencies and momenta. Left: for a point in the (ω, k) plane which is outside of the shaded region of Fig. 4.9 the "error" goes to zero for large L. Middle: inside the shaded region the error is oscillating with diverging amplitude as L goes for large values. However, for larger values of ω there is an intermediate range of L, where the relative error is smaller than 0.3. Therefore the quenched approximation is qualitatively correct. Right: for small ω the amplitude of the oscillation is become large.

Bibliography

[1] S. Sur and S. S. Lee, "Chiral non-Fermi liquids," Phys. Rev. B **90**, no. 4, 045121 (2014) [arXiv:1310.7543 [cond-mat.str-el]].

[2] J. Polchinski, "Effective field theory and the Fermi surface," In *Boulder 1992, Proceedings, Recent directions in particle theory* 235-274, and Calif. Univ. Santa Barbara - NSF-ITP-92-132 (92,rec.Nov.) 39 p. (220633) Texas Univ. Austin - UTTG-92-20 (92,rec.Nov.) 39 p [hep-th/9210046].

[3] R. Shankar, "Renormalization group approach to interacting fermions," Rev. Mod. Phys. **66**, 129 (1994).

[4] J. Hertz, "'Quantum critical phenomena',Phys. Rev. B4, 1165 (1976).

[5] A. J. Millis, "Effect of a nonzero temperature on quantum critical points in itinerant fermion systems",Phys. Rev. **B48**, 7183 (1993).

[6] H. v. Löhneysen, A. Rosch, M. Vojta, P. Wölfle, "Fermi-liquid instabilities at magnetic quantum phase transitions," Rev. Mod. Phys. **79**, 1015 (2007).

[7] L. D. Landau, "The theory of a Fermi liquid," Sov. Phys. Jetp-Ussr **3(6)**, 920-925 (1957)

[8] C. M. Varma, P. B. Littlewood, S. Schmitt-Rink, E. Abrahams and A. E. Ruckenstein, "Phenomenology of the normal state of Cu-O high-temperature superconductors," Phys. Rev. Lett. **63** (1989) 1996

[9] Y. Barlas and K. Yang, "Non-Fermi-liquid behavior in neutral bilayer graphene," Phys. Rev. B **80** (2009) 161408(R); arXiv:0908.1238 [cond-mat.mes-hall]

[10] F. Guinea and M. I. Katsnelson, "Many-Body Renormalization of the Minimal Conductivity in Graphene," Phys. Rev. Lett. **112** (2014) 116604; arXiv:1307.6221 [cond-mat.mes-hall]

[11] D. van der Marel, H. J. A. Molegraaf, J. Zaanen, Z. Nussinov, F. Carbone1, A. Damascelli, H. Eisaki, M. Greven, P. H. Kes, M. Li "Quantum critical behaviour in a high-Tc superconductor," Nature 425, 271-274 (2003); arXiv:cond-mat/0309172

[12] P. Gegenwart, Q. Si, F. Steglich, "Quantum criticality in heavy-fermion metals," Nature Physics 4, 186 - 197 (2008); arXiv:0712.2045 [cond-mat.str-el]

[13] T. Senthil, "Theory of a continuous Mott transition in two dimensions," Phys. Rev. B **78** (2008) 045109; arXiv:0804.1555 [cond-mat.str-el]

[14] T. Misawa and M. Imada, "Quantum criticality around metal–insulator transitions of strongly correlated electron systems," Phys. Rev. B **75** (2007) 115121; arXiv:cond-mat/0612632

[15] J. A. Hertz, "Quantum critical phenomena," Phys. Rev. B **14** (1976) 1165

[16] S. Sachdev, "Quantum phase transitions," Second edition, Cambridge University Press, 2011.

[17] J. Rech, C. Pepin, A. V. Chubukov, "Quantum critical behavior in itinerant electron systems: Eliashberg theory and instability of a ferromagnetic quantum critical point," Phys. Rev. B, f74(19) (2006) 195126; arXiv:cond-mat/0605306

[18] S. Chakravarty, B. I. Halperin and D. R. Nelson, "Two-dimensional quantum Heisenberg antiferromagnet at low temperatures," Phys. Rev. B **39** (1989) 2344

[19] Q. Si, J. L. Smith, K. Ingersent, "Quantum critical behavior in Kondo systems," Int. J. Mod. Phys. B **13** (1999) 2331; arXiv:cond-mat/9905006

[20] M. A. Metlitski and S. Sachdev, "Quantum phase transitions of metals in two spatial dimensions: I. Ising-nematic order," Phys. Rev. B **82** (2010) 075127 arXiv:1001.1153 [cond-mat.str-el]

[21] M. A. Metlitski and S. Sachdev, "Quantum phase transitions of metals in two spatial dimensions: II. Spin density wave order," Phys. Rev. B **82** (2010) 075128 arXiv:1005.1288 [cond-mat.str-el]

[22] T. Holder and W. Metzner, "Anomalous dynamical scaling from nematic and U(1)-gauge field fluctuations in two dimensional metals," Phys. Rev. B **92** (2015) 4, 041112 arXiv:1503.05089 [cond-mat.str-el]

[23] T. Holder and W. Metzner, "Fermion loops and improved power-counting in two-dimensional critical metals with singular forward scattering," arXiv:1509.07783 [cond-mat.str-el]

[24] S. S. Lee, "Low-energy effective theory of Fermi surface coupled with U(1) gauge field in 2+1 dimensions," Phys. Rev. B **80** (2009) 165102; arXiv:0905.4532 [cond-mat.str-el]

[25] D. F. Mross, J. McGreevy, H. Liu and T. Senthil, "A controlled expansion for certain non-Fermi liquid metals," Phys. Rev. B **82** (2010) 045121; arXiv:1003.0894 [cond-mat.str-el]

[26] A. L. Fitzpatrick, S. Kachru, J. Kaplan and S. Raghu, "Non-Fermi liquid fixed point in a Wilsonian theory of quantum critical metals," Phys. Rev. B **88** (2013) 125116 arXiv:1307.0004 [cond-mat.str-el]

[27] A. L. Fitzpatrick, S. Kachru, J. Kaplan and S. Raghu, "Non-Fermi-liquid behavior of large-N_B quantum critical metals," Phys. Rev. B **89** (2014) 16, 165114 arXiv:1312.3321 [cond-mat.str-el]

[28] R. Mahajan, D. M. Ramirez, S. Kachru and S. Raghu, "Quantum critical metals in $d = 3 + 1$ dimensions," Phys. Rev. B **88** (2013) 11, 115116 arXiv:1303.1587 [cond-mat.str-el]

[29] G. Torroba and H. Wang, "Quantum critical metals in $4 - \epsilon$ dimensions," Phys. Rev. B **90** (2014) 16, 165144 arXiv:1406.3029 [cond-mat.str-el]

[30] J. P. Blaizot and E. Iancu, "The Bloch-Nordsieck propagator at finite temperature," Phys. Rev. D **56** (1997) 7877 arXiv:hep-ph/9706397

[31] M. F. L. Golterman, "Chiral perturbation theory and the quenched approximation of QCD," Acta Phys. Polon. B **25**, 1731 (1994) arXiv:hep-lat/9411005

[32] A. Jakovac and P. Mati, "Resummations in the Bloch-Nordsieck model," Phys. Rev. D **85** (2012) 085006 arXiv:1112.3476 [hep-ph]

[33] A. Kernemann and N. G. Stefanis, "Exact Solutions for Fermionic Green's Functions in the Bloch-nordsieck Approximation of QED," Phys. Rev. D **40** (1989) 2103

[34] A. Jakovác and P. Mati, "Spectral function of the Bloch-Nordsieck model at finite temperature," Phys. Rev. D **87** (2013) 12, 125007 arXiv:1301.1803 [hep-th]

[35] A. I. Karanikas, C. N. Ktorides and N. G. Stefanis, "On the infrared structure of the one fermion Green's function in QED," Phys. Lett. B **289** (1992) 176

[36] D. V. Khveshchenko and P. C. E. Stamp, "Low-energy properties of two-dimensional fermions with long-range current-current interactions", Phys. Rev. Lett. **71** (1993) 2118

[37] L. B. Ioffe, D. Lidsky, B. L. Altshuler, "Effective lowering of the dimensionality in strongly correlated two dimensional electron gas", arXiv:cond-mat/9403023.

[38] B. L. Altshuler, L. B. Ioffe, A. J. Millis, "On the low energy properies of fermions with singular interactions", Phys. Rev. **B50**, 14048. arXiv:cond-mat/9406024.

[39] A. Allais and S. Sachdev, "Spectral function of a localized fermion coupled to the Wilson-Fisher conformal field theory," Phys. Rev. B **90** (2014) 3, 035131 arXiv:1406.3022 [cond-mat.str-el]

[40] J. Quintanilla and A. J. Schofield, "Pomeranchuk and topological Fermi surface instabilities from central interactions," Phys. Rev. B **74** (2006) 115126; arXiv:cond-mat/0601103 [cond-mat.str-el]

[41] S. A. Maier and P. Strack, "Universality in antiferromagnetic strange metals," arXiv:1510.01331 [cond-mat.str-el]

[42] A. H. Castro Neto and E. Fradkin, "Bosonization of Fermi liquids," Phys. Rev. B **49** (1994) 10877

[43] A. L. Fitzpatrick, S. Kachru, J. Kaplan, S. Raghu, G. Torroba and H. Wang, "Enhanced Pairing of Quantum Critical Metals Near d=3+1," Phys. Rev. B **92** (2015) 4, 045118 arXiv:1410.6814 [cond-mat.str-el]

[44] M. A. Metlitski, D. F. Mross, S. Sachdev and T. Senthil, "Cooper pairing in non-Fermi liquids," Phys. Rev. B **91** (2015) 11, 115111 arXiv:1403.3694 [cond-mat.str-el]

[45] J. Fröhlich and R. Götschmann, "Bosonization of Fermi liquids," Phys. Rev. B **55** (1997) 6788

[46] S. Raghu, G. Torroba and H. Wang, "Metallic quantum critical points with finite BCS couplings," arXiv:1507.06652 [cond-mat.str-el]

[47] C. Drukier, L. Bartosch, A. Isidori and P. Kopietz, "Functional renormalization group approach to the Ising-nematic quantum critical point of two-dimensional metals," Phys. Rev. B **85** (2012) 245120 arXiv:1203.2645 [cond-mat.str-el]

[48] B. Meszena, P. Säterskog, A. Bagrov and K. Schalm, "Non-perturbative emergence of non-Fermi liquid behaviour in $d = 2$ quantum critical metals," Phys. Rev. B **94**, 115134, [arXiv:1602.05360 [cond-mat.str-el]].

[49] W. Metzner, C. Castellani, C. Di Castro, "Fermi Systems with Strong Forward Scattering", Adv. in Physics **47** 317 (1998). [arXiv:cond-mat/9701012]

[50] T. Holder, W. Metzner "Fermion loops and improved power-counting in two-dimensional critical metals with singular forward scattering" Phys. Rev. **B92**, 245128 (2015). [arXiv:1509.07783 [cond-mat.str-el]]

[51] P. A. Lee, "'Gauge field, Aharonov-Bohm flux, and high-T_c superconductivity', Phys. Rev. Lett. **63**, 680 (1989).

[52] V. Oganesyan, S. Kivelson, E. Fradkin, "Quantum theory of a nematic Fermi fluid", Phys. Rev. B **64**, 195109 (2001).

[53] W. Metzner, D. Rohe, S. Andergassen, "Soft Fermi surfaces and breakdown of Fermi-liquid behavior", Phys. Rev. Lett. **91**, 066402 (2003).

[54] A. Neumayr and W. U. Metzner, "Fermion loops, loop cancellation and density correlations in two-dimensional Fermi systems,' Phys. Rev. B **58** (1998) 15449 [cond-mat/9805207]

[55] Y. B. Kim, A. Furusaki, X. G. Wen and P. Lee, "'Gauge-invariant response function of fermions coupled to a gauge field', Phys. Rev. B **50** (1994) 17917, [arXiv:cond-mat/9405083]

[56] A. L. Fitzpatrick, G. Torroba and H. Wang, "Aspects of Renormalization in Finite Density Field Theory," Phys. Rev. B **91**, 195135 (2015) [arXiv:1410.6811 [cond-mat.str-el]].

Samenvatting

De theoretische beschrijving van fermionische systemen met sterke wisselwerkingen is een zeer uitdagende open vraag in de natuurkunde. De meest bekende (maar niet de enige) experimentele realisatie van dit soort systemen zijn de koper-oxide supergeleiders die geen enkele electrische weerstand vertonen. Zelfs wanneer men een goed microscopisch model heeft voor de beschrijving van deze materialen, is het zeer moeilijk dit in macroscopische waarneembaarheden te vertalen die in principe experimenteel geverifieerd kunnen worden.

Het probleem is dat men in het geval van een zogenaamde relevante interactie geen Taylor expansie kan doen in termen van de koppelingsconstante voor de lage energieen waarin wij het meest geïnteresseerd zijn. Anderzijds — vanwege het fermionisch-teken-probleem — werken Monte Carlo numerieke technieken (die met bosonische modellen wel succesvol zijn) niet voor fermionen met eindige dichtheid.

Dit proefschrift is gericht op de toepassing van verscheidene methoden op het hierboven beschreven onderzoeksgebied. Het gemeenschappelijke thema van deze technieken is dat zij (gedeeltelijk) gemotiveerd zijn vanuit de hoge-energie-fysica: de onderzoeksrichting die zich bezig houdt met deeltjesfysica, snaar-theorie, etc.

In het Introductie hoofdstuk van dit proefschrift geven wij een overzicht van een aantal eigenschappen van Fermi-liquids (een toestand van materie die we zeer goed begrijpen) en non-Fermi-liquids (waar onze kennis tekort komt). Vervolgens introduceren wij een aantal methoden die op vaste-stof-systemen kunnen worden toegepast. Deze omvatten large-N-methoden, conformal-field-theories en holography. Bij de discussie van dit laatste punt zullen wij ook laten zien hoe deze ideeën tezamen komen in AdS/CFT en een dualiteit beschrijven tussen zwak-gekoppelde zwaartekracht-theorieën en sterk-gekoppelde large-N-systemen. Na deze algemene ideeën gaan wij over naar de presentatie van verscheidene onderzoeks-projecten.

In Hoofdstuk 2 beschouwen wij een holographisch model voor dynamische paar-vorming in supergeleiders. BCS-theorie beschrijft met succes de paar-vorming in supergeleiders waar de normale phase van het metaal een zwak-gekoppeld Fermi-liquid is. Daarentegen vertonen de hoge-temperatuurs-phase van high-$T-c$-materialen non-Fermi-liquid ge-

drag. Zoals we in de Introductie laten zien, voorspelt AdS/CFT non-Fermi-liquid toestanden in een aantal holographische modellen. Het is daarom voor de hand liggend om supergeleidend-paar-vorming in non-Fermi-liquids met AdS/CFT te bestuderen. Wij nemen een eerste stap naar dit doel door paar-vorming in een holographisch Fermi-liquid te bestuderen waarbij de ruimte-tijd geometrie die van AdS is met een hard-wall. Om dit te doen introduceren wij een parings-interactie tussen de fermionen en een order-parameter veld. Afgezien van de gefixeerde achtergronds-geometrie lossen wij het fermion-ijkveld-scalar systeem zelf-consistent op. Wij laten zien dat de studie van dit iets vereenvoudigd model nog steeds kleurrijke, en soms nieuwe ongebruikelijke natuurkunde blootlegt. We geven ook algemenere argumenten dat met de toevoeging van interacties in de bulk er subtiliteiten zijn in de gewoonlijke vertalingsregels tussen AdS en CFT.

In Hoofdstuk 3 analyseren wij een interessant sterk-gekoppeld vastestof model met een nieuwe velden-theoretische methode. Het systeem bestaat uit fermionen met eindige dichtheid (en daarom een Fermi-oppervlak) gekoppeld aan een dynamisch order-parameter-veld in 2+1 dimensies. Dit is het simpelste model dat non-Fermi-liquid gedrag vertoont als men de massa van de boson naar zijn kritieke waarde fijn stelt (massa nul in dit geval). Dit systeem is niet-perturbatief en men moet zich daarom beroepen op onconventionele technieken. Wij maken twee benaderingen. Ten eerste nemen wij aan dat de kromming van het Fermi-oppervlak klein is. Ten tweede maken wij gebruik van de zogenaamde quenched approximation, dat wil zeggen dat wij alle fermion-loops negeren. Formeel kan dit systematisch gebeuren door een aantal fermion soorten te introduceren (N_f) en vervolgens de limiet $N_f \to 0$ te nemen. Met deze vereenvoudigingen zijn wij in staat de expliciete vorm van de fermionische spectral function te bepalen. Deze laat non-Fermi-liquid gedrag zien en daarnaast een opsplitsing van het Fermi-oppervlak.

In hoofdstuk 4 vervolgen wij dit onderzoek door N_f nu eindig te houden terwijl we nog steeds de kromming van het Fermi-oppervlak klein houden. Een belangrijke vereenvoudiging die hieruit volgt is dat zelfs voor eindige N_f de boson-propagator alleen maar op één-loop niveau wordt gecorrigeerd. Deze zogenaamde Landau-damping bijdrage heeft een belangrijk gevolg in het IR regime van de fermion Green's functie. Wij analyseren deze twee-punts-functie om te verhelderen hoe het tussen de sterk-Landau-damped vorm en het quenched resultaat interpoleert.

Summary

The theoretical description of fermionic system with strong interaction is a very challenging open problem in physics. The most notable (but far from the only) experimental realization of this type of systems are the cuprate superconductors which have zero electric resistivity. Even if one has a good microscopic model for the description of these materials it is very hard to translate it to macroscopic observables which in principle can be experimentally checked.

The problem is that in case of a relevant interaction one can not Taylor expand in the coupling constant in the low-energy regime in which we are most interested. On the other hand, because of the fermion sign problem Monte Carlo numerical techniques (which are succesful with bosonic models) do not work for fermions at finite density.

This thesis is devoted to the applications of several methods to the research area described above. The common theme of these techniques is that they are (partly) motivated from high-energy physics: the research area which deals with particle physics, string theory etc.

In the Introduction chapter of this thesis we review some aspects of Fermi liquids (a state of matter we understand very well) and non-Fermi liquids (where our knowledge is limited). Then we introduce some methods which can be applied to condensed matter system. These include large-N methods, conformal field theories and holography. In the discussion of the last point we also show how these ideas come together in AdS/CFT to form a duality between weakly coupled gravitational theories and strongly coupled large-N systems. After these general ideas we turn to the presentation of several research projects.

In Chapter 2 we consider a holographic model for dynamical pairing in superconductors. The BCS-theory describes succesfully the pairing in superconducting materials when the normal phase of the metal is a weakly interacting Fermi liquid. However, in high-T_c materials the high-temperature phase possesses non-Fermi liquid behavior. As we show in the introduction, AdS/CFT predicts non-Fermi liquid states in some holographic models. It is reasonable therefore to study the superconducting pairing in non-Fermi liquids using AdS/CFT. We take the first step towards this goal by studying the pairing in a holographic Fermi-liquid where

the spacetime geometry is AdS with a hard wall. For this we introduce a pairing interaction between fermions and an order parameter field. Apart from the fixed background geometry we solve the fermion-gauge-scalar system self-consistently. We show that by studying this somewhat simplified model we still find rich, sometimes novel physics. We also argue that in case of interaction terms in the bulk there are subtleties in the usual dicitonary rules between AdS and CFT.

In Chapter 3 we analyze an interesting strongly coupled condensed matter model with a novel field theoretical method. The system at hand consists of fermions at finite density (forming a Fermi-surface therefore) coupled to a dynamical order parameter field in 2+1 dimension. This is the simplest model which displays non-Fermi liquid behavior after tuning the mass of the boson to its critical value (which is zero in our case). As this system is non-perturbative therefore we need to rely on non-standard techniques. We make two approximations. Firstly, we assume that the Fermi surface curvature is small. Secondly, we use the so-called quenched approximation, i.e. we ignore all fermion loops. Formally, this can be systematically achieved by introducing the number of fermion flavors (N_f) and taking the $N_f \to 0$ limit. With these simplification we find the explicit form of the fermion spectral function. This exhibits non-Fermi liquid behavior and also the splitting of the Fermi surface.

In Chapter 4 we continue our investigation by allowing N_f to be non-zero while keeping the Fermi surface curvature small. An important simplification is that it turns out that for small N_f the boson propagator is corrected only at one-loop. This so-called Landau-damping has an important effect to the IR region of the fermion Green's function. We analyze this two-point function in order to understand how it interpolates between the strongly Landau damped form and the quenched result.

List of Publications

The thesis is based on the following publications:

1. A. Bagrov, B. Meszena and K. Schalm, "Pairing induced superconductivity in holography," JHEP **1409** (2014) 106 [arXiv:1403.3699 [hep-th]].

2. B. Meszena, P. Säterskog, A. Bagrov and K. Schalm, "Non-perturbative emergence of non-Fermi liquid behaviour in $d = 2$ quantum critical metals," Phys. Rev. B **94** (2016), 115134, [arXiv:1602.05360 [cond-mat.str-el]].

3. B. Meszena, P. Säterskog, and K. Schalm, "Non-perturbative correlation functions of a $d = 2$ quantum critical metal", to appear

Other publications by the author are

4. B. Meszena and A. Patkos, "On the evolution of an entangled lepton-neutrino pair," Mod. Phys. Lett. A **26** (2011), 101 [arXiv:1009.5923 [hep-ph]].

Curriculum Vitæ

I was born on 31 March 1989 in Budapest, Hungary. I did my secondary education at Fazekas Mihaly high school which is a place with an exceptionally high density of future scientists and engineers.

In 2007 I started my university studies in Physics at the Eotvos Lorand University from where I received my Bachelor diploma in 2010. After this I continued my studies as a Master student in the particle physics track.

After graduation in 2012 I moved to the Netherlands to start my PhD research at the Lorentz Institute (Leiden University). I have become a member of the group of prof. Koenraad Schalm and prof. Jan Zaanen. I have conducted research at the interface between high- and low-energy physics. I was also a teaching assistant for the courses "'Effective field theory' and "Quantum field theory". During my PhD I have presented my work through talks and posters at several workshops and schools in the Netherlands, Greece, Hungary, Germany, China and Brazil.

Acknowledgments

I would like to express my gratitude to my supervisor Koenraad Schalm. He was always available for discussions and encouraged me to think independently. I would also like to thank Jan Zaanen for the interesting and enlightening discussions. Together with Koenraad they provided a lively atmosphere in our research group.

I am indebted to my other collaborators as well: Andrey Bagrov and Petter Säterskog. I believe we have formed a very good team and had a lot of fun together while doing physics. I was fortunate to share my office with Ke Liu together with his unique personality and tea factory.

I am grateful to the secretaries of the institute - Fran, Marianne and Trudy - for their kind help in practical manners. I am also thankful to other members of the group: Nick, Bartek, Vincenzo, Saso, Jaakko, Miggy, Nikos, Richard, Sasha and Robert-Jan. I will always remember the great time we had together both in the institute and outside of it.

I owe my gratitude to my parents for their continuous support. Finally, I would like to thank my beloved wife, Anna. This work would not have been possible without her love, care and patience during my PhD studies.